The Hong Kong Polytechnic University
Department of Electrical Engineering

Stochastic Studies of Overvoltages Resulting from Circuit Breaker Operation in Industrial Installations

Submitted by
Wong Sze Mei

A thesis submitted in partial fulfilment of the requirements
for the Degree of Master of Philosophy
in August 2004

CERTIFICATE OF ORIGINALITY

I hereby declare that this thesis is my own work and that, to the best of my knowledge and belief, it reproduces no material previously published or written, nor material that has been accepted for the award of any other degree or diploma, except where due acknowledgement has been made in the text.

_______________________________ (Signed)

_Wong Sze Mei____________________(Name of student)

ABSTRACT

Switching overvoltages are stochastic in nature and the conditions which may result in serious overvoltages are numerous. It has been found that switching operation of vacuum circuit breakers in motor circuits can cause large transient overvoltages at the motor terminals or the transformer terminals. By predicting these transients and applying suitable overvoltage protection, the risk of failure to equipment can be reduced.

In order to accurately predict system overvoltages, suitable simulation models are required which reflect the behaviour of the key components at power frequency as well as at frequencies corresponding to fast transients. In this research a stochastic vacuum circuit breaker model, a universal hybrid high-bandwidth (from power frequency to MHz) induction motor and a hybrid transformer model have been developed in the ATP version of the Electromagnetic Transients Program (EMTP). A large number of detailed studies were performed and the results indicate that some combinations of breaker characteristics, induction motor ratings and network topology, including system fault level, cable lengths, power factor correction capacitors and grounding practices may lead to severe reignition and voltage escalation problems. Consequently there is a need to establish, in general terms, which parameters, combinations of parameters and system configurations may lead to particularly severe transient conditions and to evaluate the performance of different protection measures. Rather than studying a large number of installations, a parametric sensitivity study was performed aimed at identifying the essential parameters that could lead to potential damage of the system equipment. Mitigating measures were also studied.

The results of the parametric sensitivity studies and the effectiveness of different protection measures are presented. Two real case studies of industrial installations in Hong Kong were carried out with one where there was a failure of a transformer attributable to VCB switching, and one where VCBs were to be installed as replacements for oil circuit breakers. The results of the case studies compare well with predictions made in the simulations.

PUBLICATIONS

1. Wong, S. M., Snider, L. A., Lo, E. W. C., "Overvoltages and reignition behaviour of vacuum circuit breakers," The International Conference on Power Systems Transients 2003 – New Orleans, 2003, Section 14a-3
2. Wong, S. M., Snider, L. A., Lo, E. W. C., Chung, T. S., "The Influence of Vacuum Circuit Breakers and Different Motor Models on Switching Overvoltages in Motor Circuits," International Conference on Electrical Engineering 2004, Sapporo, July 2004, Vol. 2, pp.355-360 (Outstanding Paper Award)
3. Wong, S. M., Snider, L. A., Lo, E. W. C., Chung, T. S., "The Influence of Vacuum Circuit Breakers and Different Motor Models on Switching Overvoltages in Motor Circuits," IEEJ Transaction on Industrial System and Electric Power Application (Submitted in July 2004)

ACKNOWLEDGEMENTS

I would like to take this opportunity to show my gratitude to the Department of Electrical Engineering for providing me with good facilities and working environment. Thanks to all the professors in the Department for giving me the support and encouragement.

I am grateful to my supervisors Dr. L. A. Snider, Dr. Edward W. C. Lo and Prof. T. S. Chung for giving me intellectual support and emphasising the meaning of research. With their advice and guidance, this research was accomplished smoothly. I am also thankful to their patience and encouragement throughout the research.

TABLE OF CONTENTS

ABBREVIATIONS

EMTP	Electromagnetic Transient Program
VCB	Vacuum Circuit Breaker
TRV	Transient Recovery Voltage
SCR	Short circuit ratio
BV	Breakdown Voltage
HF	High Frequency
SSFR	Standstill Frequency
PRBS	Pseudorandom Binary Sequence

CHAPTER 1 INTRODUCTION

The main contributions in this thesis are (i) the development of improved stochastic models of vacuum circuit breakers, (ii) the development of hybrid models of induction motors and transformers valid over a wide bandwidth, (iii) parametric sensitivity studies, including effects of cable and motor grounding, power factor correction, cable lengths, etc, (iv) stochastic studies aimed at determining representative overvoltages in industrial power delivery networks, and (v) evaluation of the effectiveness of overvoltage protection measures.

1.1 BACKGROUND

Over the past several years, electrical equipment and installations have become increasingly vulnerable to transient overvoltages arising from lightning and switching transients. Interrupting current in an inductive load is well known to generate overvoltages that can cause dielectric breakdown of insulation. The loads do not have to be large: for example Martzloff and Hahn (1970) found that when a vacuum cleaner was unplugged while the motor was running, there was an arc created in the air at the socket where the connection was broken. They found that a transient overvoltage with a peak value between 1.4 and 2.5 kV was injected into the 120V mains.

Transient overvoltages studies and overvoltage protection in industrial power systems are recognized as crucial for the reliability of the electrical supply and equipment, especially in critical electrical services, such as in airports and hospitals. The IEC Standard on Insulation Coordination in Low Voltage Systems (IEC 2000) devotes a large part of the application guide to mitigation of overvoltages, and suggests ways to sectionalize an electrical installation into regions where given values of overvoltages will not be exceeded. However, the mitigation measures, involving judicial placement of metal oxide arresters and other voltage limiting devices are still lacking, and failures attributable to overvoltages are still not uncommon.

The overvoltage protection problem is exacerbated by the difficulty of accurately predicting overvoltages, since they are stochastic in nature, and in order to accurately predict system overvoltages, suitable simulation models are required which reflect the behaviour of key components at power frequency as well as at frequencies corresponding to fast transients.

1.2 OVERVOLTAGES GENERATED BY VACUUM CIRCUIT BREAKERS

Among the most onerous overvoltages in industrial systems are those arising from interruption of inductive currents by vacuum circuit breakers (VCBs) (Greenwood et al. 1988, Colombo et al. 1988, Reckleff et al. 1988 and Eichenberg 1998). When a circuit breaker is opened, the two electrical networks at either side of the breaker are disconnected and each of the networks proceeds to redistribute its trapped energy. As a result of this energy redistribution, each network will develop a voltage that appears simultaneously at the respective terminals of the breaker. The algebraic sum of these two voltages represents the Transient Recovery Voltage (TRV) and this phenomenon depends on the conditions that prevail at the moment of the interruption of current. TRV rises almost instantaneously once the contacts of the breaker start parting and its magnitude can normally get higher than 2 p.u. if no protection method is applied.

In the case of VCBs the overvoltages can be much higher owing to the ability of VCBs to interrupt very fast changing current, which leads to a virtual chopping of current before the current reaches a natural zero. This current chopping leads to high overvoltages in inductive loads and transformers.

1.2.1 Current chopping and arc physics

Theoretically, current flow in a vacuum circuit breaker should be interrupted when current reaches its natural zero. However in practice current is interrupted prior to a natural current zero with values ranging between 3A to 12A due to arc instabilities. This phenomenon is called “current chopping” and can result in substantial overvoltages owing to the “trapped” stored energy in the magnetic field of apparatus such as motors and transformers. The consequential higher magnitude TRV thus enhances the likelihood of reignition, where the arc between the contacts is re-established, to be followed by another interruption. The process may be repeated several times, leading to an escalation of overvoltages, and potential damage to equipment.

When the contacts of a vacuum interrupter separate, a metal vapour arc discharge develops and flows through the plasma in the gap between the contacts until the next current zero. The arc is then extinguished and the conductive metal vapour condenses on the metal surfaces of the contacts within a matter of microseconds. Consequently the dielectric strength of the gap builds up very rapidly.

At currents under 10kA, the vacuum arc burns as a diffuse discharge. At high values of current the arc changes to a constricted form with an anode spot. A constricted arc that remains on one spot for too long can thermally over stress the contacts to such a degree that the deionization of the contact zone at current zero can no longer be guaranteed. To overcome this problem the arc root must be made to move over the contact surface. In order to achieve this, contacts are so shaped that the current flow through them results in a magnetic field being established which is at right angles to the arc axis. This field causes the arc root to rotate rapidly around the contact resulting in a uniform distribution of the heat over its surface. Contacts of this type are called radial magnetic field electrodes and they are used in the majority of circuit breakers for medium voltage application.

A new design of vacuum interrupter had been developed (Greenwood 1994) in which the arc is altered from a diffusion to a constriction state by subjecting the arc to an axial magnetic field. Such a field can be provided by leading the arc current through a coil suitably arranged outside the vacuum chamber. Alternatively the field can be provided by designing the contact to give the required contact path. Such contacts are called axial magnetic field electrodes. This principle has advantages when the short circuit current is in excess of 31.5 KA. Both designs, however, are subject to current chopping.

Current chopping is due to a breakdown of necessary conditions to maintain emission of electrons at the cathode. It has been shown that arc extinction in gaseous interrupting media can be attributed to arc columnar effects. In a vacuum interrupter, however, the absence of columnar effects at low currents suggests that the sudden arc cessation is dominated by cathode processes. It is speculated that current chopping is a direct result of vacuum arc instabilities, and is shown to be equivalent to spontaneous extinction of a dc arc after a certain lifetime (Smeets et al. 1989). In a similar study, instabilities were said to be short peaks in arc voltage in low-current vacuum arcs (Smeets et al. 1992). It was concluded that current chopping takes place as a result of a high-frequency arc current oscillation with increasing amplitude. This oscillation is excited periodically at the current minima by a series of instabilities in a self-enhancing way. The dc lifetime is related to arc instabilities, which are believed to be manifestations of an ion deficiency in the near-anode plasma. The deficiency is in turn caused by a discontinuity in the ionized mass flow from the cathode spot into the plasma.

The arc-interruption properties of a vacuum interrupter depend largely on the material and geometry of the contacts. Over the period of their development, various types of contact material have been used. Currently it is accepted that an oxygen free copper chromium alloy is the best material for high voltage VCBs. With this alloy, chromium is distributed throughout the copper in the form of fine grains, such that this material combines good arc extinguishing characteristics with a reduced tendency to contact welding and provides low chopping current when interrupting inductive currents.

Arcing time is the time between the contact separation and the following current zero; the quenching capability represents the high frequency current clearing capability. The breaker parameters affected by arc physics which have significant effects on overvoltages caused by current interruption include arcing time, quenching capability, chopping current magnitude and rate of dielectric recovery, all of which depend on the interrupter contact material. Furthermore, Greenwood et al. (1989) stated that *di/dt*, the rate of change of current, was believed to be an important criterion for predicting the behaviour of vacuum switches under conditions where reignitions and voltage escalation can occur. If *di/dt* exceeds a certain value (say 1000A/μs (Helmer et al. 1996)), conduction continues straight through the current zero with the formation of a new cathode spot on the former anode. Interruption will take place for lower *di/dt*'s.

1.2.2 Voltage escalation and reignition behaviour

At the initial stage of contact separation, the build-up of the TRV usually prevails over the rate of recovery of dielectric strength. As a result, reignition takes place and interruption cannot be brought about until the next zero passing of phase current. However, studies have shown that the ability of vacuum switching devices to interrupt high frequency currents can lead to repeated reignitions and voltage escalation.

Smeets et al. (1993) preformed a study of two different types of contact material of vacuum interrupters, and four types of reignitions following high-frequency current zero were observed. They are classified according to the duration between interruption and reignition. He concluded that a series of reignitions can consist of 4 distinct types of reignitions. Also, the effect of high-frequency arcing breakdown voltage and the high-frequency interruption ability were found for the two materials.

It was found that the reignition and escalation problems are more severe with protective capacitors connected to the system side for relatively low load shedding at short arc duration (Glinkowski et al. 1997). To study the most severe reignition/escalation behaviour of the vacuum generator circuit breaker, the vacuum switching device was characterized by the Breakdown Voltage (BV) strength and the high frequency current clearing capability or derivative of the current (*di/dt*) characteristic. The results show that higher escalation voltages are more likely to occur if the vacuum generator circuit breaker exhibits a medium range BV characteristic and that the chance of getting escalation may occur when the system side capacitance is comparable with the generator side capacitance.

In another study of voltage escalation in vacuum switching operations, the focus was on the interruption of motor inrush current (Greenwood et al. 1988). The successive trapping of magnetic stored energy in the motor winding and its subsequent release to the motor and cable capacitance were believed to cause a sequence of escalating voltage surges. The analysis was done in such a way to examine the consequences of variation of one parameter while keeping others constant. The conclusion was that switch designers should aim for a low *k* factor, defined as the increase in dielectric strength with distance, and low *di/dt* interrupting capability in order to alleviate the problem.

Studies of interrupting starting current of motors by VCB were carried out with different sets of combination of *k* factor and the high frequency (HF) interrupting capability (Chaly et al. 1996). It was found that HF interrupting capability is important for high power motors connected by short cables to the VCB when the HF current does not pass through zero. Generally, increasing the *k* factor lowers the maximum overvoltages but serious overvoltages can still possibly occur. It is suggested that VCBs should be supplied together with the proper protection against such overvoltages.

Owing to the large number of parameters which can affect current chopping, it is difficult to develop a deterministic model of a VCB. A stochastic approach is used in this research, whereby the above breaker parameters are taken into account by randomly selecting variables within representative ranges. This model serves well in statistical overvoltage studies.

CHAPTER 2 SIMULATION TOOLS FOR OVERVOLTAGE STUDIES

It is apparent that transient problems cannot be solved by hand except in the simplest circuits containing a small number of elements. Computer simulation techniques are required in order to determine magnitudes and waveshapes of transients and how components or systems behave when subjected to prescribed transients.

2.1 EMTP

In this research I used the ElectroMagnetic Transient Program (EMTP) (Dommel 1986) which is a well-proven and comprehensive computer program designed to solve electrical transient problems in lumped active and passive circuits, distributed circuits, or combinations thereof. EMTP is an internationally acclaimed program used to solve electromagnetic transient problems, and can solve any networks of interconnections of resistors, inductors, capacitors, single and multiphase pi-circuits, distributed-parameter lines, as well as machines and control systems. EMTP uses nodal analysis and solves the system differential equations using the trapezoidal rule of integration with a fixed time step. The solution is very efficient, and as such EMTP is one of the most suitable tools for solving large networks. In contrast, state-space simulation tools, such as Matlab, use a variable time step, and provide very accurate solutions for highly nonlinear systems. The cost, however, is solution time: the time step becomes very small at high nonlinearities, consequently the solution time becomes very long. For large networks, typical of power systems the solution time becomes excessive.

EMTP also comprises comprehensive models of electrical, hydro and thermal machines such that electromechanical transients including the dynamics of electrical machines can also be studied. The ATP (Alternate Transients Program) version of EMTP (Meyer et al. 1987 - 1995), which was used in this research, includes simulation tools for control systems called Transient Analysis of Control Systems (TACS) and MODELS. The former can represent different blocks in control systems while the latter was incorporated into the ATP version of EMTP to simulate complex systems. MODELS is a high-level language similar to C and was used in this research for simulation of the complex equations and control algorithm related to the circuit breaker model. The interface between electrical network and TACS or MODELS is established by exchange of signals such as node voltages, switch currents, switch status, time-varying resistances, voltage and current sources. Figure 2-1 shows the simulation flow in EMTP as well as the relationship between the electric network and the control systems as used in this research.

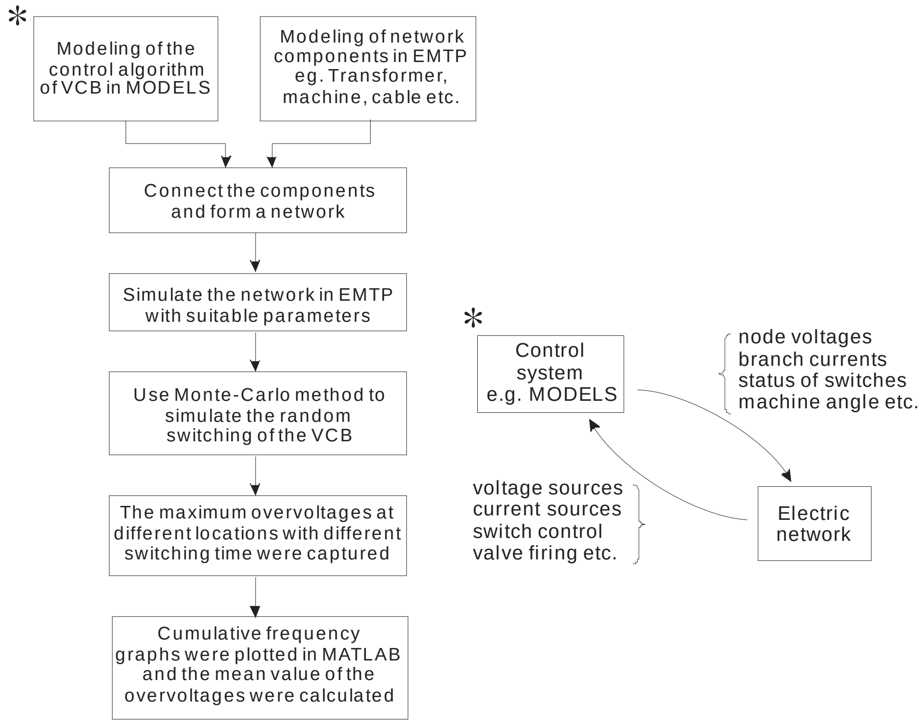

Figure 2-1 Simulation flow of EMTP

2.1.1 Trapezoidal rule and numerical oscillations

EMTP uses the trapezoidal rule of integration to solve ordinary differential equations. The trapezoidal rule of integration uses a fixed time step and provides fast and efficient solutions, however it is notorious for giving rise to numerical oscillations in some circumstances. A brief explanation of the use of the trapezoidal rule follows.

A system can be described as a set of n^{th} order ordinary differential equations,

$$\left[\frac{dx}{dt}\right] = [A][x] + \left[g(t)\right] \qquad (2\text{-}1)$$

where [A] is a constant square matrix and *g(t)* is a vector of known forcing functions. This can be rewritten as:

$$[x(t)] = [x(t-\Delta t)] + \int_{t-\Delta t}^{t} \{[A][x(u)] + [g(u)]\} du \qquad (2\text{-}2)$$

By using linear interpolation on [*x*] and [*g*] between *t-Δt* and *t* and assuming that for the time being [*x*] is known at *t*, (note that in reality it is not necessarily true), we get,

$$[x(t)] = [x(t-\Delta t)] + \frac{\Delta t}{2}[A]\{[x(t-\Delta t)] + [x(t)]\} + \frac{\Delta t}{2}\{[g(t-\Delta t)] + [g(t)]\} \qquad (2\text{-}3)$$

This method also implies that the areas under the integral of equation (2-3) are approximated by trapezoids, which is why the rule gets its name.

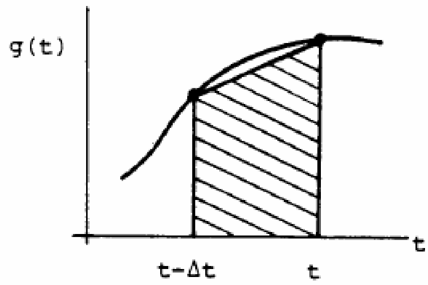

Figure 2-2 Trapezoidal rule of integration

The main drawback with the trapezoidal rule is encountered when simulating a step change in current through an inductor or a step change in voltage across a capacitor since both of these cause numerical oscillations. Consider a simple case of switching off an inductor: there will be voltage oscillations even though the switch opening occurs at a current zero. This is in fact inherent to the trapezoidal rule of integration which is used to work out solution for all the programs in the software. This is illustrated in the following equation:

$$i_L(t) = i_L(t-\Delta t) + \frac{1}{L}\int_{t-\Delta t}^{t} v_L(u)du \qquad (2\text{-}4)$$

since $i_L(t)$ and $i_L(t-\Delta t)$ equal zero, we have,

$$\frac{1}{L}\left(\frac{v_L(t-\Delta t) + v_L(t)}{2}\right)\Delta t = 0 \Rightarrow v_L(t) = -v_L(t-\Delta t) \qquad (2\text{-}5)$$

As a result, the voltage will alternate about the time axis, changing at each time step from equal positive to negative magnitudes. Figure 2-3 is an example of such a numerical oscillation.

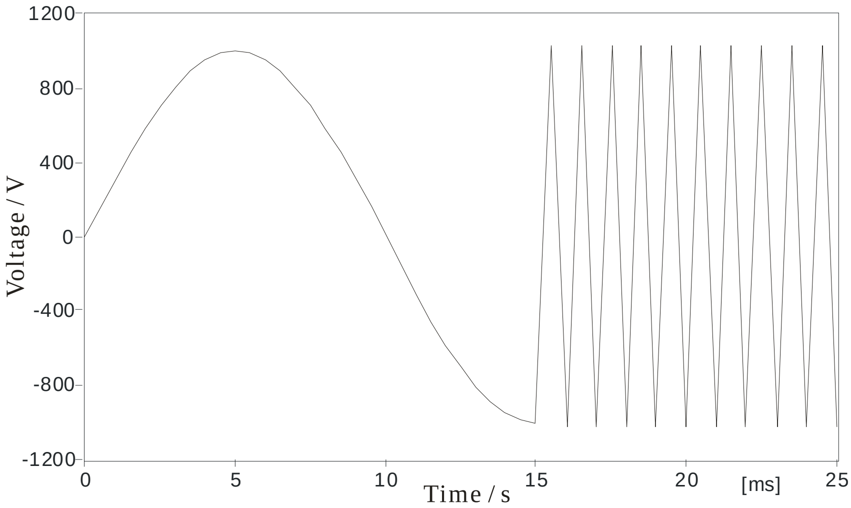

Figure 2-3 Inductor voltage V_L as a result of numerical oscillation

In this example as illustrated in the Figure 2-3, the voltage oscillates between -1000 and 1000 at each time step of 0.5ms. These oscillations might be confused with oscillations caused by the LC circuit which could induce oscillations with high natural frequency and amplitude. However, it is in fact quite easy to distinguish the two kinds of oscillations: numerical oscillations take place at each time step defined by the user (i.e. Δt) and true solution is always given by the average value of the oscillations. So in the above example, the true solution would be zero. Oscillations caused by LC circuits usually have smaller natural frequency and, for a properly chosen time step, the magnitude will not change with the change of time step.

Numerical oscillations can be damped by means of connecting resistors in series or in parallel with the capacitive or inductive element concerned respectively. Problems arising out of inductor switching can be solved by connecting an appropriate damping resistance, R_p, across the inductor concerned (IEEE Working Group 15.08.09 1999). For critical damping the resistance is given by

$$R_p = 6 \cdot \frac{2L}{\Delta t} \qquad (2\text{-}6)$$

Similarly, an appropriate resistance, R_s, connected in series with a capacitance can critically damp numerical oscillation and the resistance is given by

$$R_s = \frac{1}{6} \cdot \frac{\Delta t}{2C} \qquad (2\text{-}7)$$

However, in practice critical damping is not sufficient since the formulae relate to only simple circuits having one capacitor or one inductor. For more complex networks the optimal values are obtained by trial and error using the critical values as starting points.

2.1.2 Time step

Results from EMTP are discrete because variables are calculated at each time step during compilation. The time step is usually set to be at the most a tenth of the time period of the highest frequency of the system. For example, if the resonant frequency of an LC circuit is 1kHz, the time step has to be less than 0.1msec.

2.1.3 TACS and MODELS

TACS is a simulation module for time-domain analysis of control systems. It was originally developed for the simulation of HVDC converter controls. For TACS, a block diagram representation of control systems is used. TACS can be used for the simulation of (i) HVDC converter controls, (ii) excitation systems of synchronous machines, (iii) power electronics and drives and (iv) electric arcs (circuit breaker and fault arcs).

MODELS is a general-purpose description language supported by an extensive set of simulation tools for the representation and study of time-variant systems. It is a high-level language similar to C and can be used for simulation of complex equations and control algorithms.

The description of each model is enabled using free-format, keyword-driven syntax of local context and that is largely self-documenting. It provides the EMTP user with a tool for specifying and modifying the value of the numerical and logical quantities that can be used for controlling the operation of the electrical components of the simulated system.

One of the important features is its ability to define local limits, minima and maxima, on the size of the local time step to be used for the step-by-step solution of a model. When a model is called from outside for updating its internal state to a new simulation time, the interval of time since the last call for update determines the step that the model can use to carry out its operation. This outside step, being too large or too small, may not be properly scaled to the fineness of the representation needed to follow the internal dynamic operation of the model. An appropriate range of time steps can be maintained by specifying a minimum and/or a maximum limit on its size. If the outside time step is too large for the model, that is, larger than the specified maximum, the model will subdivide the outside step into finer internal steps. If the outside time step is too small for the model, that is, smaller than the specified minimum, the model will ignore the request for the update, which will provide no significant change in the state of the model.

CHAPTER 3 MODELLING OF CIRCUIT ELEMENTS

Studies of TRV and voltage escalation have been limited owing to the deficiencies of the breaker models. A few different mathematical circuit breaker models exist and in general they all take into account arc thermal instabilities, however there is no existing universal precise arc model because of the complexity of the arc physics. Some models are characterized by experimentally measured parameters to describe the statistical properties of different phenomena taking place in the breaker opening process.

The predicted transient overvoltage depends not only on the characteristics of the circuit breakers, we also need to know how other circuit elements will behave under switching operations. The development of simulation models requires a very detailed knowledge about the transient behaviour of each component. To avoid an unusual number of model parameters, relevant and irrelevant effects need to be separated. It is frequently sufficient to represent each circuit element by its inductance, or power frequency reactance, though resistance may also be taken into account on some occasions and the traditional equivalent circuits for machines are examples. The transient model is different and it must take into account the capacitance of components, since this plays such an important role in the transient response. To this extent the transient model is significantly more complicated.

The evaluation also requires knowledge of the value of components: the inductances, capacitances, and resistances of the elements involved. The inductive reactance of most power system components is often available from the manufacturer. On the other hand, the capacitance of the components is not provided by the manufacturer and usually obtained by test.

The form of a model depends on how it is to be used. Take an induction motor for example: if the primary interest is in the terminal response as a component in a system, we would use one model, but if we are concerned with events within the motor (example, the transient stresses on the winding insulation), a different and more complex model would be required.

Moreover, the degree of detail in modelling also depends on the position of the component in the system with respect to the event creating the disturbance. If a switch is being opened or closed, or if a fault occurs, the impact will be greatest on components close to the switch or fault, therefore, these components should be modelled in more detail than required for remote components, which may be relatively unaffected by the transient event.

This research is aimed at determining the fast-front statistical overvoltages that may result from operation of vacuum circuit breakers in typical industrial installations. For the purposes of this study a comprehensive circuit breaker model was developed which accounts for the stochastic behaviour of the arc interruption process. As has been previously discussed, the arc interruption process can lead to onerous overvoltages, particularly to equipment with windings, such as motors and transformers, owing the high turn-to-turn stress that may result because of the highly non-uniform distribution of the fast-front overvoltage across the winding. However this project is not dealing with this aspect of the problem, but concentrates on the prospective magnitude of the overvoltages that may be produced by operation of VCBs. To this end, the study requires, in addition to the comprehensive circuit breaker models, other circuit elements models which are required to represent the correct propagation media and/or termination impedances for incident surges, and this is the focus of the development of these models in this research. Simulation models of induction motors, transformers and cables have been developed for the studies of switching overvoltages and these models reflect the required termination impedance at both operating frequency and high frequencies. In the following, the various models will be presented.

3.1 VACUUM CIRCUIT BREAKERS

There are several references in the literature pertaining to the development of VCB models (Thuries et al. 1986 and St-Jane et al. 1983). A realistic model simulated in EMTP was proposed (Phaniraj et al. 1988) and the initial stages of the contacts opening were modelled by a constant arc voltage until the inception of the arc instability period and the voltage was determined by either the equations of the Avdonin Model, the Urbanek Model or the Kopplin Model. It was believed that this procedure could provide suitable initial values for the arc equations and minimize the numerical problems due to the sudden voltage change. The statistical properties of the current chopping level, the cold dielectric strength of the vacuum gap high-frequency-current extinction of the vacuum discharge were incorporated into the interrupter model and it was implemented in EMTP using the MODELS module (Helmer et al. 1996). An algorithm similar to that developed by Janko Kosmac and Peter Zunko (1995) was employed, with a different empirical formula for chopping current. The probability of multiple re-ignitions was determined by the relative difference of *di/dt* and the high frequency quenching capability of the specific vacuum circuit breaker. Owing to the stochastic nature of these models, numerous simulations were needed to study the severity of TRV.

3.1.1 My approach

Models of specific circuit breakers would require experimental determination of the relevant parameters, and as such it is virtually impossible to develop a generic deterministic model. Moreover, those models would only be applicable to systems showing arcing phenomenon which match the conditions at which the measurements are made. This restricts the applicability of such models.

Modern overvoltage and insulation coordination studies are based on Monte Carlo techniques (IEC 1996): i.e. stochastic studies where statistical overvoltages distributions are determined by simulating random breaker operations within an electrical cycle. The distribution is often characterized by what is known as the *statistical overvoltage*, which is the overvoltage which has a 2% probability of being exceeded. Consequently, it is appropriate to develop a stochastic breaker model which would serve well in statistical overvoltage studies.

Stochastic models, rather than being based on measured parameters, are based on choices of random values from a range of typical values for each of the related variables during a Monte Carlo simulation, in order to determine the statistical overvoltages that may result from vacuum circuit breaker switching.

Vacuum circuit breakers have been modelled using a time-variable arc resistance, (Phaniraj et al. 1988, Kosmac et al. 1995 and Thomas et al. 1995) or by an ideal controlled switch (i.e. either an open circuit or a closed circuit) (Greenwood et al. 1988, Phaniraj et al. 1988 and Glinkowski et al. 1997), as shown in Figure 3-1.

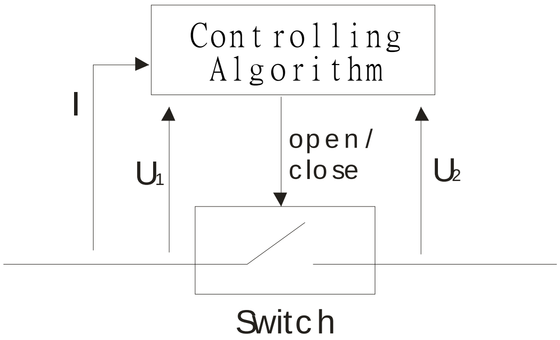

Figure 3-1 Model of Vacuum Circuit Breaker

While the variable resistance approach can, in theory, better represent the arc voltage during the arc-interruption process, the arc voltage in vacuum interrupters is very low, of the order of a few tens of volts, (as compared to the kV rated voltage) and has little effect on the development of the transient recovery voltage. Consequently the stochastic breaker model developed in this research is based on a controlled switch, where the MODELS module was employed to control the statistical variables.

The generic stochastic model incorporates different stochastic properties inherent to the breaker operation to control the actual state of the breaker during the computer simulation by considering different properties of the breakers:

- The random nature of arcing time
- The ability of the breaker to chop the current before its natural zero
- The characteristic recovery dielectric strength between contacts when opening
- The quenching capability of high frequency current at zero crossing

The performances of combinations of the stochastic properties of the breakers with representative networks were analyzed towards determining parameter sensitivity and worse case scenarios.

After the contacts of a breaker mechanically open, the dielectric strength between them increases as a function of time, and a ‘race’ between the transient recovery voltage (TRV) and the dielectric strength develops. When the TRV exceeds the withstand voltage of the gap, a closing signal is sent to the switch, so that a reignition is simulated. Reopening can occur if the rate-of-change of the current at a current zero has a value lower than the critical value of a pre-defined quenching capability. An opening signal is then sent to the switch. If this extinction is followed by a new reignition, the above procedure starts again until the dielectric strength between the contacts can withstand the TRV. This mechanism is shown in Figure 3-2 and the flow chart for the simulation algorithm is shown in Figure 3-3.

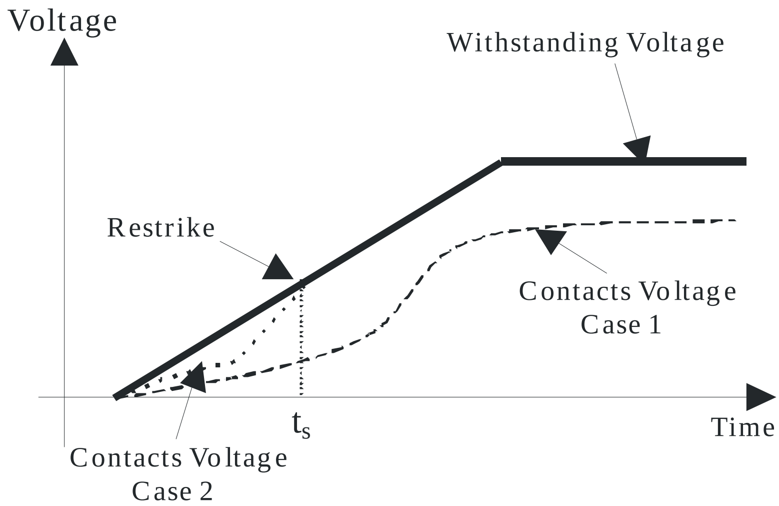

Figure 3-2 Withstand voltage – time characteristic of a VCB

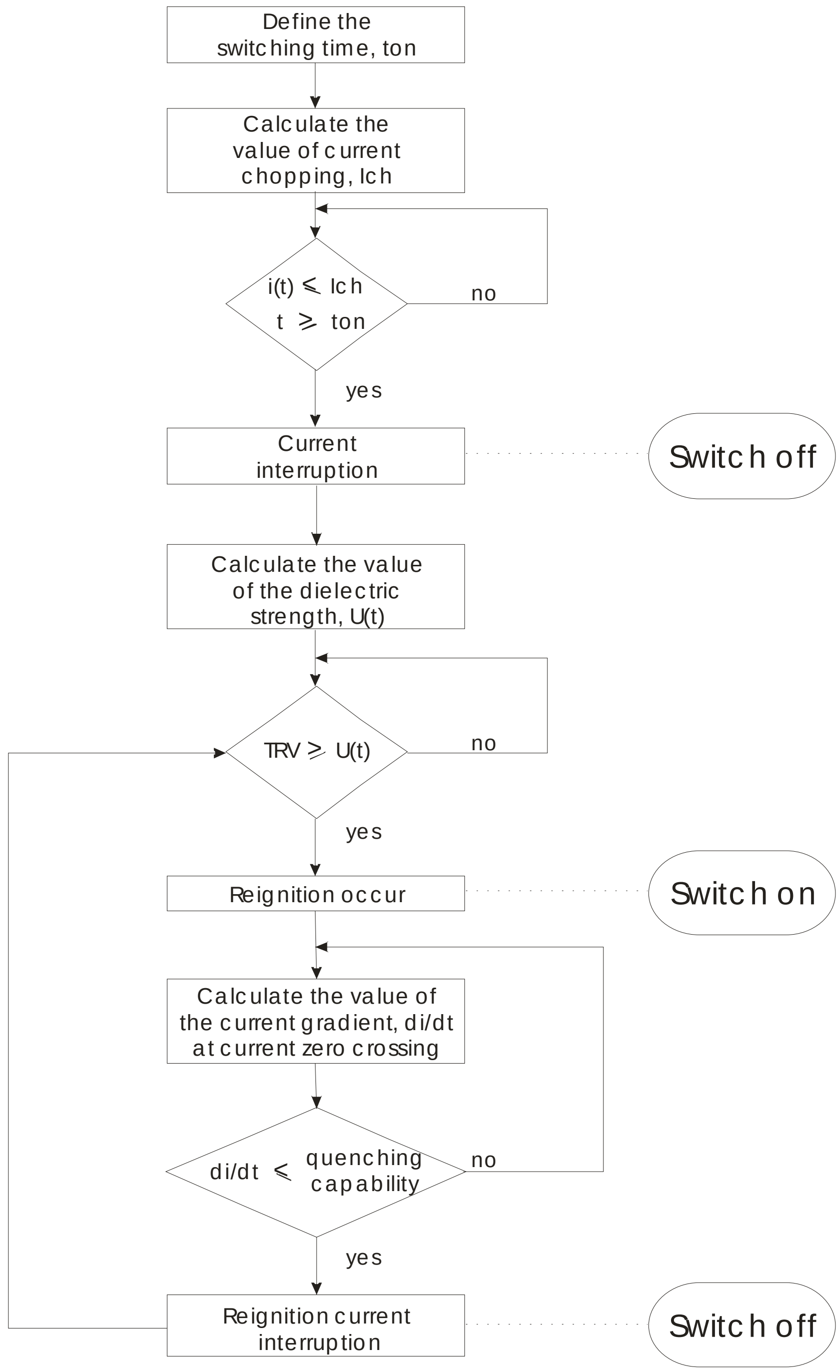

Figure 3-3 Simulation flow chart for the VCB model

3.1.1.1 Arcing time

The arcing time of the breakers is the time between the contact separation and the following current zero. Since it is random in nature the breaker can begin to open with uniform probability at any point in a cycle, a uniform distribution was used in this research to determine the physical opening time of the contact which in turn determines the arcing time.

3.1.1.2 Dielectric strength recovery

There are two breakdown mechanisms: the first one is the breakdown of a cold gap, while the second one refers to a gap which has reignited, such that residual charge carriers exist near the cathode and the breakdown occurs at lower voltages. In this research, only the cold gap breakdown is considered since when the preceding arc current does not exceed several hundred Amperes, the relevant breakdown voltage under the influence of the TRV is equivalent to the cold gap breakdown voltage (Lindmayer et al. 1984). The literature shows that a linear dependency of dielectric strength and contact distance can be assumed during the first millimetre of the contact separation (Glinkowski et al. 1997). A typical relation is as follows:

$$U = A(t - t_{open}) + B \qquad \text{where } t > t_{open} \qquad (3\text{-}1)$$

where U is the value of the dielectric strength, t_{open} is the moment of contact separation, A represents the slope and B represents the intercepts of the equation. The values of the constants A and B in (3-1) for four typical dielectric strength characteristics are shown in Table 3-1.

A (V / µs)	B (V)
2	0
20	0
30	1000
50	0

Table 3-1 Dielectric strength of VCB

The value of U calculated with (3-1) is assumed to be the mean value of a Gaussian distribution with a standard deviation of 15%. (Helmer et al. 1996).

3.1.1.3 Current chopping

The actual chopping current is non-deterministic, however earlier research established different mean chopping levels (Phaniraj et al. 1988 and Kosmac et al, 1995) for different load currents and contact material. In this research, the mean chopping current is estimated according to (Phaniraj et al. 1988):

$$\overline{I_{ch}} = (\omega \cdot \hat{i} \cdot \alpha \cdot \beta)^q \qquad (3\text{-}2)$$

with $\omega = 2 \cdot \pi \cdot 50Hz$

$\hat{i} =$ amplitude of the 50 Hz current

$\alpha = 6.2 \cdot e^{-16} s$

$\beta = 14.3$

$q = (1 - \beta)^{-1}$

The chopping currents derived from this equation correspond to those of modern vacuum circuit breakers, which use Cu/Cr contacts. Hence, the chopping current tends to increase with smaller inductive currents, and this agrees with the observation that the overvoltages tend to be higher when switching small inductive loads. The statistical nature of the chopping current in the simulation is represented by a Gaussian distribution with the mean value calculated from equation (3-2), and truncated at +/- two standard deviations, taken to be 15% of the mean value. The breaker current is assumed to be chopped immediately once the absolute value of the current exceeds the statistically determined value.

3.1.1.4 High frequency quenching capability

A reignition occurs when the TRV exceeds the dielectric strength of the breaker contacts. The actual frequency of the high frequency current associated with arc instability of the breaker is determined by a model comprising inductance and capacitance. This high frequency current will be superimposed on the power frequency current. When the high frequency current gets larger in magnitude than the power frequency current, it can force current zeros at times other than those expected to occur normally with power frequency current. Most vacuum circuit breakers have the ability to quench this high frequency current and therefore the current may be quenched in one of its zero crossings at high frequency.

The rate-of-change of the current at a current zero determines whether or not there is a successful extinction. The high frequency quenching capability of typical vacuum circuit breakers is found to be in the range of several hundred A/μs (Phaniraj et al. 1988). This value can be a constant or a function of the time after contact separation as shown in equation (3-3):

$$\frac{di}{dt} = C(t - t_{open}) + D \qquad \text{where } t > t_{open} \qquad (3\text{-}3)$$

where *di/dt* is the quenching capability, t_{open} is the moment of contact separation, *C* represent the slope and *D* represent the intercept with the ordinate. Pairs of typical values of the constants *C* (which can be positive or negative) and *D* are shown in Table 3-2. It is assumed that when the absolute value of the rate-of-change of the current at a current zero is above this *di/dt* limit, arc extinction will not occur.

C (A / (μs)^2)	D (A / μs)
-0.034	255
0	100
0	600
0.31	155

Table 3-2 Quenching capability of VCB

3.1.2 Evaluation circuit

The circuit, shown in Figure 3-4, represents a typical medium voltage industrial supply network where critical transient situations may occur, and is expected to produce severe overvoltages since the load is not complex (i.e. there are no other cables connected) and there are no power factor correction capacitors connected. Resistor R_b was included to account for the natural damping that occurs in practice. R_a has a negligible value and is there for current measuring purposes for MODELS. R_c is connected across inductor L_s to damp numerical oscillations (a consequence of the trapezoidal rule of integration) which are brought about by the inductive current interruption.

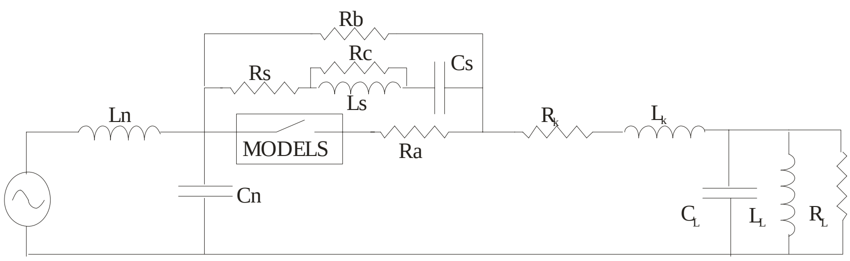

Figure 3-4 Evaluation circuit

	R_S = 50Ω	R_k = 2Ω	R_L = 10kΩ	R_a = 1x10^{-5}Ω
L_n = 5mH	L_S = 50nH	L_k = 40μH	L_L = 120mH	R_b = 9500Ω
C_n = 0.1μF	Cs = 200pF		C_L = 10nF	R_c = 1.33Ω

The results shown in Figures 3-5, 3-6, 3-7 and 3-8 are based on the case with the following parameters: the range of arcing-time was 100 – 200 μs, the rate-of-change of the dielectric strength was chosen to be 50 V/μs while the quenching capability was set to 100 A/μs.

The voltage across the breaker oscillates at a high frequency immediately after current interruption at about 0.7ms. This oscillation is a result of interaction between the longitudinal capacitance of the breaker C_S, the parasitic capacitance to ground at the load side of the breaker C_L and the cable inductance L_k. The oscillation frequency is given by:

$$f_1 \approx \left(2 \cdot \pi \cdot \sqrt{L_k \cdot \frac{C_S \cdot C_L}{C_S + C_L}} \right)^{-1} \approx 1.8\mathrm{MHz}$$

The first TRV peak of the oscillation is called suppression peak (Figure 3-5) and its value is:

$$V = I_{ch} \sqrt{\frac{L_k}{C_{//}}} = 2782\mathrm{V}$$

where $C_{//} = \dfrac{C_S \cdot C_L}{C_S + C_L}$

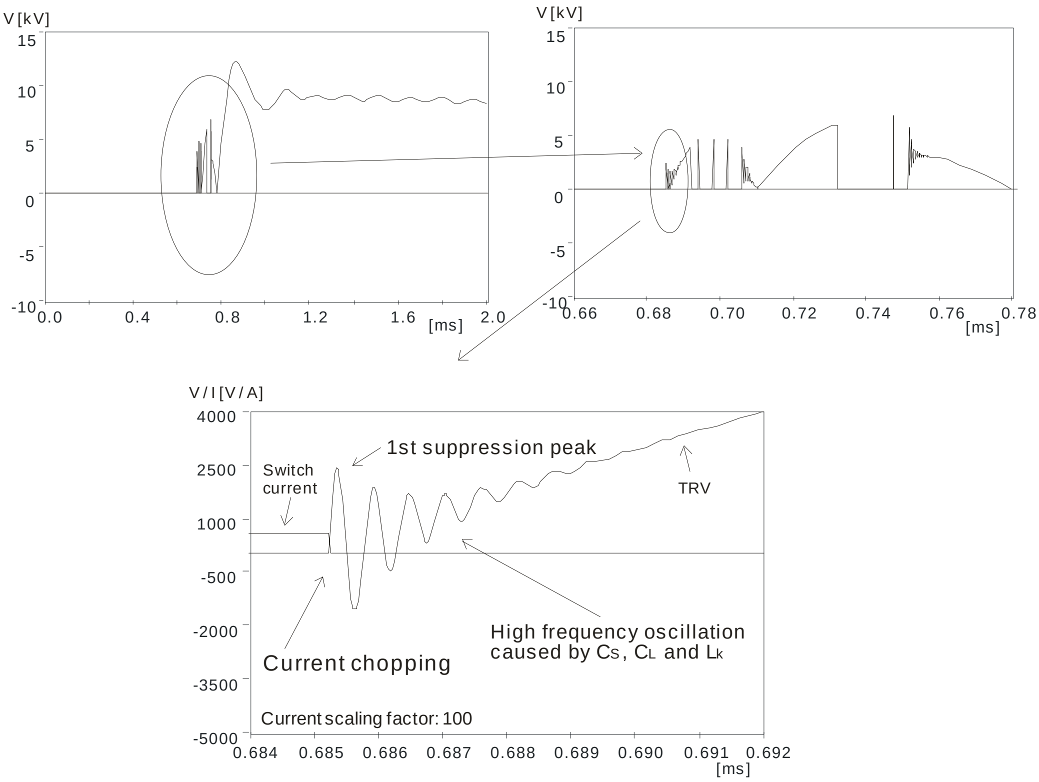

Figure 3-5 Typical TRV waveforms

Following the decay of the initial transient, a much lower frequency dominates. This is caused by the interaction of the load stray capacitance C_L and the inductive load L_L. The frequency is given by:

$$f_2 \approx \frac{1}{2 \cdot \pi \cdot \sqrt{L_L \cdot C_L}} = 4.6\text{kHz}$$

Had there been no reignition, the TRV would have risen to a magnitude given by:

$$V = I_{ch}\sqrt{\frac{L_L}{C_L}} \;=\; 21.3\text{kV}$$

However, if the TRV exceeds the dielectric strength of the breaker, re-ignition will occur as shown in Figure 3-6.

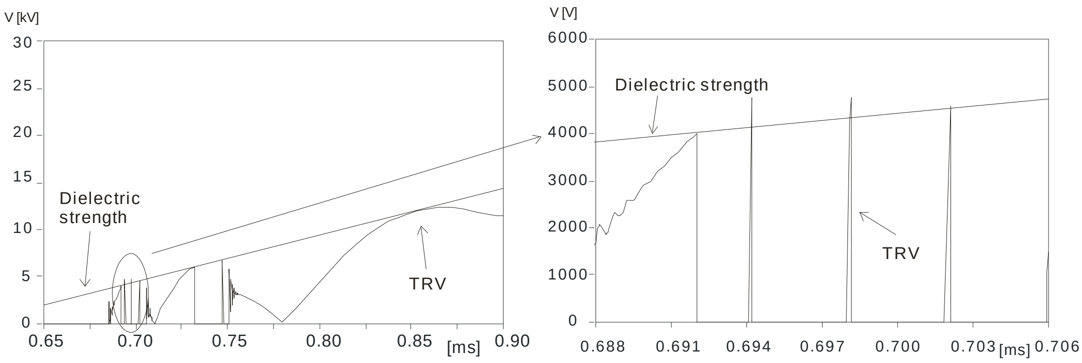

Figure 3-6 Race of TRV and the dielectric strength

The arc re-establishes and current starts to flow through the gap. The current waveshape comprises two frequency components as show in Figure 3-7.

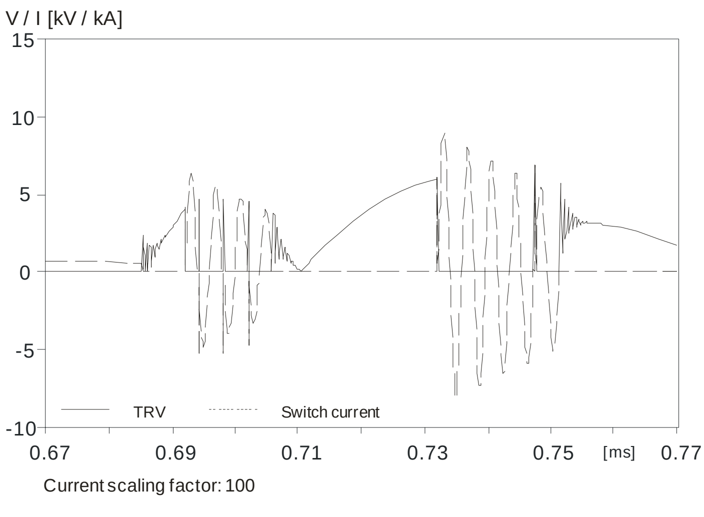

Figure 3-7 Arc re-establishment

The first one is a result of interaction of L_S and C_S and the second one is a result of interaction of L_k and C_L. The first frequency component I_{f3} is:

$$f_3 \approx \frac{1}{2 \cdot \pi \cdot \sqrt{L_S \cdot C_S}} \approx 50\text{MHz}$$

Owing to the high frequency, this component is quickly damped and is not quenched at its zero crossing. The second frequency component I_{f4} becomes dominant and its frequency is given by:

$$f_4 \approx \frac{1}{2 \cdot \pi \cdot \sqrt{L_k \cdot C_L}} \approx 0.25\text{MHz}$$

This second frequency component is interrupted at a zero-crossing and the TRV rises again. As this process repeats, the magnitude of TRV escalates at each re-ignition owing to the increase of stored energy in the inductors from previous re-ignitions.

Also, the dielectric strength is increasing during the whole process since the contacts are separating and once the contacts become sufficiently far apart the dielectric strength prevails over the TRV and no more re-ignitions take place. This is shown in Figure 3-8.

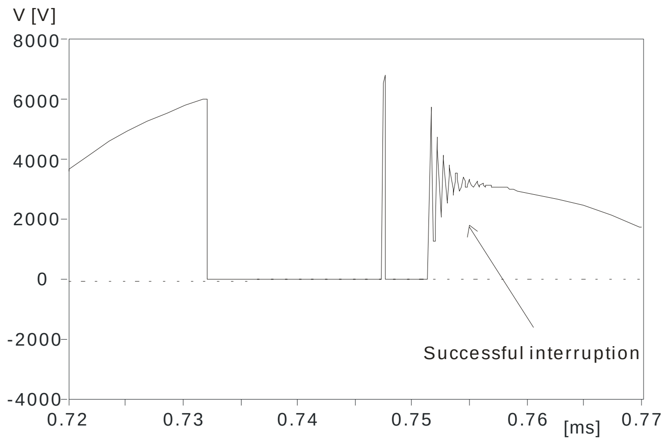

Figure 3-8 Successful interruption

3.2 INDUCTION MOTOR MODELS

Valid modelling of the termination impedance presented by induction motors is an important factor for an accurate overvoltage analysis. The model should provide a valid representation of the termination of the feeding cable over a frequency range from power frequency to high-frequency (MHz). Furthermore the model must present the correct back EMF for a variety of switching situations. As discussed previously, the distribution of the voltage stress across the motor winding is not considered in this study, since the intention is to determine the overall magnitude of the overvoltage and to this end, the correct termination impedances at both operating frequency and high frequencies of the induction motor models are required.

There are several approaches to model induction motors. The most common models comprise passive networks of resistance and capacitance and inductance. For power frequency performance studies motor models can be represented by lumped *R* and *L* parameters and slip (Ueno et al. 1984) as shown in Figure 3-9. In EMTP (Dommel, 1986), the power frequency representation of induction motors can be represented by using the type 19 Universal Machine source model, which is a d-q dynamic model, where the mechanical system of the motor is represented by branches of an electrical network. Consequently, this induction motor model can adequately represent the back EMF and can capture the low-frequency transients at different loads and modes of operation.

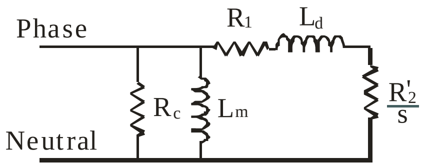

Figure 3-9 Single-phase representation of equivalent circuit model of induction motor

3.2.1 My approach

It was found that most of the induction motor models found in the literature were unable to represent both the power frequency and the high-frequency characteristics of the motor when presented to the incident fast-front surge travelling from the vacuum circuit breakers. In this research several different models of induction motors were evaluated and based on this work, a universal hybrid high-bandwidth (from power frequency to MHz) induction motor model was developed in order to obtain a global representation taking into account the low- and high-frequency components of the impinging surge. The universal high-bandwidth hybrid induction motor model comprises two components: one the d-q dynamic model represents the behaviour at operating frequency and the other, a passive network represents the high-frequency transient behaviour: its topology is discussed below.

3.2.1.1 D-Q dynamic model

A representation of the ATP/EMTP power-frequency/dynamic model of an induction motor is shown in Figure 3-10. This model presents the appropriate back EMF and can capture the low-frequency transients at different modes of operation of the induction motor. The mechanical system of the motor is represented by branches of an electrical network as shown in the figure.

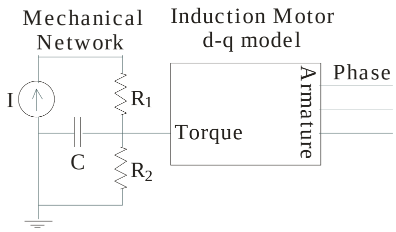

Figure 3-10 Three-phase representation of d-q dynamic model of induction motor

The torque and the speed characteristics of a simulated induction motor subject to disconnection and reconnection are shown in Figure 3-11. At 1 second the motor is disconnected and the electromagnetic torque and the speed drop to zero. The motor is reconnected at 15 seconds and the torque and speed recover as shown in Figure 3-11. Figure 3-12 shows the TRV, and the beat frequency owing the changing frequency of the back EMF during disconnection is evident.

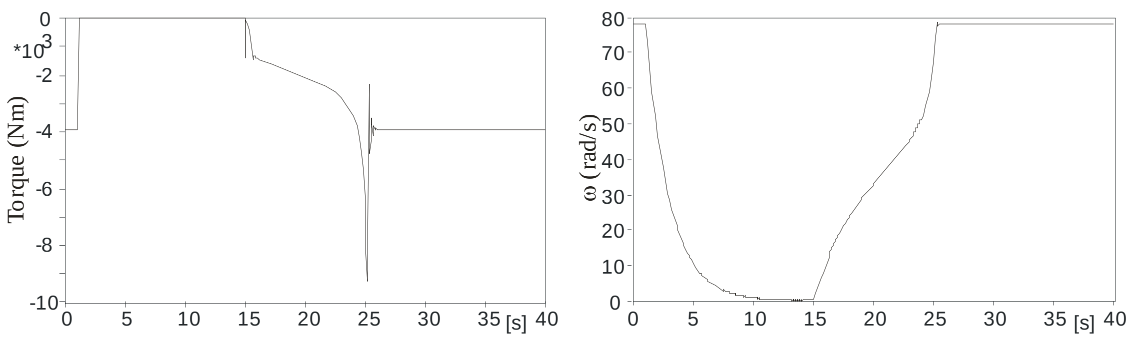

Figure 3-11 Torque and speed of an induction motor

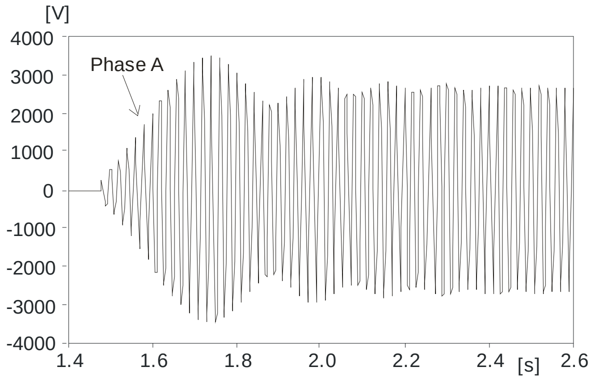

Figure 3-12 TRV during switch off a running induction motor

3.2.1.2 High frequency model

For high frequency studies a lumped resistor can be used to represent the equivalent surge impedance of the motor and lumped capacitors can be used to represent the parasitic capacitances (Dick et al. 1988 and Reckleff et al. 1988). The required parameters, however, are not readily available for specific motors, and system identification methods have been used to obtain parameter estimations. These methods can be broken into two classes: offline and online. Offline techniques include model parameter extraction from standstill frequency response (SSFR) data obtained when the motor is at rest and disconnected from the main power supply (Wills et al. 1989). Online techniques make use of cross correlation between the output and input, which is a pseudorandom binary sequence (PRBS) signal (Benn et al. 2003). Frequency dependent models of induction motors using network synthesis method is another approach for modelling (Grandi et al. 1997, Boglietti et al. 1999 and Moreira et al. 2002). The frequency response of the phase-to-neutral impedance and phase-to-ground impedance are evaluated experimentally to characterize the motor in the high-frequency range.

The topology of a generic model used in this research was developed based on measurements made on a small machine. The relevant parameters corresponding to a larger machine were obtained through extrapolation since it was not possible to perform the measurements on a large machine. However the techniques used in this research can be applied to large machines in order to obtain the parameters of a particular machine.

The phase to neutral impedance and the phase to ground impedance were obtained using the connections shown in Figure 3-13.

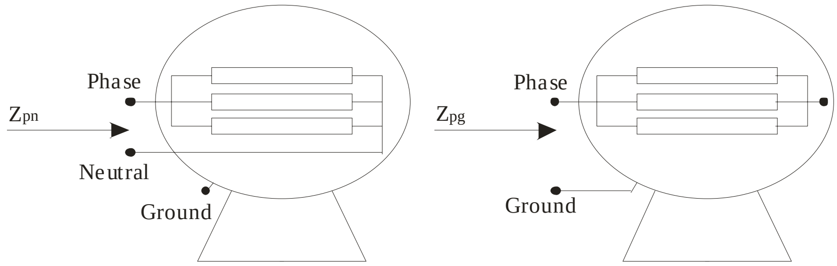

Figure 3-13 Connections and impedances for the frequency analysis

The frequency response seen at the phase-to-neutral and phase-to-ground terminals was measured in the 100Hz to 5MHz range using an impedance analyzer HP4192A. The frequency responses of several different passive networks, shown in Figure 3-14, were compared with the measured frequency response of the induction motor. In these networks R_e accounts for the losses introduced by eddy currents inside the magnetic core, C_g represents the winding-to-ground capacitance, R_g is added to represent the dissipative effects that are present in the motor frame resistance and R_t, L_t, and C_t capture the second resonance in the frequency response, which is related to the winding turn-to-turn capacitance.

From the frequency response obtained experimentally, the parameters of the high frequency model can be calculated using the expressions (3-4) – (3-10) (Moreira et al. 2002), in which f_{low} and f_{high} are the lowest (100Hz) and the highest (5MHz) test frequencies in the impedance measurements, respectively.

$$C_g \approx \frac{1}{6(2\pi f_{low})Mag\{Z_{pg}\}_{f_{low}}} \qquad (3\text{-}4)$$

$$R_g \approx 3 \times Real\{Z_{pg}\}_{f_{high}} \qquad (3\text{-}5)$$

$$C_t \approx \frac{C_g}{10} \qquad (3\text{-}6)$$

$$R_t \approx 3 \times Real\{Z_{pn}\}_{f_{zero-Z_{pn}}} \qquad (3\text{-}7)$$

$$L_t \approx \frac{1}{C_t}\left(\frac{1}{2\pi f_{zero-Z_{pn}}}\right)^2 \qquad (3\text{-}8)$$

$$R_e \approx 3 \times Mag\{Z_{pn}\}_{f_{pole-Z_{pn}}} \qquad (3\text{-}9)$$

$$L_d \approx \frac{2}{C_g}\left(\frac{1}{2\pi f_{pole-Z_{pn}}}\right)^2 \qquad (3\text{-}10)$$

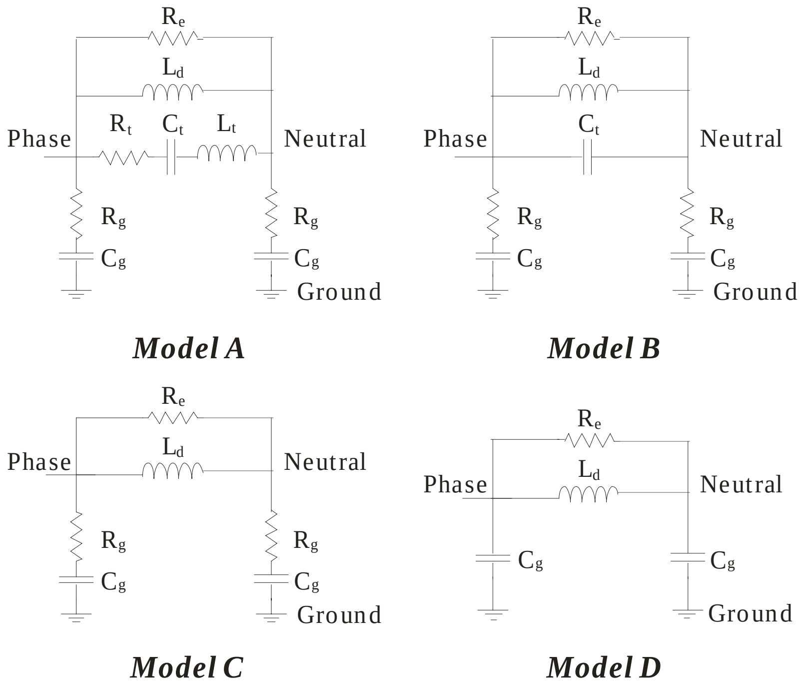

Figure 3-14 Different high frequency induction motor models

Figure 3-15 shows that the frequency response of Model D was the closest to that of the experimental result.

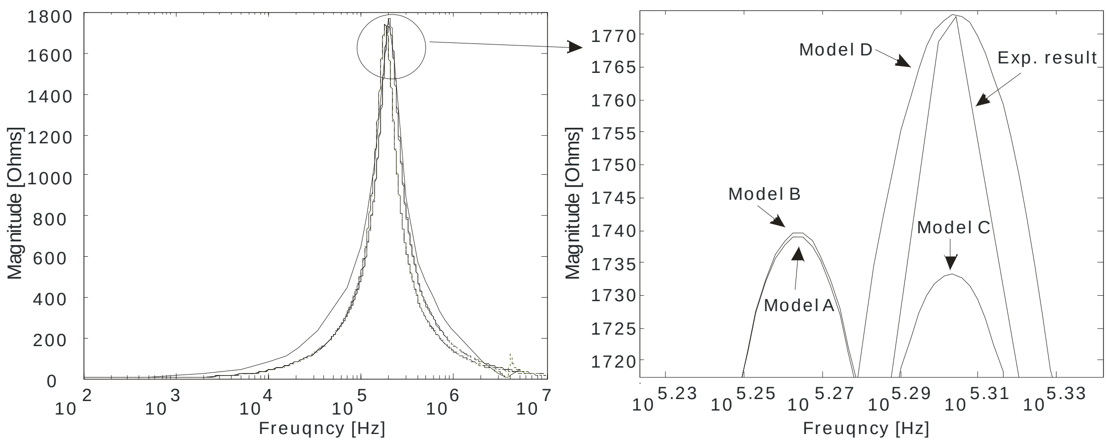

Figure 3-15 Comparison of the phase-to-neutral frequency responses

All the models were incorporated into a simple circuit to investigate the effect on the resulting overvoltages. It was found that there is little significant difference in the results obtained with the different models. Consequently model D, which is simple while the response compares well with the experimental results, was used for the overvoltage studies.

Figure 3-16 demonstrates a trend of the grounding capacitance magnitude as a function of the motor rated power P_r as found in Boglietti et al. (1999). The mean square straight line, also shown in Figure 3-16, has the following equation:

$$C_g = 0.0086 + 0.529\ln(P_r) \qquad (3\text{-}11)$$

where C_g is in nF and P_r is in kW

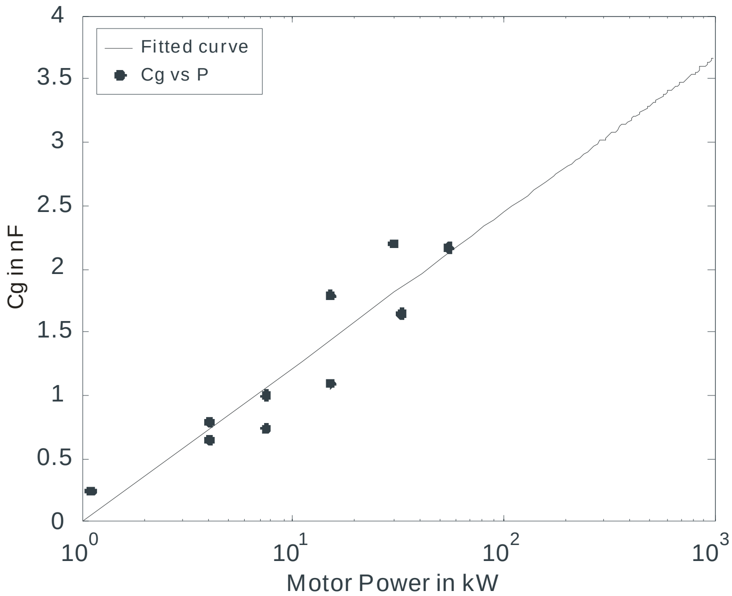

Figure 3-16 Capacitance C_g as a function of the motor rated power

A sensitivity study was performed on the demonstration circuit shown in Figure 3-19 using both sets of values, from the literature and from the mean square straight line. No significant differences were found in the overvoltage results. Consequently, for other motors with different power ratings, the corresponding values of *Cg* were chosen from (3-11).

Additionally, Figure 3-17 shows the damping factor as a function as of the motor rated power. The transfer function of Model D is:

$$\frac{LCs^2 + \frac{L}{R}s + 1}{2sC(\frac{LC}{2}s^2 + \frac{L}{R}s + 1)}$$

and the characteristic equation is

$$\frac{LC}{2}s^2+\frac{L}{R}s+1=0 \quad \Rightarrow s^2+\frac{2}{RC}s+\frac{2}{LC}=0$$

$$Hence\begin{cases}2\zeta\omega_n=\dfrac{2}{RC}\\ \omega_n=\dfrac{2}{LC}\end{cases}$$

The damping ratio ζ therefore is equal to $\frac{1}{\sqrt{2}R}\sqrt{\frac{L}{C}}$. No obvious correlation seems to exist, and the damping ratio was assumed to be 0.5 for other motors with different power rating. As with *Cg*, variations in ζ were found to have little effect on the results.

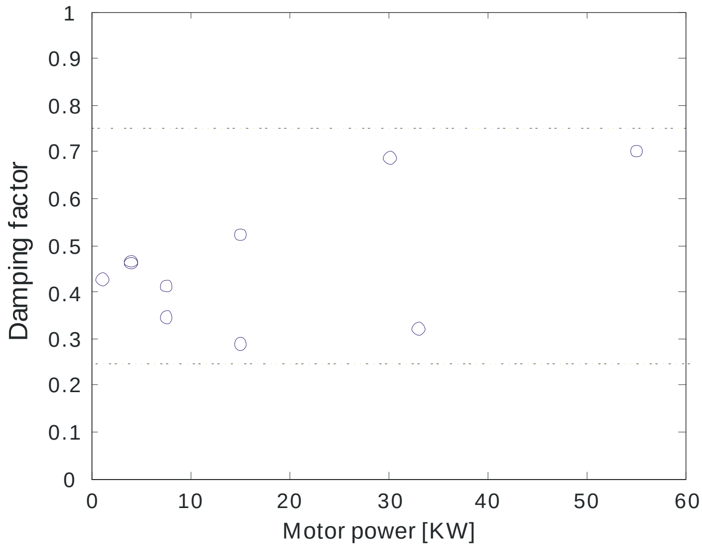

Figure 3-17 Damping factor as a function of rated power

3.2.1.3 Universal high-bandwidth hybrid model

A hybrid model was formed by interconnecting the high frequency model with the D-Q dynamic model, as shown in Figure 3-18, in order to obtain a global solution taking into account the high and low frequency phenomena.

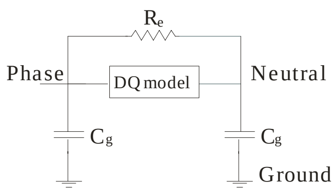

Figure 3-18 Universal high-bandwidth hybrid model

3.2.2 Evaluation circuit

The transient overvoltage behaviour of the above induction motor models (including equivalent circuit model, high-frequency models, power-frequency / dynamic models, and combinations between them) were compared and incorporated into an evaluation circuit shown in Figure 3-19.

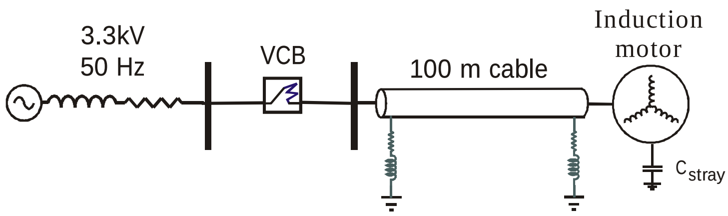

Figure 3-19 Evaluation circuit to verify the transient overvoltage behaviours

It is clear that the characteristics of the overvoltages obtained at the terminals of the induction motor are dependent on the induction motor model. In Figure 3-20, which corresponds to the equivalent circuit model shown in Figure 3-9, the back EMF of the motor is not represented, consequently the breaker TRV and the voltage transients at the motor terminals are not fully represented.

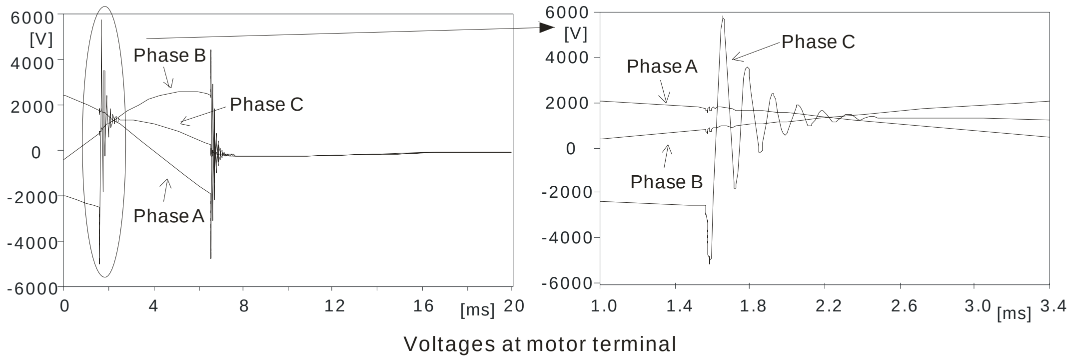

Figure 3-20 Transient voltage response from model shown in Figure 3-9

Figure 3-21 shows results obtained using the D-Q dynamic model shown in Figure 3-10, which represents the running mode of the motor. The high frequency oscillations corresponding to the interaction between the capacitance of the cable and inductance of the motor are evident, however the interaction with other circuit elements, such as those associated with the turn-to-turn capacitance, are missing. Similar results, corresponding to the starting mode of the motor are shown in Figure 3-22.

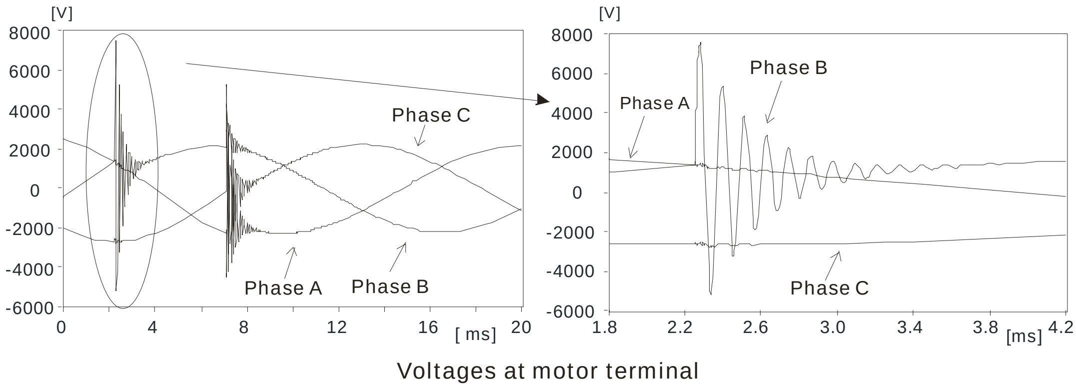

Figure 3-21 Transient voltage response from model shown in Figure 3-10 (running motor)

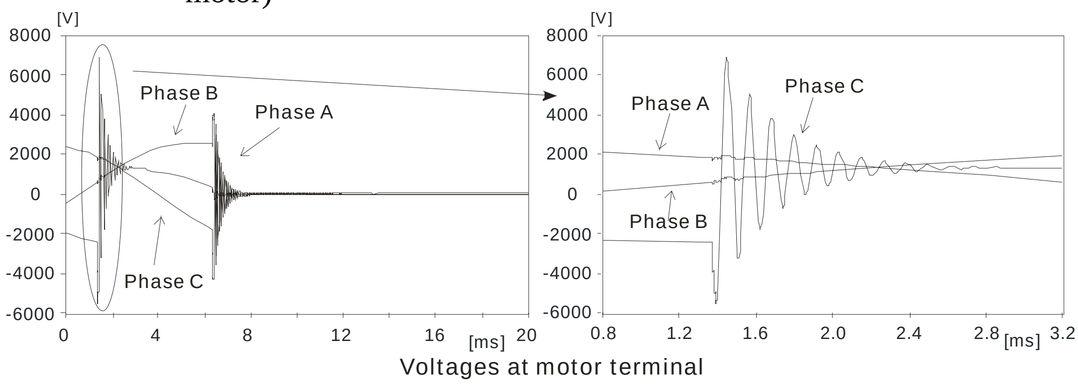

Figure 3-22 Transient voltage response from model shown in Figure 3-10 (starting motor)

In Figure 3-23, which corresponds to the Model D shown in Figure 3-14, the high frequency response is similar to that reported by other authors (Boglietti et al. 1999 and Moreira et al. 2002), however the power frequency response is not represented.

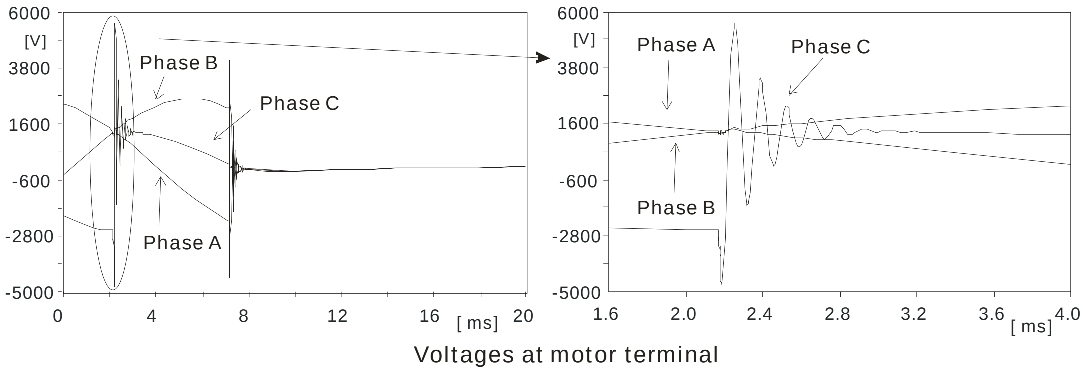

Figure 3-23 Transient voltage response from model shown in Figure 3-14

In Figures 3-24 and 3-25, which correspond to a model comprising a combination of the models shown in Figures 3-18, both the high frequency and the power frequency responses are represented for both the running mode and starting mode of the induction motor.

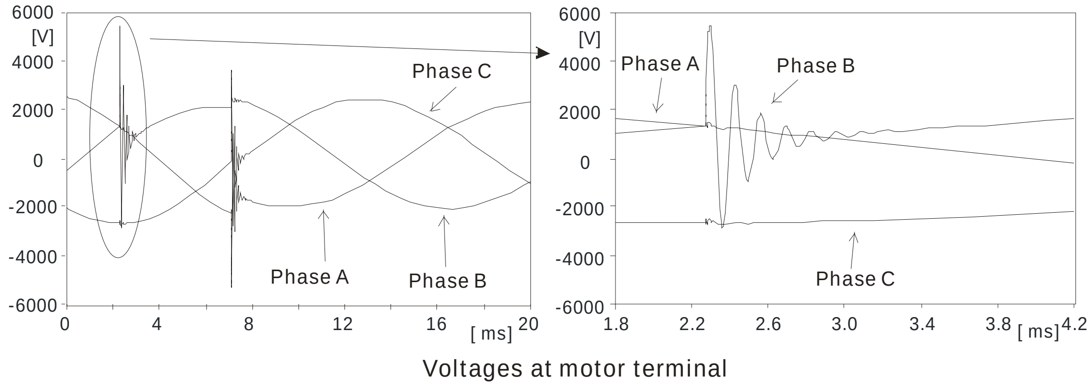

Figure 3-24 Transient voltage response from model shown in Figure 3-18 (running motor)

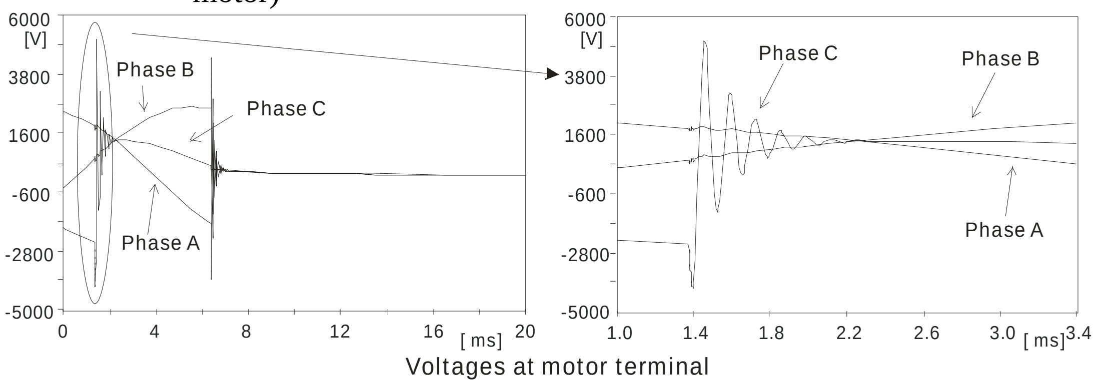

Figure 3-25 Transient voltage response from model shown in Figure 3-18 (starting motor)

From the above results it can be concluded that the universal induction motor developed in this research can represent both the low- and high-frequency phenomena with standard simulation software for a broadband overvoltage study.

3.3 TRANSFORMER MODELS

A complex model of a transformer would require representing every turn and all mutual couplings, inductive and capacitive, with every other turn. Such a model is unnecessary unless detailed information about turn-to-turn stress is required, otherwise something much more tractable will suffice. The model chosen will depend on the purpose it is to serve. The simplest model can be a transformer being switched at no load. A model for studying the transfer of surges from winding to winding is more complicated, requiring representation of both magnetic as well as capacitive coupling, and depends on the nature of the surge being transferred. The most complex models are those required for the study of the internal voltage distributions and oscillations within the transformer when the equipment is subjected to different stimuli.

Many papers deal with the frequency dependence or the high-frequency characteristics of a transformer model (Avila-Rosales et al. 1982, Vaessen 1988, Wilcox et al. 1991 and 1992, deLeon et al. 1992, Morched et al. 1993 and Chimklai et al. 1995) and several research projects have been oriented to the design and the identification of the parameters of the high frequency transformer black box models (Soysal 1993, CIGRE 1994, Keradec 1994 and Miri 1997). To represent the frequency response of transformers, simple linear equivalent circuit (Avila-Rosales et al. 1982 and Morched et al. 1993), transfer functions (Soysal 1993 and Keradec 1994), and state equations (deLeon et al. 1992) have been used. Modal theory is another approach for modelling the transformer model (Wilcox et al. 1991 and 1992). This method is rather complex and may not be convenient for power systems surge analysis, because of the focus on internal winding representation.

There is a high frequency transformer model in the ERPI version of the EMTP which leads to a nodal admittance matrix which is complex symmetrical and frequency dependent (Morched et al. 1993). However, this model does not exist in ATP/EMTP but some papers show that accurate models can be achieved using a basic model combined with frequency dependent series branches and a network of capacitances (Chimklai et al. 1995 and Ueda et al. 1997).

3.3.1 My approach

The essential element is how the transformers behave under fast transient surge. When we consider the overvoltages under the switching operations of vacuum circuit breaker, it is necessary to represent the transformer including the ferromagnetic nonlinearities as well as the correct termination impedance of the cable.

The transformer was modelled by EMTP's saturable transformer model with capacitance elements to represent capacitive coupling and stray capacitance. The transformer in the evaluation circuit is a 5MVA, delta/wye, 11kV/3.3kV with leakage impedance of 8%. The circuit diagram and the calculation for all the parameters are given below:

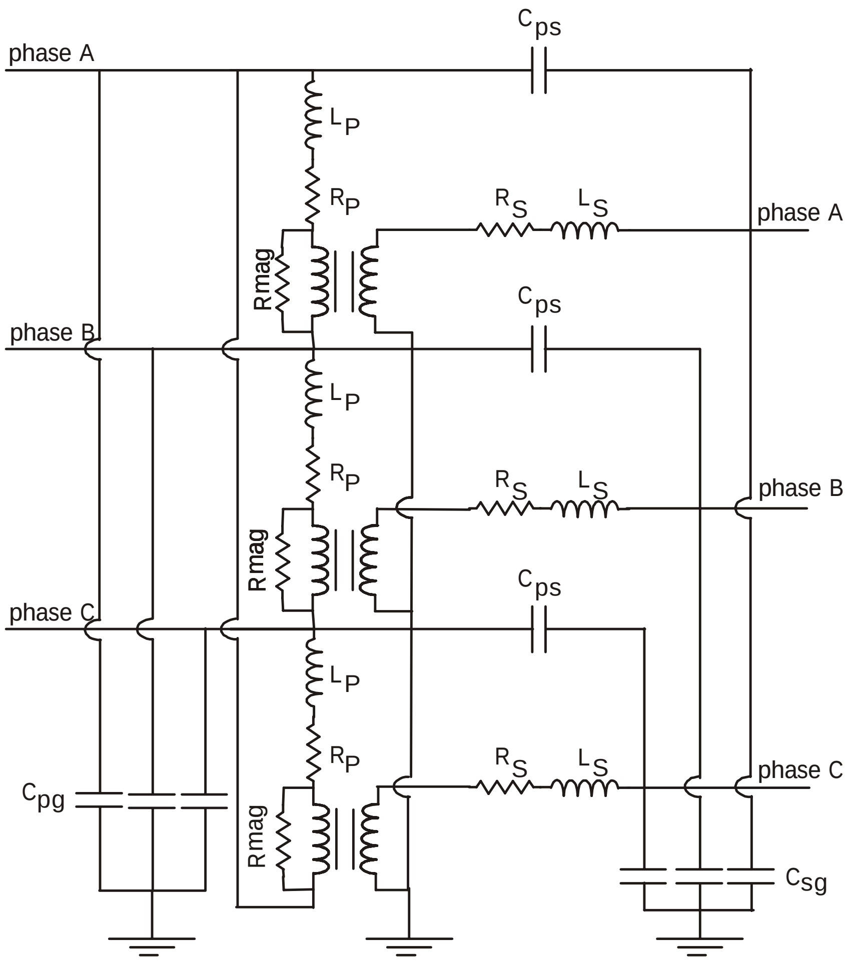

Figure 3-26 Delta / wye saturable transformer

(a) Rated voltage

Since it is an 11 kV/3.3 kV delta star transformer, the rated voltage at primary is 11 kV while that at the secondary is given by: $V_{secondary} = \frac{3.3kV}{\sqrt{3}} = 1.905kV$ because of the star connection.

(b) R_{mag}

The resistance representing the core loss of the transformer is very high, $50\text{k}\Omega$, since the core losses resulting from an impulse are small and offer little damping to very fast front surges.

(c) Leakage impedance

Assuming equal per unit leakage impedance for the primary and secondary windings, the values are obtained as follows:

$$S = 5MVA$$

$$Z_{Bpri} = \frac{kV^2}{MVA} = \frac{11^2}{5} = 24.2\Omega$$

$$Z_{pri} = Z_{pu} \times Z_{Bpri} = \frac{8\%}{2} \times 24.2 = 0.968\Omega$$

with the typical ratio of reactance X to resistance R, $\frac{X}{R} = 10$

and $Z^2 = R^2 + X^2$, *we have*

$$R_{pri} = 3 \times 0.09632 = 0.289\Omega$$

$$L_{pri} = 3 \times 3.066 \times 10^{-3} = 9.198mH$$

for delta connection

while $Z_{B\sec} = \frac{kV^2}{MVA} = \frac{3.3^2}{5} = 2.178\Omega$

$$Z_{\sec} = Z_{pu} \times Z_{B\sec} = \frac{8\%}{2} \times 2.178 = 0.08712\Omega$$

$$R_{\sec} = 8.67 \times 10^{-3}\Omega$$

$$L_{\sec} = 0.2759mH$$

for wye connection

(d) Current/flux pair and current/voltage pair

The current/flux pairs in the model were obtained by running an EMTP subroutine SATURA (Meyer et al. 1987 - 1995), which converts current/voltage to current/flux pairs. The first knee point is assumed to be the magnetizing current with voltage at 1 p.u..

The parameters of the saturable transformer model are summarized in Table 3-3.

Rated voltage at primary side	11kV
Rated voltage at secondary side	1.905kV
Leakage impedance	8%
Resistance across magnetizing branch: R_{mag}	50kΩ
Primary leakage resistance: R_p	0.289Ω
Primary leakage inductance: L_p	9.198mH
Secondary leakage resistance: R_s	$8.67 \times 10^{-3}\Omega$
Secondary leakage inductance: L_s	0.2759mH
First knee point: I / ϕ pair	1.07A / 49.52 Vs
Capacitance between primary winding and ground	7nF / phase
Capacitance between secondary winding and ground	7nF / phase
Capacitance between primary and secondary winding	4nF / phase

Table 3-3 Parameters for transformer model

3.3.2 Evaluation circuit

The transformer model was incorporated into the circuit shown below. The VCB was switched off and the voltage at the transformer terminal was measured and the results are shown in Figure 3-28.

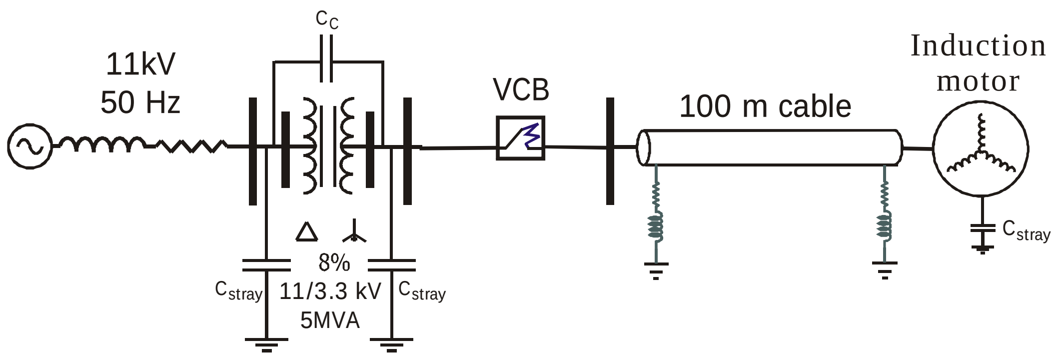

Figure 3-27 Evaluation circuit to verify the transient overvoltage behaviours

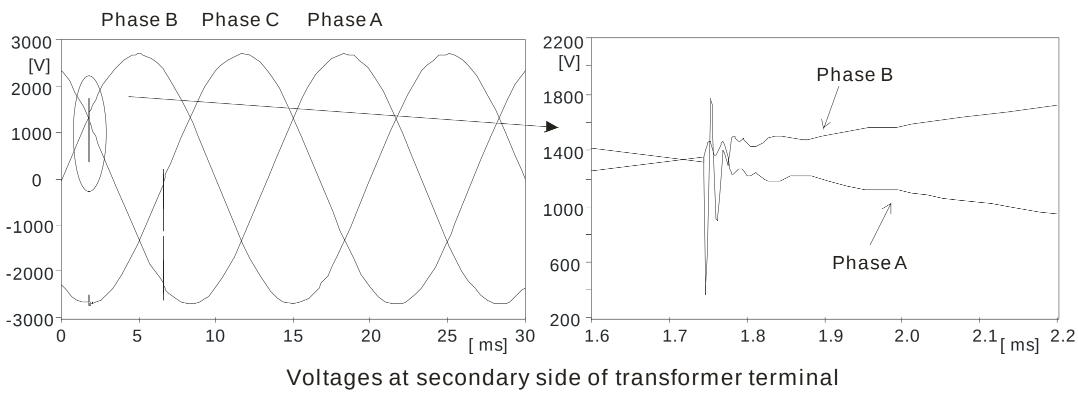

Figure 3-28 Transient voltage response with transformer model

From the above results it can be concluded that the high bandwidth transformer developed in this research can represent both the low- and high-frequency phenomena with standard simulation software for a broadband overvoltage study.

3.4 CABLE MODELS

For the simulation of fast transients, adequate estimation of power cable parameters is needed in order to obtain an accurate computation of the overvoltages. Distributed-parameter representation provides more accurate results in the study of high frequency transients than the lumped-parameter models (Krause et al. 1972). However, lumped-parameter representation of the transmission line can be successfully used to analyze the overvoltage phenomena if an adequate number of segments is used in the calculation (Moreira et al. 2001). With regard to the properties of the line, early papers have proposed the use the lossless characteristics (Jouanne et al. 1996), which lead to a considerable amount of inaccuracy owing to underdamping. The use of a distortionless line representation was proposed in (Skibinski et al. 1998). Preliminary investigations indicate that it is still not sufficiently accurate to investigate the overvoltage problem, especially for very long cable drives. Distortion has been demonstrated to be important for an accurate analysis of overvoltages (Moreira et al. 2001).

EMTP (Dommel 1986) provides several kinds of line modelling for both distributed-parameter and lumped-parameter representation. They can be categorized into two classes, the constant-parameter line model and the frequency dependent line models such as JMARTI line model and the SEMLYEN line model, which take into account the influence of frequency on the line.

3.4.1 My approach

EMTP provides several alternatives for line modelling. In this research, the JMARTI frequency dependent line/cable model was used. The parameters of the cables were obtained by employing the subroutine CABLE CONSTANTS in EMTP using the dimensions, geometrical and physical data of the cables.

The JMARTI models are fitted in a frequency range specified with the number of decades from the lowest frequency point and the number of sample points per decade. The model also requires a frequency where the transformation matrix is calculated and a steady state frequency to calculate steady state parameters.

3.4.2 Evaluation circuit

The cable model was incorporated into the circuit shown below. The cable is energized from a voltage source, and a comparison of the voltage waveforms at the cable ends between cable model with and without frequency dependence was made. As shown in Figure 3-30, the damping in the model without frequency dependence is significantly less than the model with frequency dependence.

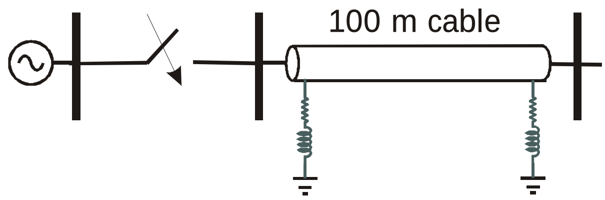

Figure 3-29 Evaluation circuit to verify the transient overvoltage behaviours

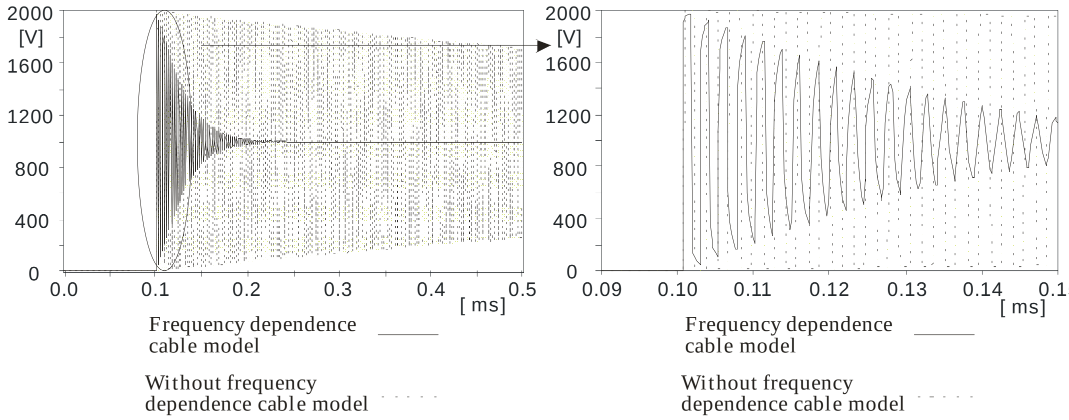

Figure 3-30 Transient voltages response at cable receiving terminals with different type of cable model

Clearly, the JMARTI model is more representative of high frequency damping and it uses is mandatory in this project.

CHAPTER 4 PARAMETRIC SENSITIVITY STUDIES

Switching overvoltages are stochastic in nature and the conditions which may result in serious overvoltages are numerous. Rather than studying a large number of typical installations, the parametric sensitivity studies performed are aimed at identifying the essential parameters that could lead to potential damage of the system equipments.

The concept of parametric sensitivity studies is to hold all parameters constant except one, and evaluate the results corresponding to a credible range of the subject parameter. In this research, the parameters and switching operations were studied.

4.1 STUDIES ON VCB PARAMETERS

As discussed in Chapter 3, the breaker model chooses random values for the most significant parameters from a range of typical values found in the literature, corresponding to typical breaker designs. These parameters include: arcing time, chopped current magnitude, dielectric strength recovery and quenching capability.

Combining the current chopping, dielectric strength and the quenching capability characteristics of the breaker leads to sixteen different breaker models. Incorporation of three ranges of the arcing time (200 - 300μs, 100 - 200μs , 0 - 100μs) results in a total of forty-eight models which were developed and analyzed using the representative circuit shown in Figure 4-1. Appendix A shows the parameters of the cases with the above combinations. The Monte Carlo study was based on a sample of 100 switchings for each case and for each switching the stochastic variables were randomly chosen as previously described.

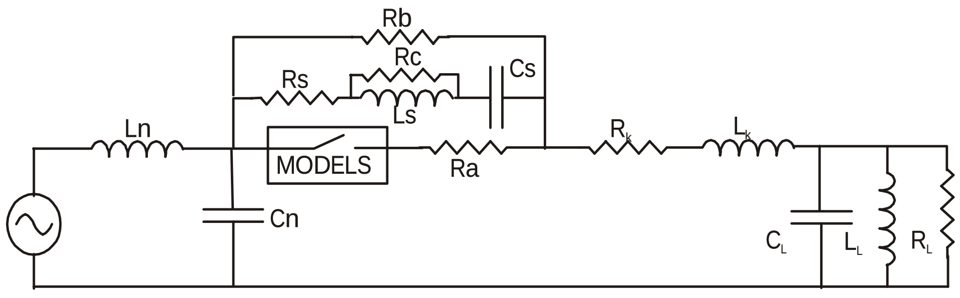

Figure 4-1 Evaluation circuit

4.1.1 Different termination types

When a vacuum circuit breaker reignites during an open operation, voltage escalation occurs and the interruption process can terminate in one of three ways:

- The breaker can successfully interrupt at the end of the high frequency reignition sequence. The gap successfully recovers after a series of restrikes. This is referred to termination mode A.
- The breaker fails to interrupt the high frequency current, the power frequency current takes over and the final interruption is accomplished at the next power frequency current zero. This is designated a termination mode B.
- The breaker fails to interrupt and may cause harm to itself and/or connected equipment.

4.1.2 Variation of dielectric strength

When the rate-of-change of the dielectric strength is decreased to 30 V/μs while keeping all the other parameter as the same as the previous case, the termination mode changes from type A to type B. As shown in Figure 4-2, the current cannot be interrupted at high frequency and the conduction period of the high frequency component was lengthened to around 3 ms, also the number of reignitions increased.

As the reignitions repeat, eventually a point must be reached when the power frequency current is greater than the high frequency current. Then, the conduction period is diminished: the power frequency conduction resumes, and there can be no recovery until the next power-frequency based current zero.

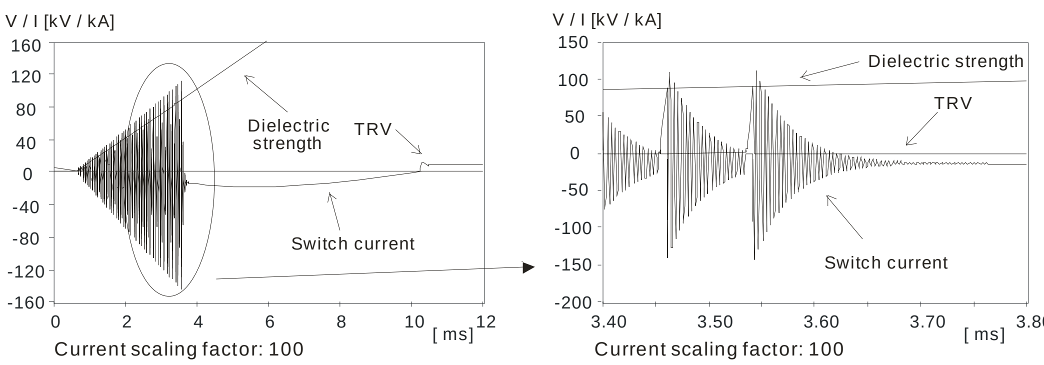

Figure 4-2 Unsuccessful interruption of high frequency current

When the rate-of-change of the dielectric strength is gradually decreased from 50 V/μs to 2 V/μs, with all other characteristics and parameters remaining constant, the escalation voltage will increase until the termination mode changes from mode A to mode B as illustrated in Figure 4-3.

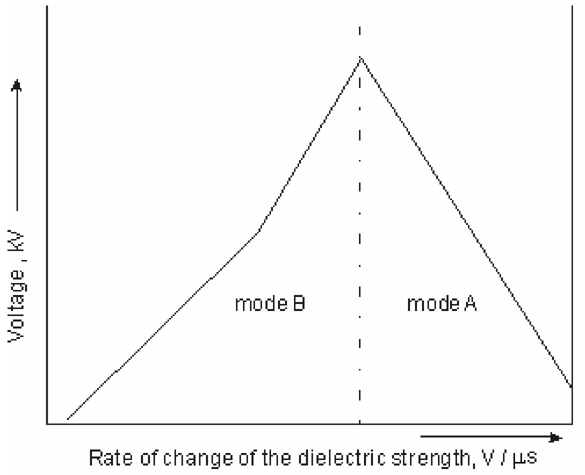

Figure 4-3 Recovery voltage vs rate-of-change of the dielectric strength

In termination mode A, it was found that the conduction period of high frequency current I_{f4} is longer when the rate-of-change of the dielectric strength decreases from 50 V/μs to 20 V/μs as shown in Figure 4-4. Consequently, the voltage escalates and more reignitions occur.

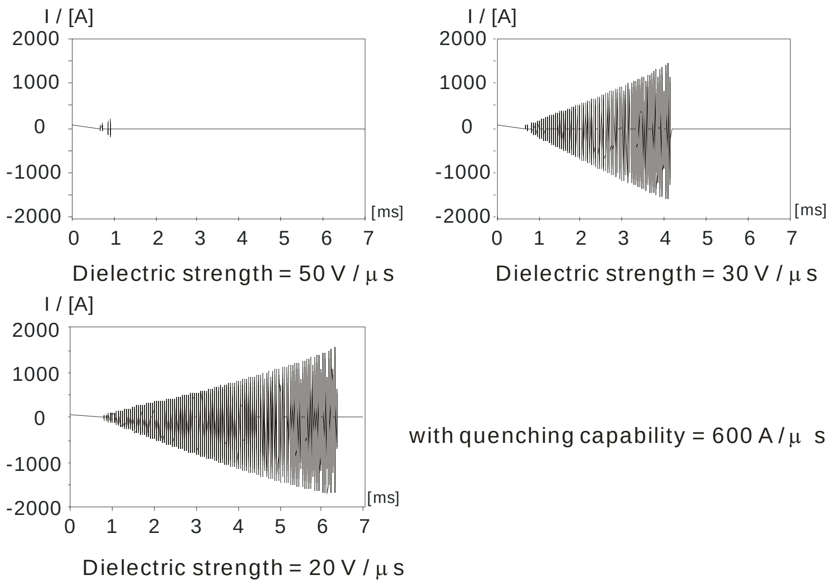

Figure 4-4 Current through the breaker with varying the rate-of-change of dielectric strength but keeping the quenching capability constant

On the other hand, when considering termination mode B, it was established that the higher the rate-of-change of the dielectric strength, the higher of the magnitude of the high frequency current I_{f4} and the longer its conduction period, as illustrated in Figure 4-5.

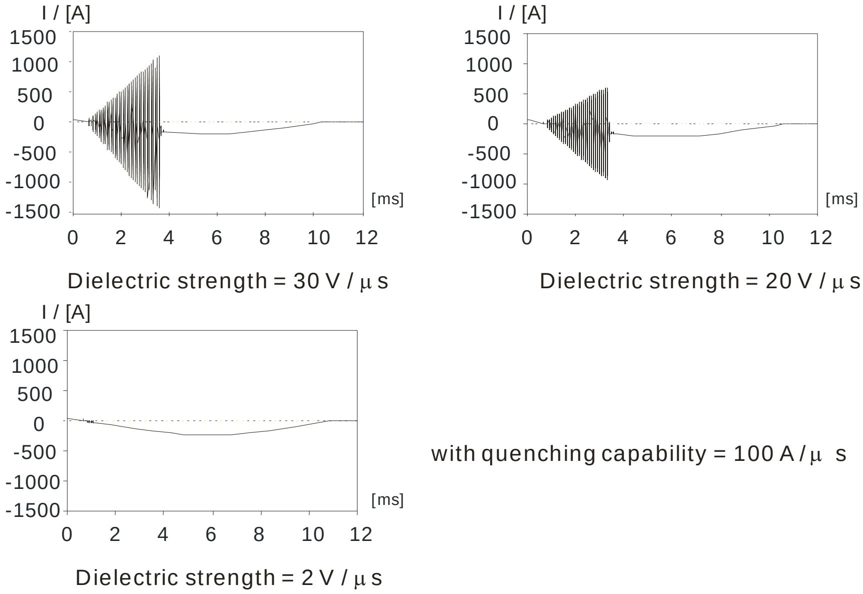

Figure 4-5 Current through the breaker with varying the rate-of-change of dielectric strength but keeping the quenching capability constant

Consequently, the escalation voltage is most severe when the rate-of-change of the dielectric strength is in the middle range between 50 V/μs and 20 V/μs.

4.1.3 Variation of quenching capability

The variation of the quenching capability also affects the interruption of the high frequency current. As shown in Figure 4-6, the higher the quenching capability, the higher the TRV and more reignitions occur. On the other hand, when the quenching capability is too small, the current may not be chopped during the high frequency period and this will result in failure of interruption. Additionally when the quenching capability decreases to zero, the breaker will fail to interrupt.

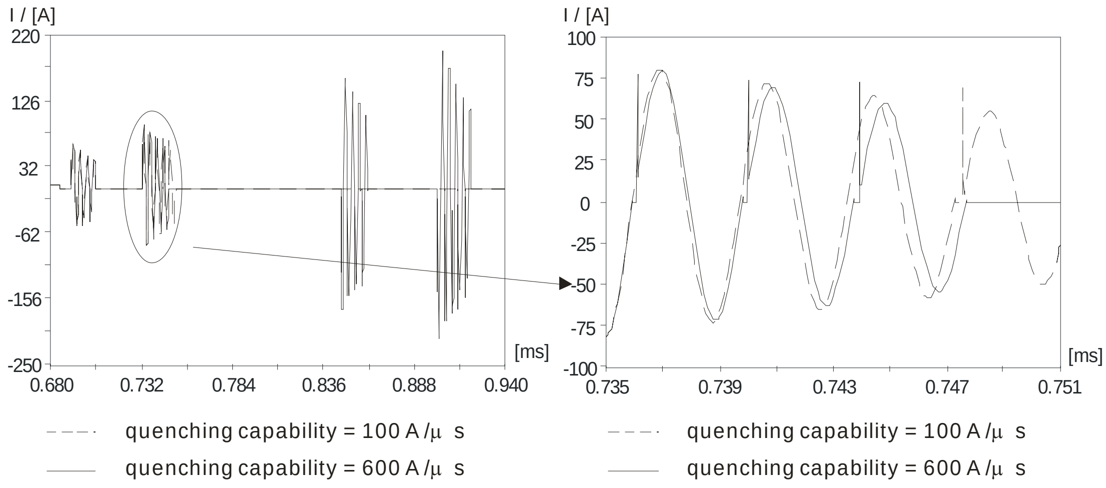

Figure 4-6 The current pattern with variation of the quenching capability

When comparing the influence of the quenching capability with the rate-of-change of the dielectric strength on the escalation voltage, as shown in Figures 4-4, 4-5 and 4-6, it was found that the effect of the quenching capability is not as significant as the rate-of-change of the dielectric strength. The quenching capability affects the termination mode of breakers with the same rate-of-change of the dielectric strength. When the quenching capability is large, the termination mode is likely to be mode A. Consequently, as demonstrated in Figure 4-7, the peak of the characteristic shown in Figure 4-3 shifts when the quenching capability varies.

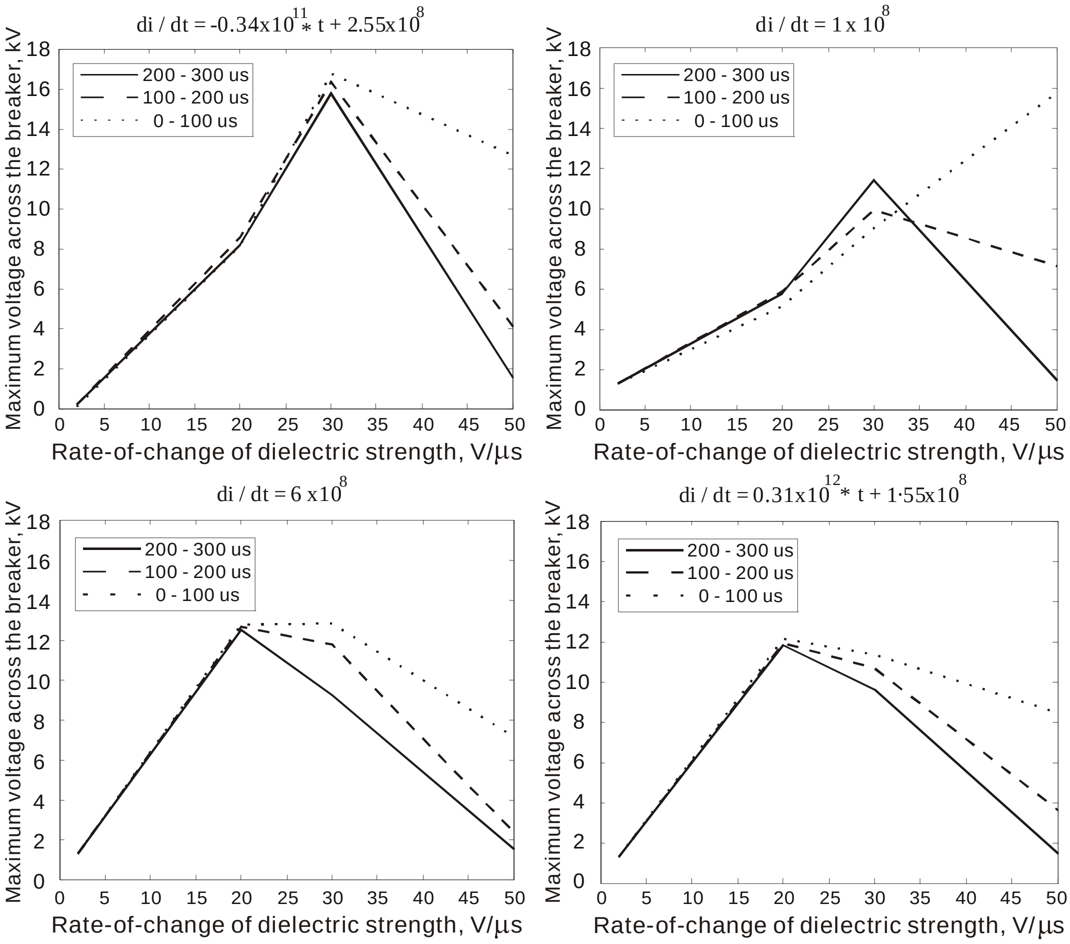

Figure 4-7 Influence of the rate-of-change of the dielectric strength on the recovery voltage

4.1.4 Summary

Based on the results shown in Appendix B and Appendix C, Figure 4-8 summarizes the effect of the rate-of-change of the dielectric strength and the quenching capability of the vacuum circuit breaker models with different arcing time ranges on the escalation voltage. It was found that some combinations of the breaker characteristics may lead to reignition/voltage escalation problems. When the rate-of-change of the dielectric strength is between 20 and 30 V/μs (middle range), the escalation voltage is usually higher than other cases. Moreover, when the arcing time is close to the current zero (ranging from 0 – 100 μs), the escalation voltage is more severe than that corresponding to arcing times ranging from 100 μs to 300 μs. Also, high escalation voltage usually appears when the termination mode is mode A (successfully interrupt at the end of the high frequency reignition sequence), or if the quenching capability decreases with time.

The result of the statistical TRV calculation shows that the rate-of-change of the dielectric strength and the arcing time of the breaker are the most important for the estimation of the TRV, while the influence of the quenching capability on the escalation voltage is less pronounced.

Consequently, when estimating the overvoltages resulting from the operation of vacuum circuit breakers in the system, it is suggested to consider the middle range of the rate-of-change of the dielectric strength to look for the worst case in order to provide the most appropriate protection scheme.

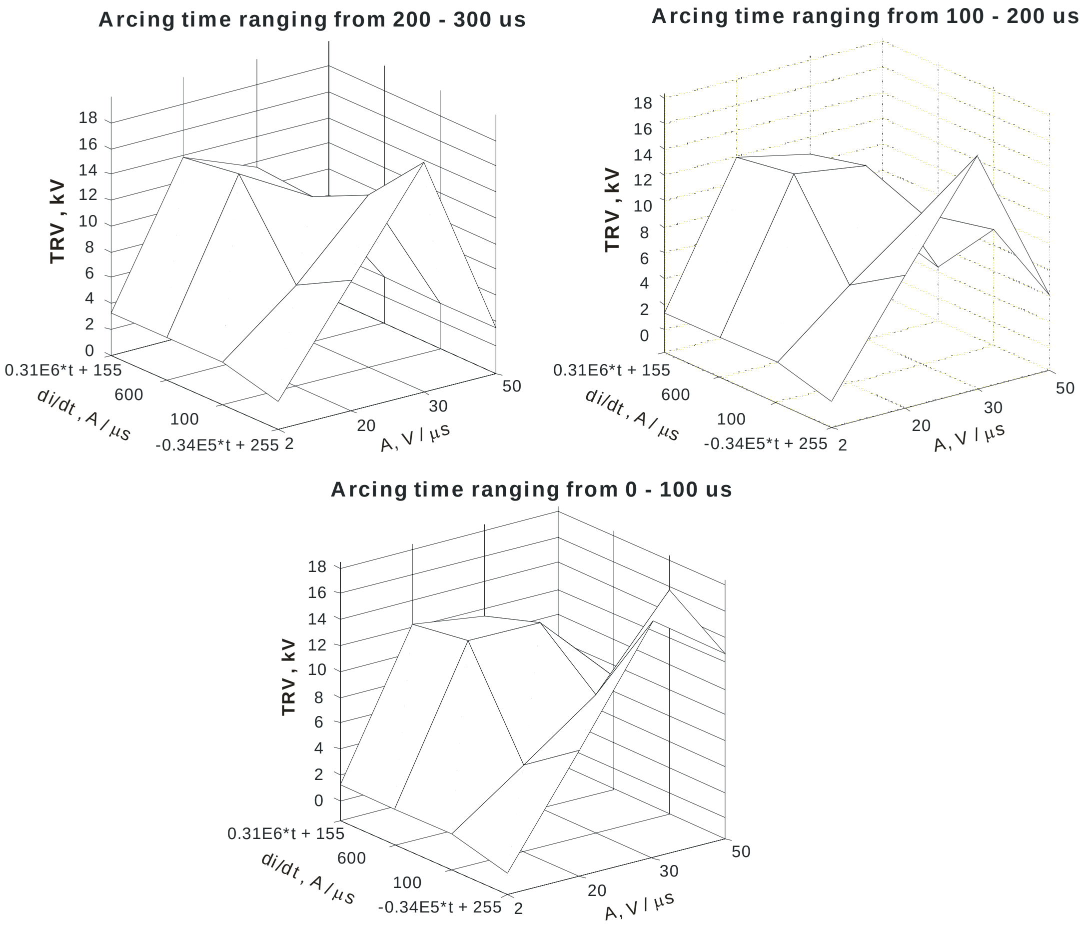

Figure 4-8 Escalation voltages as a function of the breaker model characteristics

4.2 STUDIES ON OTHER CIRCUIT PARAMETERS

The following parameters governing the severity of switching overvoltages were evaluated in a parametric sensitivity study, using the network shown in Figure 4-9 and the results of varying different parameters are shown below.

1. Short circuit ratio
2. Source types
    - Inductive
    - Complex
3. Transformer connection
4. Cables connecting the motor to the breaker, the motor to the power factor correction capacitors
    - Type of cable model
    - Cable length
    - Grounding practices
5. Rating of power factor correction capacitors
6. Motors running condition

The network comprises an 11kV source with fault level of 50MVA, a 5 MVA, 11 kV/3.3 kV delta star-grounded transformer with leakage impedance of 8%, a vacuum circuit breaker, a 20m cable connecting the motor to the breaker, and a 420kW induction motor.

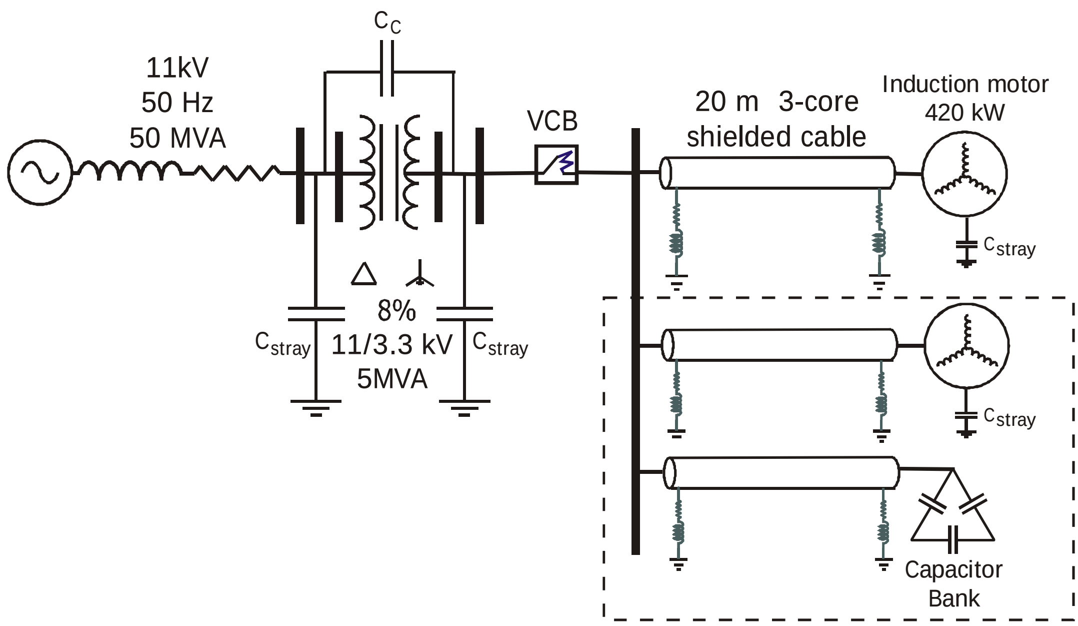

Figure 4-9 Evaluation circuit to perform parametric sensitivity studies

4.2.1 Short circuit ratio

As shown in Figure 4-10, the short circuit level does not have a strong influence on the fast-front overvoltages.

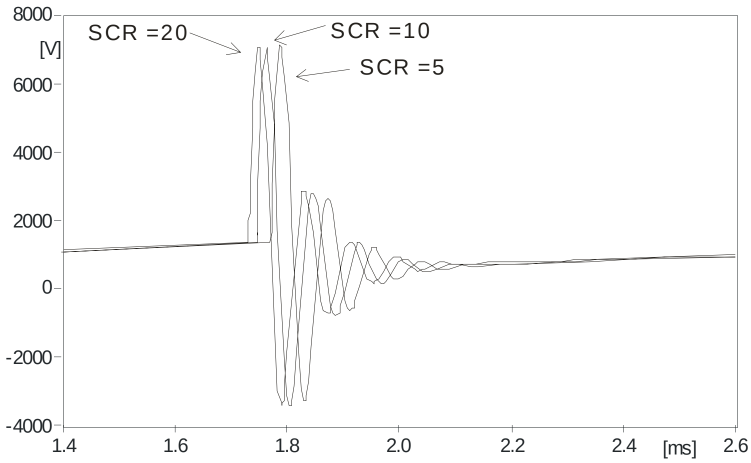

Figure 4-10 Effect of short circuit ratio – voltage at motor terminal

4.2.2 Source type

Figure 4-11 shows that the overvoltage for a complex source is less severe than that for an inductive source, as expected. This is because the surge impedance presented by other cables connected at the switching bus act to reduce the level of the incident wave.

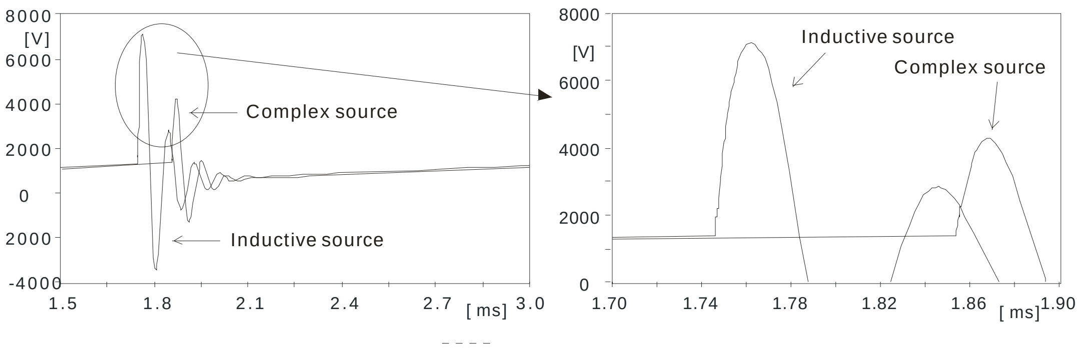

Figure 4-11 Effect of source type – voltage at motor terminal

4.2.3 Transformer connection

When the transformer is ungrounded at the low voltage side, the voltage at the motor terminal contains more oscillations than at the transformer with a grounded neutral. As shown in Figure 4-12, the overvoltages at the motor terminal for both cases are similar.

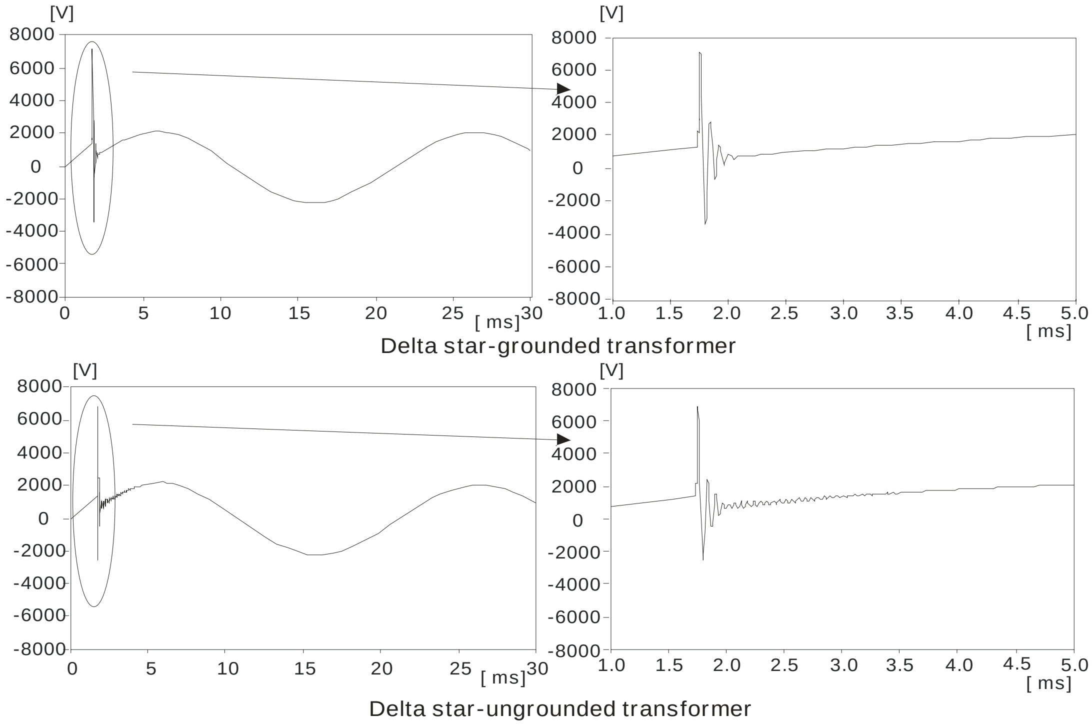

Figure 4-12 Effect of transformer connection – voltage at motor terminal

4.2.4 Type of cable model (motor)

As shown in Figure 4-13, the damping in the model without frequency dependence (Cable CONSTANT model and pi-section model) is, as expected, less than the model with frequency dependence.

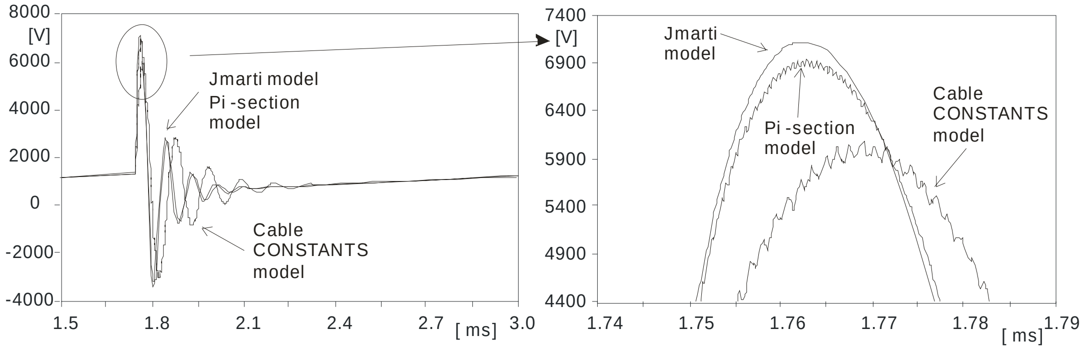

Figure 4-13 Effect of cable type – voltage at motor terminal

4.2.5 Grounding of cable sheath (motor)

It was found that the overvoltages are similar for different grounding practices. In Figure 4-14, the voltages at the motor terminal are similar as those for the case with cable sheath grounded at both ends while the voltages at motor terminal are similar for the case with cable sheath grounded at sending end and ungrounded at both ends.

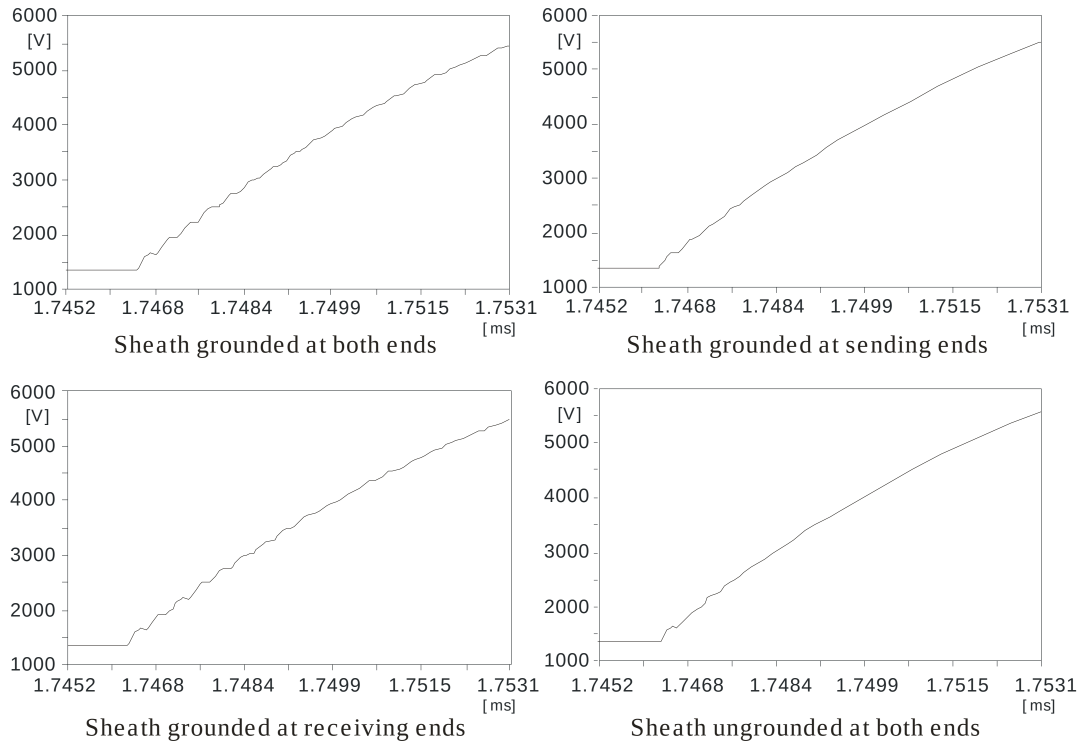

Figure 4-14 Effect of grounding of cable sheath – voltage at motor terminal

4.2.6 Cable length (motor)

The results indicate that shorter cables lead to higher overvoltages as shown in Figure 4-15. This is because surge impedance of the network formed by the motor inductance and the cable capacitance is higher for shorter cables, and higher surge impedance leads to higher suppression peaks for a given chopping current.

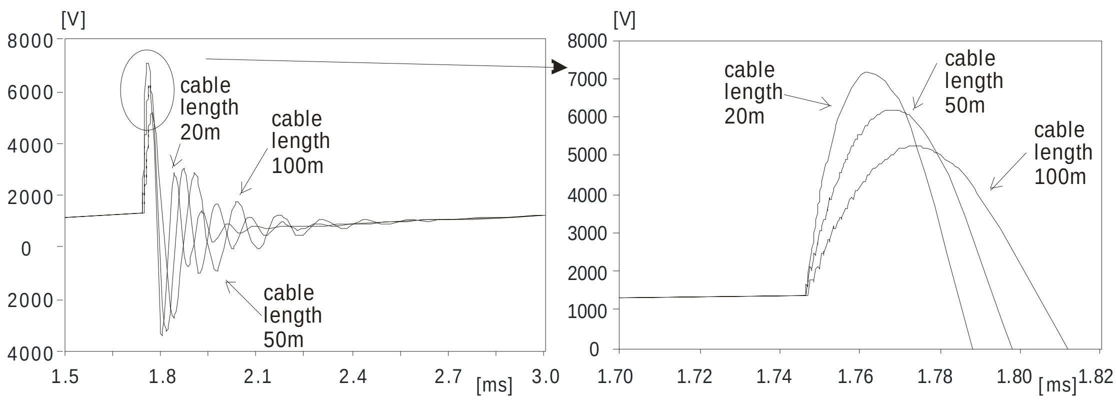

Figure 4-15 Effect of cable length – voltage at motor terminal

4.2.7 Present of power factor correction capacitors

The presence of power factor correction capacitors precludes high overvoltages to be generated at the motor terminal, as shown in the following figures. However, the power factor correction capacitors introduce more low frequency oscillations of the voltage at the motor terminal.

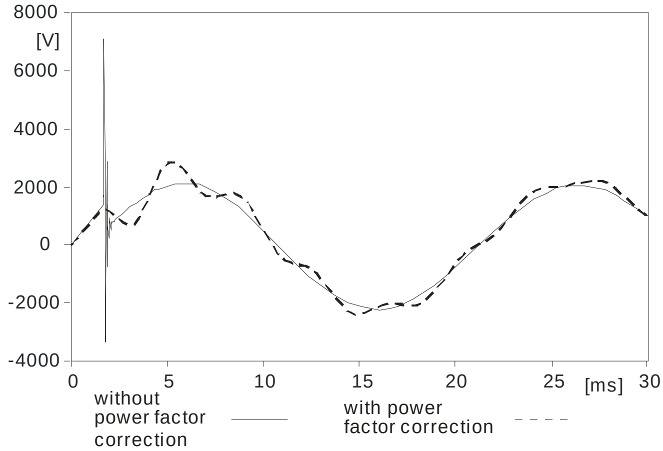

Figure 4-16 Effect of presence of power factor correction capacitors– voltage at motor terminal

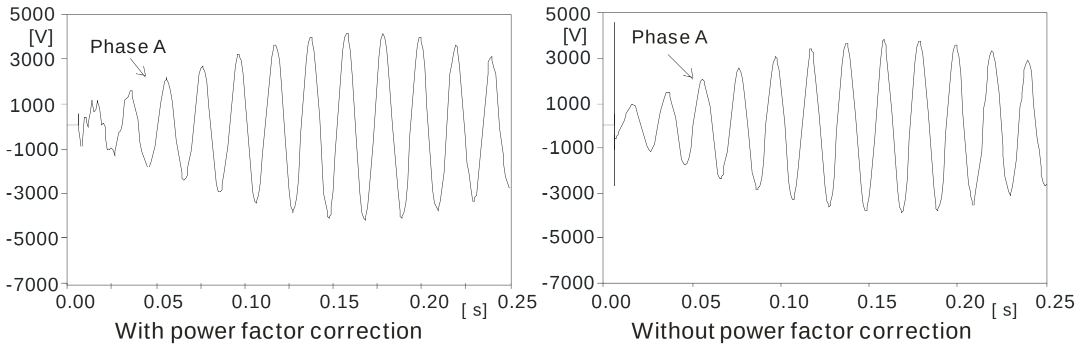

Figure 4-17 Effect of presence of power factor correction capacitors – voltage across breaker

4.2.8 Cable length (power factor correction capacitors)

The location of the power factor correction capacitors does not have an obvious effect on the overvoltage generated at the motor terminal. It only affects the low frequency oscillation at the motor terminal. The closer the power factor correction capacitors to the motor terminal, the higher the frequency content of the oscillation produced. The effect on the peak magnitude of the overvoltages produced however is small.

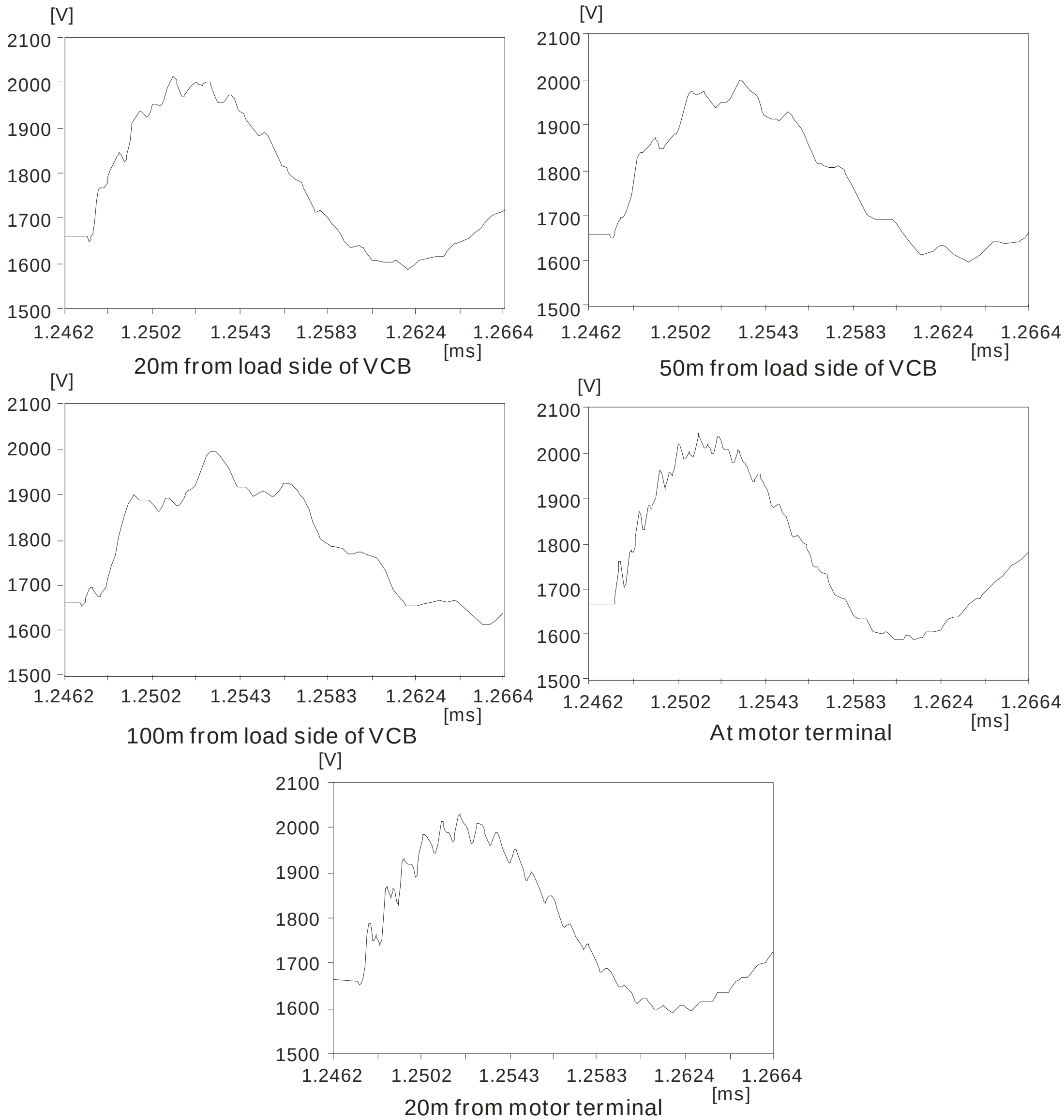

Figure 4-18 Effect of location of power factor correct capacitors – voltage at motor terminal

4.2.9 Rating of power factor correction capacitors

The ratings of the power factor correction capacitors are 86kVAr to bring the power factor up to 0.92 and 35kVAr to bring the power factor up to 0.88. As shown in Figure 4-19, the low frequency oscillation is more onerous with the 35kVAr capacitor bank.

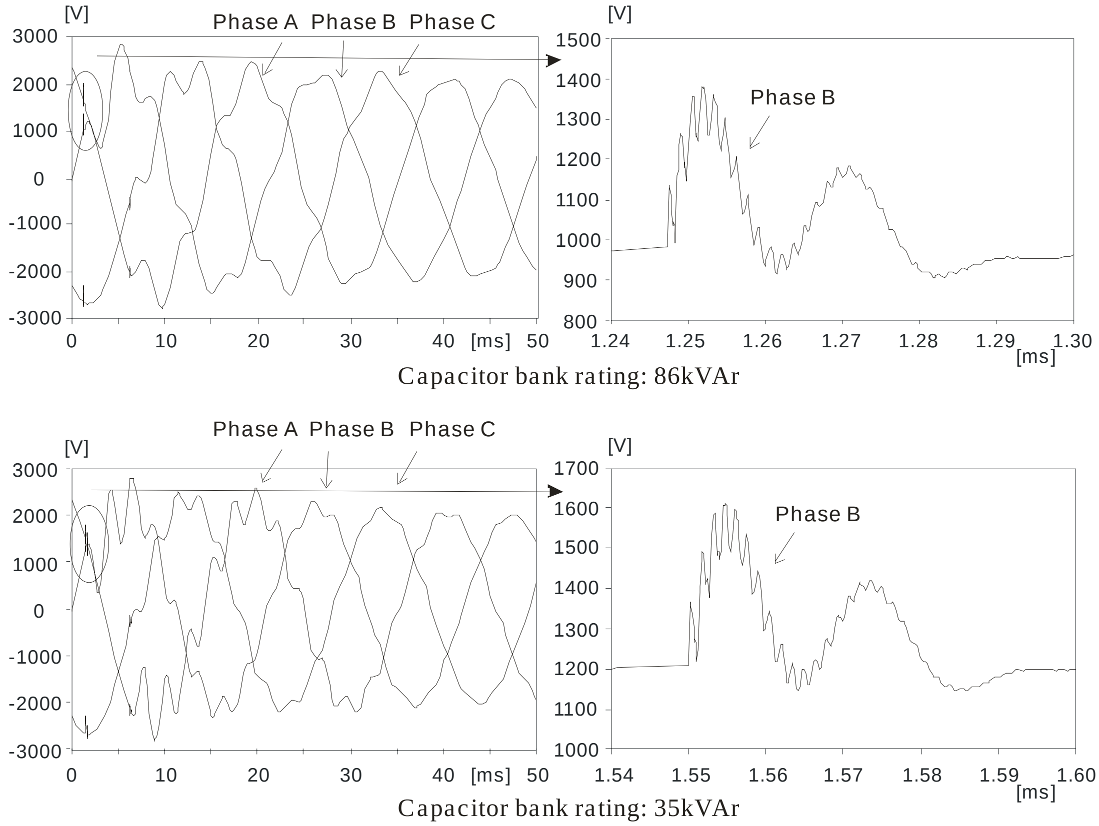

Figure 4-19 Effect of rating of power factor correction capacitors – voltage at motor terminal

4.2.10 Motor condition

A running motor continues to generate back EMF after it is switched off. Thus the voltage across the vacuum circuit breaker builds up very slowly as the applied voltage of the system and the back EMF of the motor drift apart. On the other hand, aborting a motor start may generate severe overvoltage since the motor has no back EMF and therefore behaves like a reactor. As shown in Figures 4-20 and 4-21, the overvoltages generated in a starting motor are more severe than a running motor. Moreover, the probability of reignition to occur is higher when switching off a starting motor than a running motor.

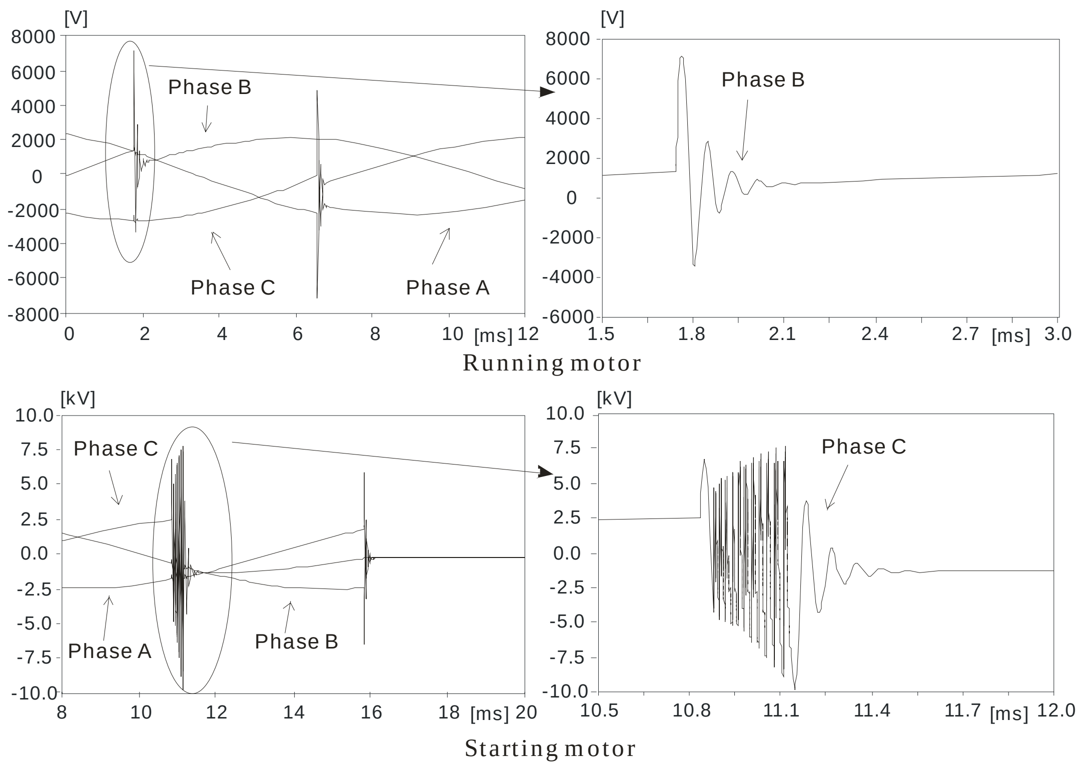

Figure 4-20 Effect of motor running condition – voltage at motor terminal

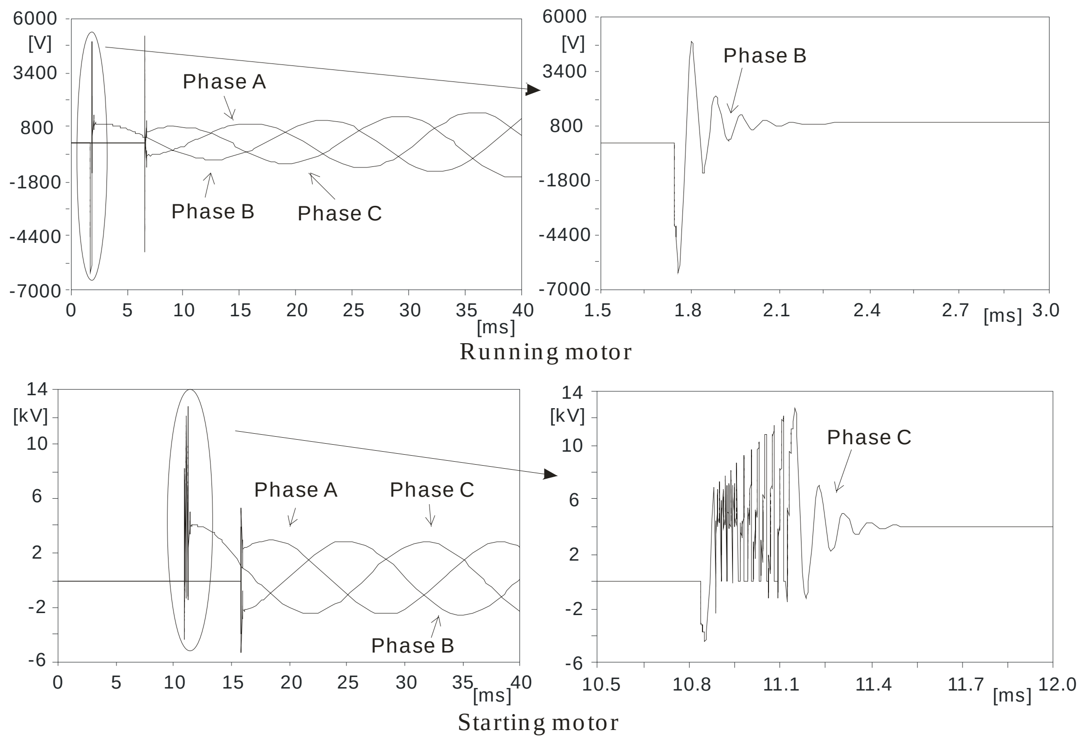

Figure 4-21 Effect of motor running condition – voltage across the breaker

4.3 STATISTICAL OVERVOLTAGES

Monte Carlo methods were used to study the stochastic properties of overvoltages. The distribution curves of statistical overvoltages of different voltage quantities for the cases can be found in Appendix D. The mean values and the 2% overvoltages in each case were recorded and they are listed in the following table:

Case No.	Variation parameters	Voltage at motor terminal (p.u.)	
		Mean	2 %
1	-	2.96	3.68
2	SCR: 20	2.98	3.65
3	SCR: 5	2.97	3.70
4	Complex source type	1.77	2.04
5	Transformer connection: delta-star ungrounded	2.92	3.45
6	Motor cable type: pi section model	3.02	3.63
7	Motor cable type: Constant parameters model	2.48	3.07
8	Grounding of motor cable: grounded at receiving end	2.96	3.46
9	Grounding of motor cable: grounded at sending end	2.98	3.46
10	Grounding of motor cable: ungrounded at both ends	2.99	3.58
11	Motor cable length: 50m	2.56	3.10
12	Motor cable length: 100m	2.16	2.63
13	Capacitor bank rating and location: 86kVAr, at motor terminal	1.05	1.26
14	Capacitor bank rating and location: 86kVAr, 20m from motor terminal	1.05	1.26
15	Capacitor bank rating and location: 86kVAr, 20m from load side of VCB	1.05	1.27
16	Capacitor bank rating and location: 86kVAr, 50m from load side of VCB	1.05	1.25
17	Capacitor bank rating and location: 86kVAr, 100m from load side of VCB	1.05	1.18
18	Capacitor bank rating and location: 35kVAr, 20m from load side of VCB	1.05	1.27
19	Motor starting	2.61	10.08

Table 4-1 Mean and 2% overvoltages for different cases

As can be seen in Table 4-1, the mean and 2% overvoltages at the motor terminal are not much influenced by the short circuit ratio as well as the transformer connection. Moreover, the grounding practices of the cable sheath do not have much of an effect on the overvoltages at the motor terminal.

The simulation models of the cable were compared by studying Case 1, Case 6 and Case 7. It was found that the frequency dependent model can well represent the damping. Case 1, Case 11 and Case 12 compared the effect of the cable length on the overvoltage at the motor terminal. It is clear that longer cables reduce the overvoltages generated.

When power factor correction capacitors were connected, the overvoltages generated at the motor terminals were precluded. The length of the cable connecting the motor to the power factor correction capacitors and the rating of the power factor correction capacitors does not have much of an impact. However, with smaller ratings of power factor correction capacitors, the low frequency oscillation was found to be more severe.

Finally, it was found that when switching off a starting motor with no power factor capacitors connected, onerous overvoltage can occur and the 2 % overvoltage was found to be more than 10 p.u..

CHAPTER 5 PROTECTIVE MEASURES

The control of overvoltages is defined as "the condition within a system wherein the expected transient overvoltages are limited to a defined level". There are two kinds of control (i) *protective control* where specified attenuation means limit the prospective transient overvoltages to a defined level (arresters, surge suppressers, etc.), and (ii) *inherent control* where the characteristics of the system can be expected to limit the prospective transient overvoltages to a defined level (statistics, experience, measurements, network topology). In this research the effectiveness of protective control has been evaluated.

5.1 SURGE PROTECTIVE DEVICES

Surge protective devices (SPD's) comprise series or parallel devices which block (series) or divert (parallel) incoming surge energy. They comprise devices such as gas tubes and semi-conductors, each of which have relative advantages in terms of energy absorption characteristics, speed of operation, and mode of operation. Another commonly used protective device, the RC damper, serves to modify the shape on the incident waveform, making it less onerous to the protected equipment.

5.1.1 Metal oxide varistors

Metal oxide varistors (MOV's) are among the most commonly used surge protection devices in industry. They offer fast response, excellent clamping, reasonable energy absorption capability, and they are cheap. Unlike gas tubes, they are not crow-bar devices, and do not require series resistors.

The choice of device, location, installation method and adequate grounding practices act together to provide adequate surge protection. Whatever device is used it must be installed properly, and it is usually here that surge protection often fails. Even relatively short lead lengths represent a significant travel time to a fast front surge. For example, a 10 kV surge with a time-to-crest of 0.5μs will result in an *effective protective level* at the terminals of the equipment of some 600V higher than the clamping voltage of the MOV.

Figure 5-1 shows the results of an EMTP simulation, which further demonstrates this effect: note the difference in the voltage developed at Node 2, with and without representation of the lead length.

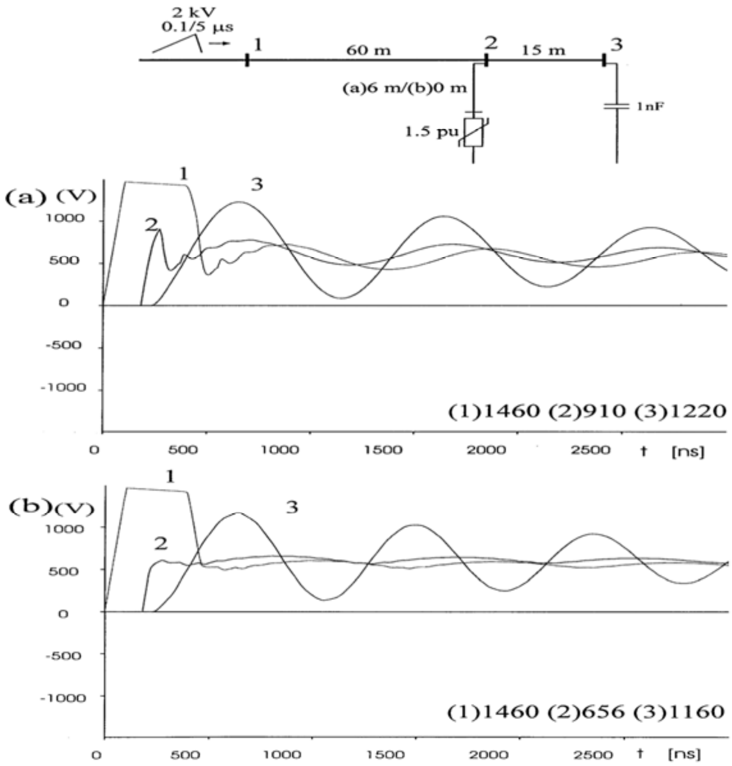

Figure 5-1 Effective of lead length on protective level of MOV

It is significant that in the case of the transformer failure discussed below, there were improperly installed surge arresters and the low voltage winding which failed was inadequately protected.

5.1.1.1 Simulation of MOVs

In EMTP, there is a supporting program to obtain the V/I characteristics of arresters with different ratings. This supporting routine can derive a true non-linear representation for a zinc-oxide surge arrester (MOV), starting from manufacturer's data for the surge arrester. The non-linear V/I characteristics is approximated by an arbitrary number of exponential segments. By inputting a set of V/I data in p.u., arresters with different ratings can be generated by specifying the voltage rating in individual cases. The data used were from the manufacturer and the V/I curve is shown below:

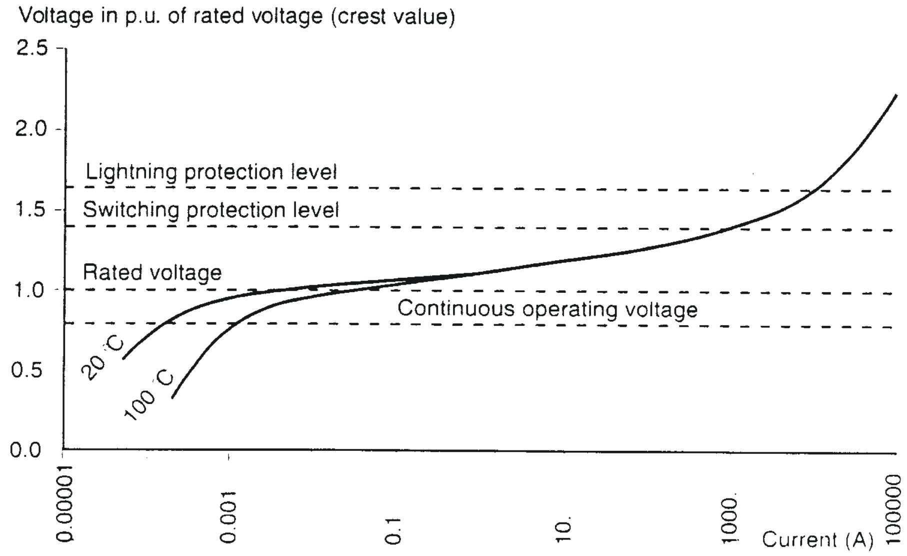

Figure 5-2 Arrester characteristics

5.1.2 RC dampers

Surge arresters limit the magnitude of the voltage surge but do not modify its rate of rise. The RC damper, typically comprising a series connection of a capacitor of the order of a microfarad with a resistor of some 50Ω is another protection device. RC dampers reduce the rate of rise of the incident waveform, thereby rendering the overvoltage less onerous to the protected equipment. Furthermore by approximately matching the surge impedance of the connecting cable with a series resistor, they act to reduce the reflected component of the overvoltage transmitted to the protected equipment. The series resistor also assists in damping transient oscillations.

5.2 EVALUATION CIRCUIT

Different protection measures were applied to the network shown in Figure 5-3. The protective measures evaluated include:

- Arrester at motor terminal
- Arrester at motor terminal with 6m separation distance
- Arrester at transformer low voltage side
- Arrester at transformer low voltage side with 6m separation distance
- Arresters across the vacuum circuit breaker
- RC damper at motor terminal
- RC damper at transformer terminal

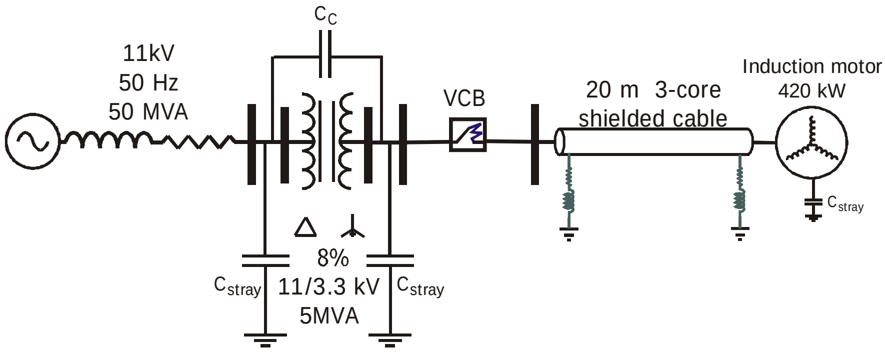

Figure 5-3 Evaluation circuit to perform protective measures studies

The cases are listed in Table 5-1.

Case No.	Protection applied
1	Nil
2	3kV arrester at motor terminal
3	3kV arrester at motor terminal with 6m separation distance
4	3kV arrester at transformer low voltage side
5	3kV arrester at transformer low voltage side with 6m separation distance
6	3kV arresters across the vacuum circuit breaker
7	RC damper at motor terminal: R = 30Ω C = 0.2μs
8	RC damper at transformer terminal: R = 30Ω C = 0.2μs

Table 5-1 Different cases for overvoltage study

5.2.1 No protective devices

Ways to reduce the magnitude of TRVs were implemented and incorporated into the 8 cases. Figure 5-4 shows some results from Case 1 which has no protection applied. The figure shows the magnitude of the voltage at motor terminal, transformer low voltage side and across the breaker. Note that the voltage at the transformer low voltage side terminal is more than 15kV and the TRV is more than 20kV.

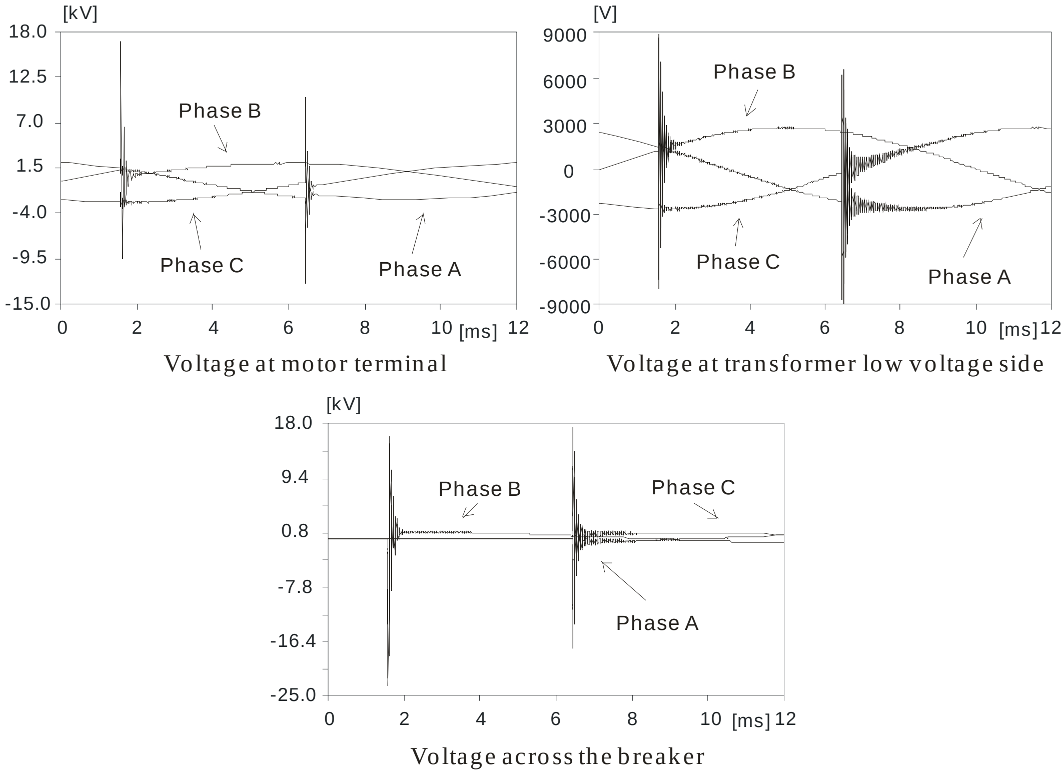

Figure 5-4 Transient voltage response without protective devices connected

5.2.2 Arrester at motor terminal

Figure 5-5 shows the network with 3kV arresters connected at each of the phase of the motor terminal. Figure 5-6 shows the typical waveforms and it shows that overvoltages appear at phase B first when compared with other phases. Therefore the arrester at phase B operates first and absorbs the greatest amount of energy.

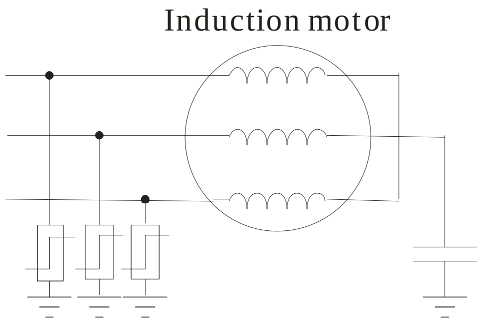

Figure 5-5 Arresters at induction motor terminal

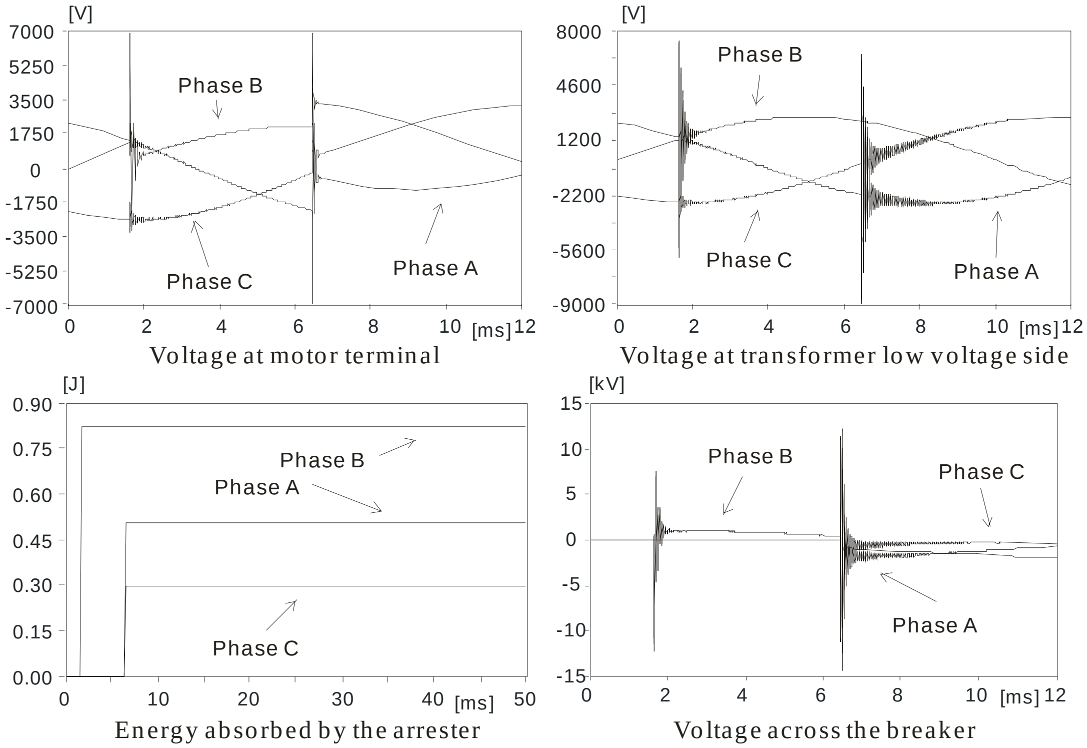

Figure 5-6 Transient voltage response with arresters at motor terminal

5.2.3 Arrester at motor terminal with 6m separation distance

Figure 5-7 shows the network with 3kV arresters connected at the phases of the motor terminal with 6m separation. Figure 5-8 shows the typical waveforms: the overvoltages in this case are very close to those of the previous case, since the steepness of surge is reduced after passing the cable and consequently the separation distance has less of an effect.

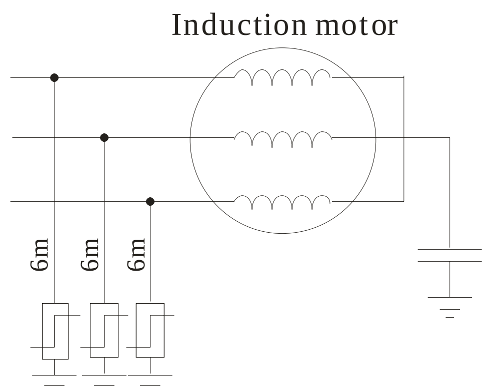

Figure 5-7 Arresters at induction motor terminal with 6m separation distance

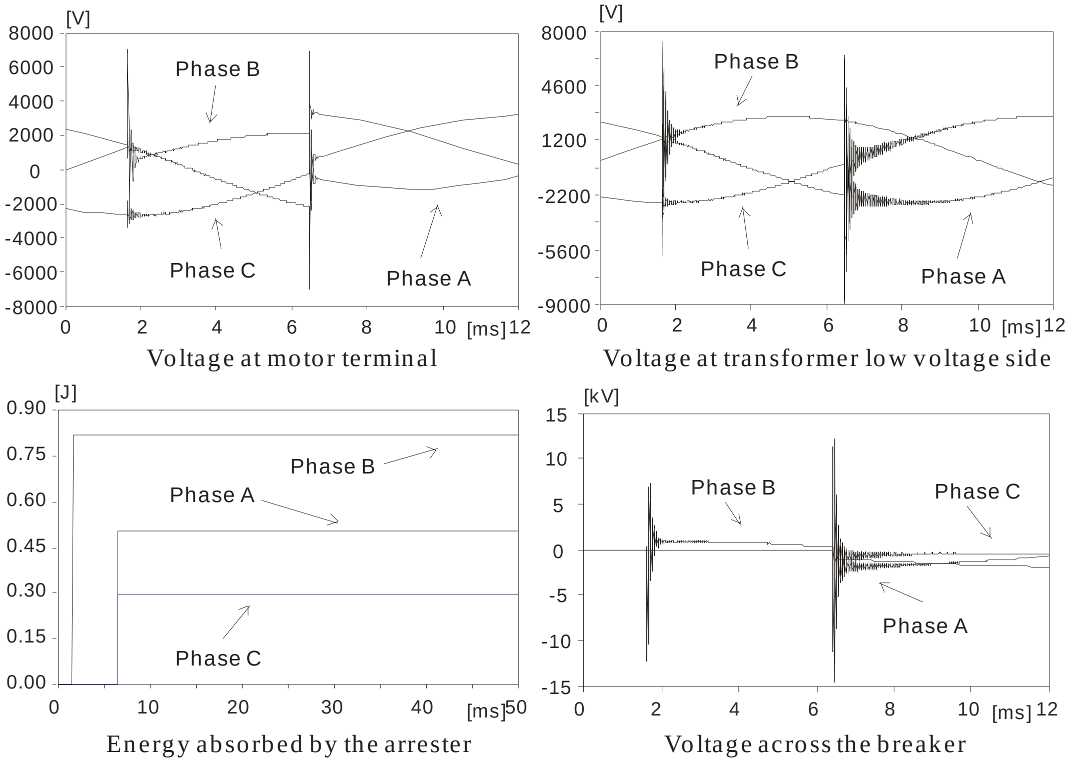

Figure 5-8 Transient voltage response with arresters at motor terminal with 6m separation distance

5.2.4 Arrester at transformer terminal

Figure 5-9 shows the network with 3kV arresters connected at each of the phase of the transformer low voltage side. Figure 5-10 shows the typical waveforms and it shows that overvoltages at the motor terminal and TRV are more severe than those of Case 2.

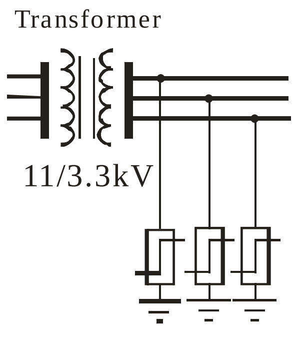

Figure 5-9 Arresters at transformer low voltage side

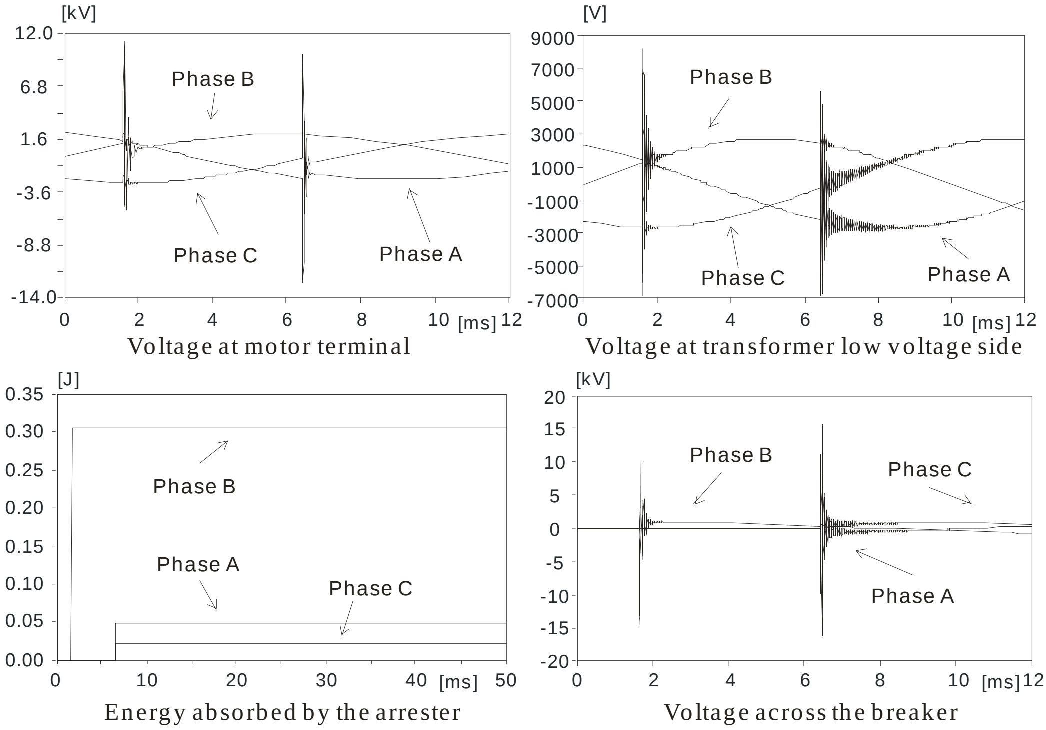

Figure 5-10 Transient voltage response with arresters at transformer low voltage side

5.2.5 Arrester at transformer terminal with 6m separation distance

Figure 5-11 shows the network with 3kV arresters connected, with 6m lead length, at each phase of the transformer low voltage side. Figure 5-12 shows the typical overvoltage waveforms at the transformer low voltage side and it is apparent that they are more severe than those of the previous case. This is because at the transformer low voltage side, which is the source side of the VCB, the surge front is relatively steep when compared to that at the motor terminal, hence the separation distance has more effect on the effective protective level of the arrester.

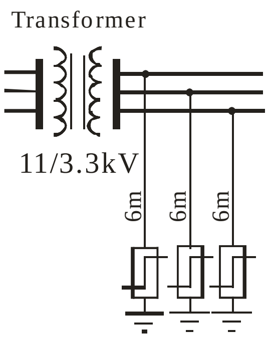

Figure 5-11 Arresters at transformer low voltage side with 6m separation distance

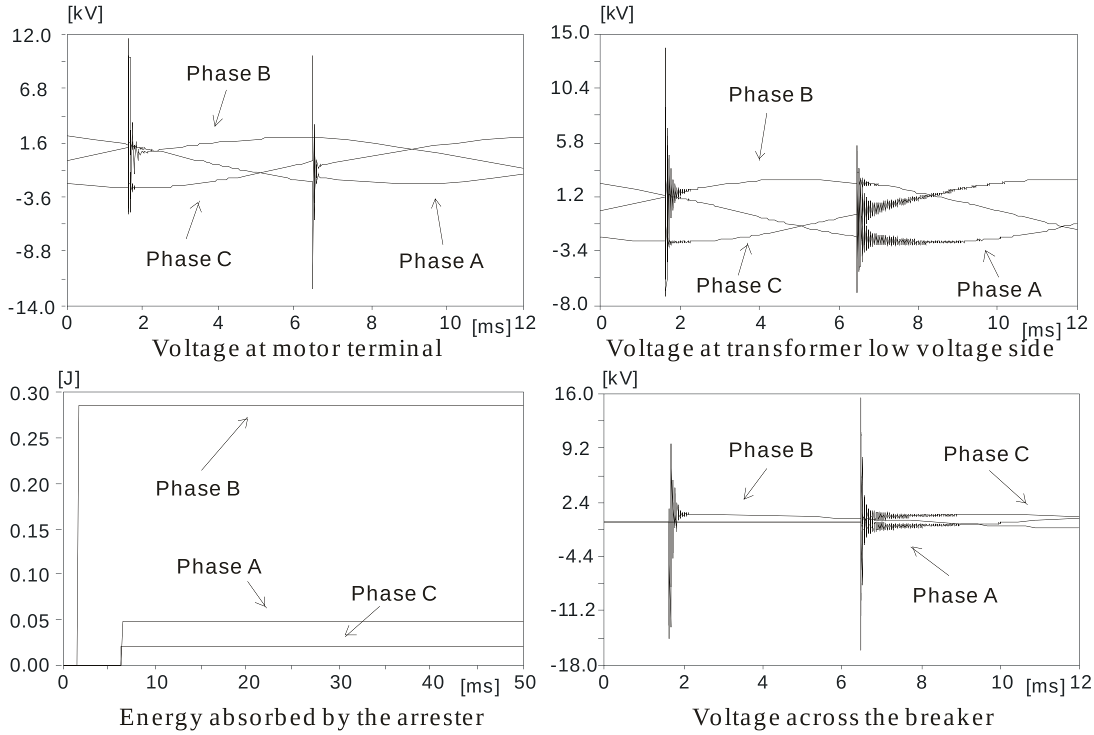

Figure 5-12 Transient voltage response with arrester at transformer low voltage side with 6m separation distance

5.2.6 Arresters across the vacuum circuit breaker

Figure 5-13 shows the network with 3kV arresters connected longitudinally across each phase of the breaker. These arresters limit the TRV and typical waveforms are shown in Figure 5-14. When compared with Figure 5-3 which refers to Case 1, it is clear that the TRV is reduced from 25kV to 8kV. Hence it is more effective to reduce the TRV when the arresters are connected across the breaker.

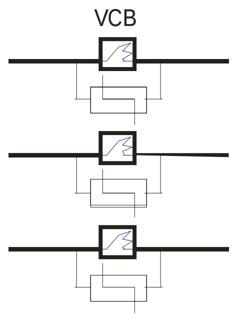

Figure 5-13 VCB with arresters connected across it

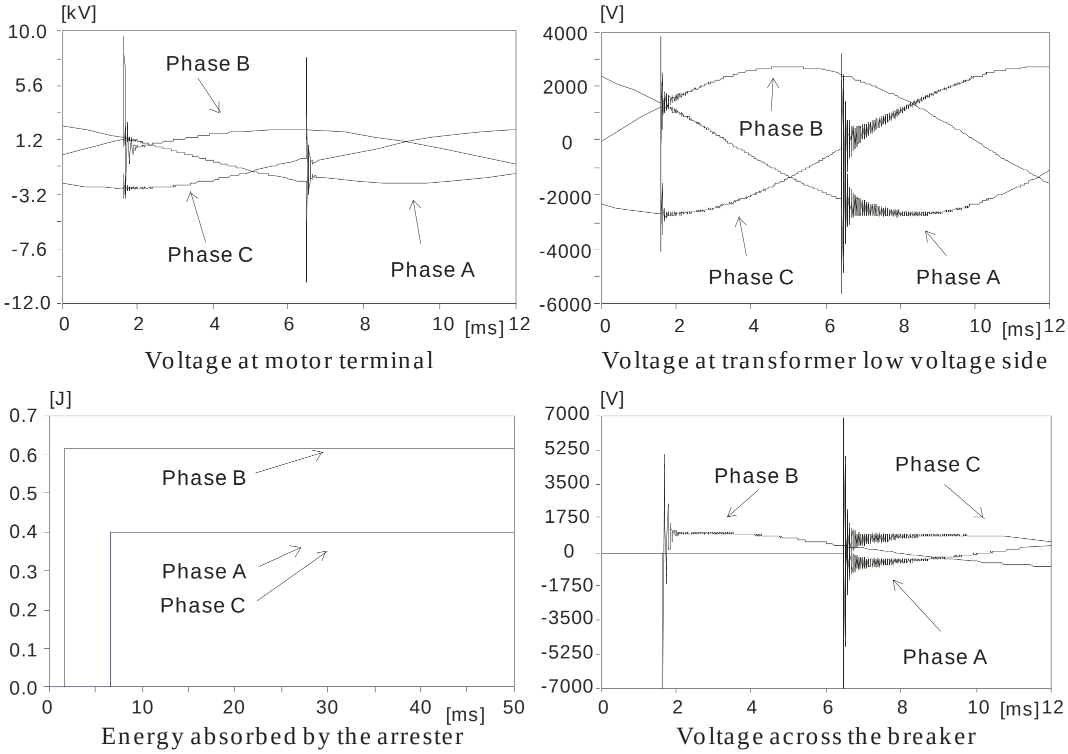

Figure 5-14 Transient voltage response with arresters across the breaker

5.2.7 RC damper at motor terminal

Another protection method studied is the use of RC dampers to ground at the motor terminals as shown in Figure 5-15. The effect of the RC damper is to reduce the steepness of the incident surge. The resistor, matched to the surge impedance of the cable, helps to reduce the reflected component of the travelling wave. When compared with Figure 5-4 which refers to Case 1, it is clear that the TRV is reduced from 20kV to 9kV and the voltage at motor terminal is reduced from 15kV to 4kV.

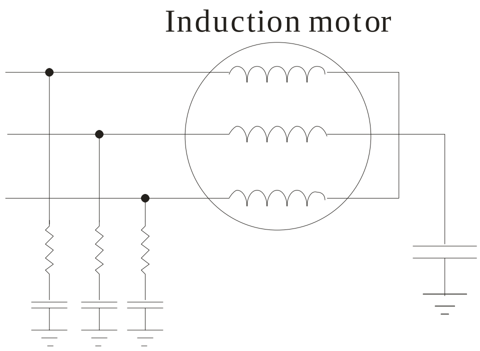

Figure 5-15 RC dampers at induction motor terminal

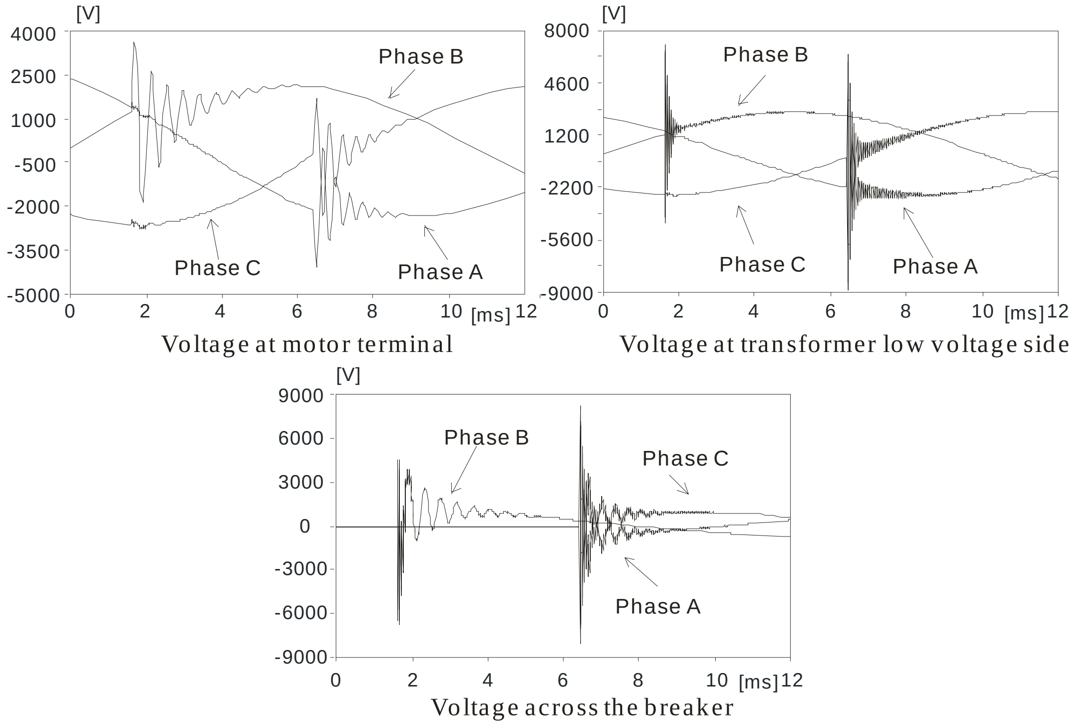

Figure 5-16 Transient voltage response with RC dampers at motor terminal

5.2.8 RC damper at transformer terminal

Figure 5-17 shows the network with RC dampers connected at transformer low voltage side. As shown in Figure 5-18, the overvoltage at transformer low voltage side is limited to less than 3kV. However, the TRV and the overvoltage at the motor terminal are not limited by the RC damper.

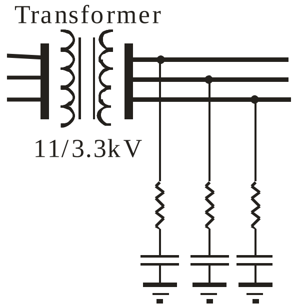

Figure 5-17 Transformer with RC dampers connected at its terminal

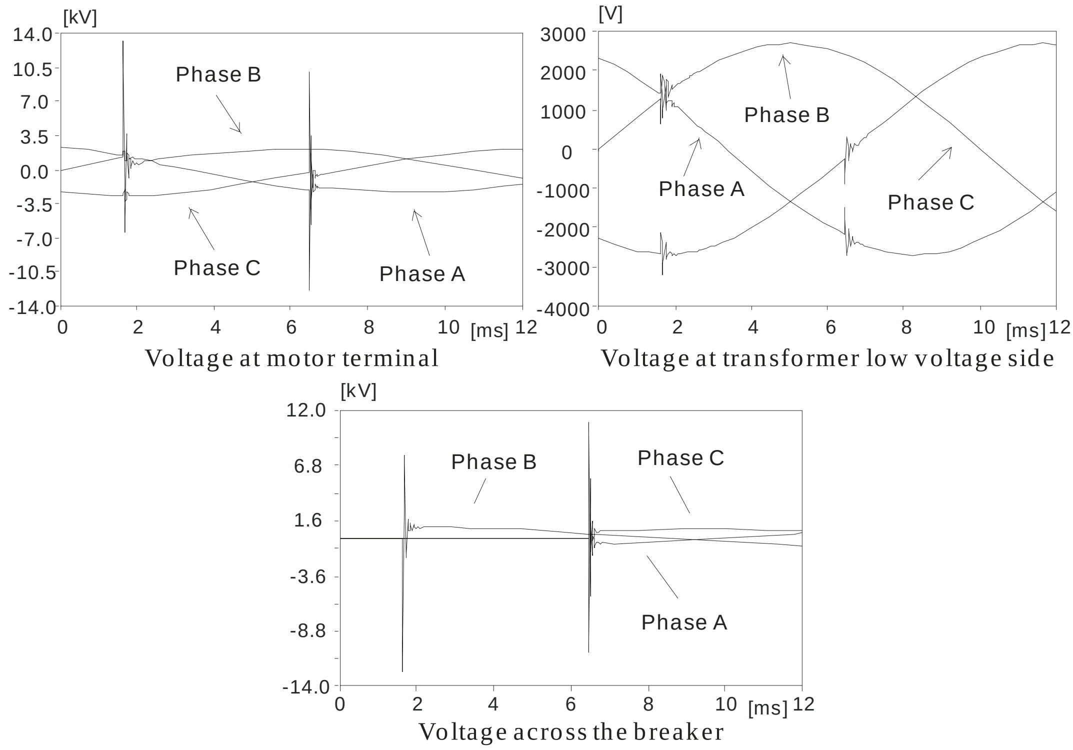

Figure 5-18 Transient voltage response with RC dampers at transformer low voltage side

5.3 STATISTICAL OVERVOLTAGES

Monte Carlo methods were used to determine the statistical overvoltages. One hundred simulations were run for each case, and the relevant cumulative probability distributions for some cases are shown in Figures 5-19 to 5-22.

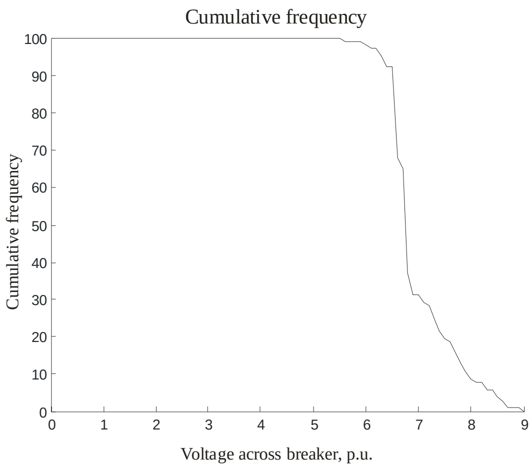

Figure 5-19 TRV, Case 1

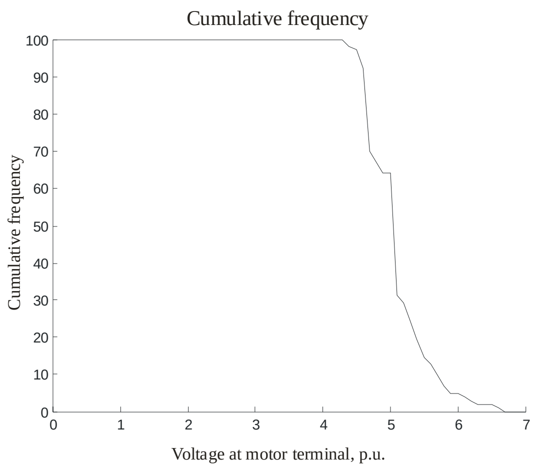

Figure 5-20 Voltage at motor terminal, Case 1

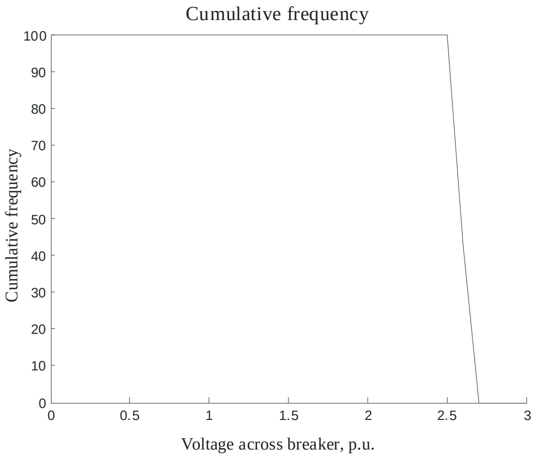

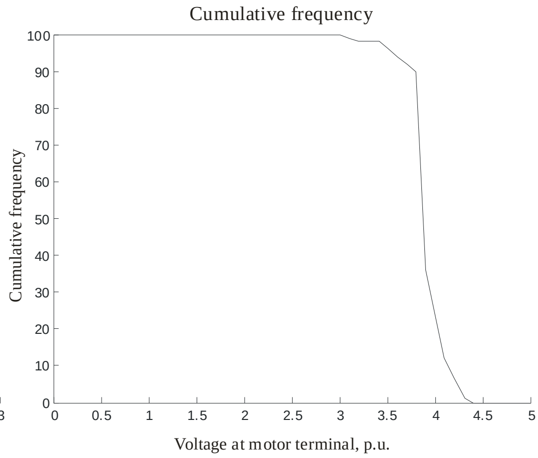

Figure 5-21 TRV, Case 6 Figure 5-22 Voltage at motor terminal, Case 6

The above figures show results for Case 1 and Case 6. Case 1 has no protection method applied and Case 6 has a 3kV arrester connected across the breaker. It is obvious that both the magnitude of TRV and voltage at motor were reduced in the case where arresters were applied. (The statistical results for other cases can be found in Appendix E) The mean values and the 2% overvoltages in each case were recorded and they are listed in the following table:

Case No.	Voltage at motor terminal (p.u.)		Voltage across breaker (p.u.)		Voltage at transformer low voltage side (p.u.)	
	Mean	2%	Mean	2%	Mean	2%
1	5.043	6.294	6.753	8.647	3.371	6.394
2	2.557	2.691	5.400	6.196	3.393	4.045
3	2.644	2.700	5.376	6.285	3.376	4.057
4	5.054	6.549	6.533	7.798	2.558	3.080
5	5.054	6.400	6.445	7.600	2.589	5.250
6	3.874	4.283	2.588	2.695	2.077	2.650
7	1.560	1.850	3.076	3.650	3.362	3.900
8	4.971	6.550	4.664	6.250	1.233	3.050

Table 5-2 Mean and 2% overvoltages for different case

As can be seen in Table 5-2, the mean and 2% TRVs without any protection device are more than 6.5 p.u. and 8.5 p.u. respectively. Case 2 and Case 3 have arresters connected to ground at the motor terminals and there is a significant reduction in the statistical overvoltages. Note that the lead length has less of an effect. The arresters have little effect on the TRV and the voltage at transformer low voltage terminals.

Cases 4 and 5 have arresters connected to ground at the transformer low voltage side. There is a significant reduction in the statistical overvoltage, however the effect of the lead length is more pronounced than with the previous case. The TRV and the statistical overvoltages at the motor terminal are not significantly reduced.

The most effective protection method is Case 6 which has arresters connected across the breaker. The 2% overvoltages of all locations are less than 4.5 p.u. and the TRV is reduced by more than 50% when compares with the statistical overvoltages of Case 2 and Case 3 (arresters connected to ground at motor terminal).

RC damper to ground at motor terminal and transformer low voltage side are applied in Cases 7 and Case 8 respectively. The table shows that the overvoltage at the motor terminal is reduced significantly when the RC damper is connected at the motor terminal. Moreover, the 2% overvoltages at other locations are also reduced. When the RC damper is connected to the transformer low voltage side, the reduction on the TRV is not as much as in the previous case because without the cable there is no reflected wave.

CHAPTER 6 CASE STUDIES

Two industrial installations in Hong Kong were studied, one where there was a failure of a transformer attributable to VCB switching, and one where VCBs were to be installed as replacements for oil circuit breakers.

6.1 INDUSTRIAL INSTALLATION IN HONG KONG – PAPER MILL

An employee on duty in the control room of a paper mill in Hong Kong switched off a large induction motor and heard a loud "bang" sound, following which a section of the paper making plant, which was the only section running at the time, was de-energised. As shown in Figure 6-1, the transformer appeared to have failed owing to consequential damage to the winding insulation following a flashover of the C-phase and neutral leads over the top end of the low voltage winding. It was suspected that a transient overvoltage resulting from switching of a lightly loaded induction motor by a vacuum circuit breaker led to the failure (Snider 1997). A simulation of the network, using my model of the vacuum circuit breaker, revealed that the significant overvoltages could be generated by the VCB.

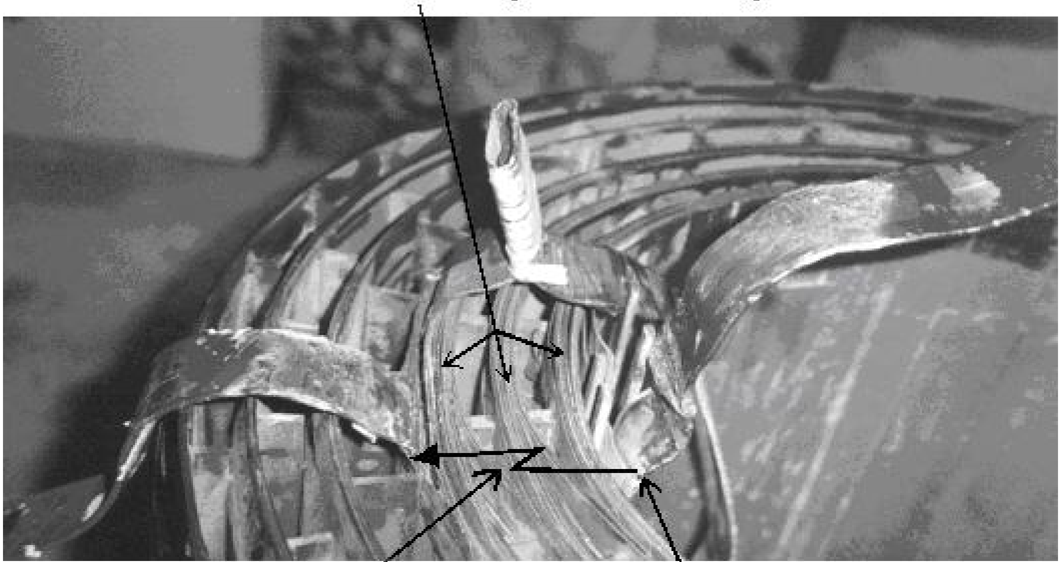

Figure 6-1 Failed transformer

6.1.1 Simulation network and parameters

The one-line diagram of the supply circuit is shown in Figure 6-2 with the stochastic model of vacuum circuit breaker and the developed circuit models. An arrester was installed at the low voltage side of the transformer, however the low voltage lead of the arrester was connected to the enclosure rather than the transformer neutral (through the paint, which was not removed), so the effective connection length is very long. Note that the question marks represent the unknown values, where the connections were made through paint (high values of resistances were used).

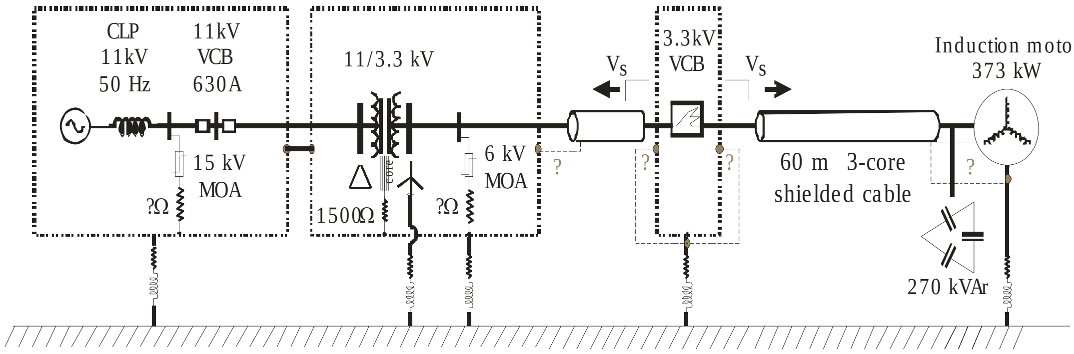

Figure 6-2 Single line diagram of the supply circuit

This is a typical case where the simulation is difficult since there are many unknown parameters. For example, the actual withstand voltage characteristics and the chopping current characteristics for the vacuum circuit breaker are not known, however the stochastic breaker model, covering a range of typical values, serves well towards the determination of the statistical overvoltages, which in turn serve as good indicators of potential problems.

The simulated circuit was simplified to include the crucial components which could influence the magnitude of the TRVs produced and shown in Figure 6-3.

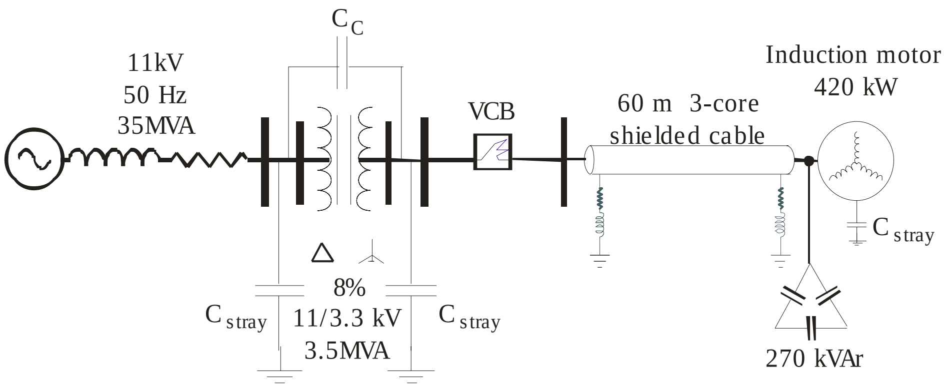

Figure 6-3 Simplified single line diagram of the supply circuit

The fault level, based on estimates from the electrical supply company, is ten times of the transformer rating and the leakage impedance of the transformer was assumed to be 8%. The nominal withstand voltage curve was set to 20kV/ms, and the nominal current quenching capability was set to 600A/µs. A range of chopping current values was used and was represented by a Gaussian distribution with a mean value of 10A and standard deviation of 15%, typical of older breakers. The cable was assumed to be a 120mm^2 PVC shielded cable. The parameters of the induction motor model were found by the method described in Chapter 3.

6.1.2 Typical results – simulation

Typical waveform of TRV and motor voltage following opening of VCB

The overvoltages generated are stochastic, and one of the typical cases (not the 'worst') is shown in Figure 6-4. The transient recovery voltage across the breaker for this case is about 3 p.u. and it comprises different frequency components. These frequency components are a result of superposition of the interaction of the capacitances and inductances in various parts of the network. The overvoltage generated at the transformer low-voltage side is about than 3.7 p.u.. Note that the delta connected power factor correction capacitors preclude high-frequency phase-to-phase oscillations.

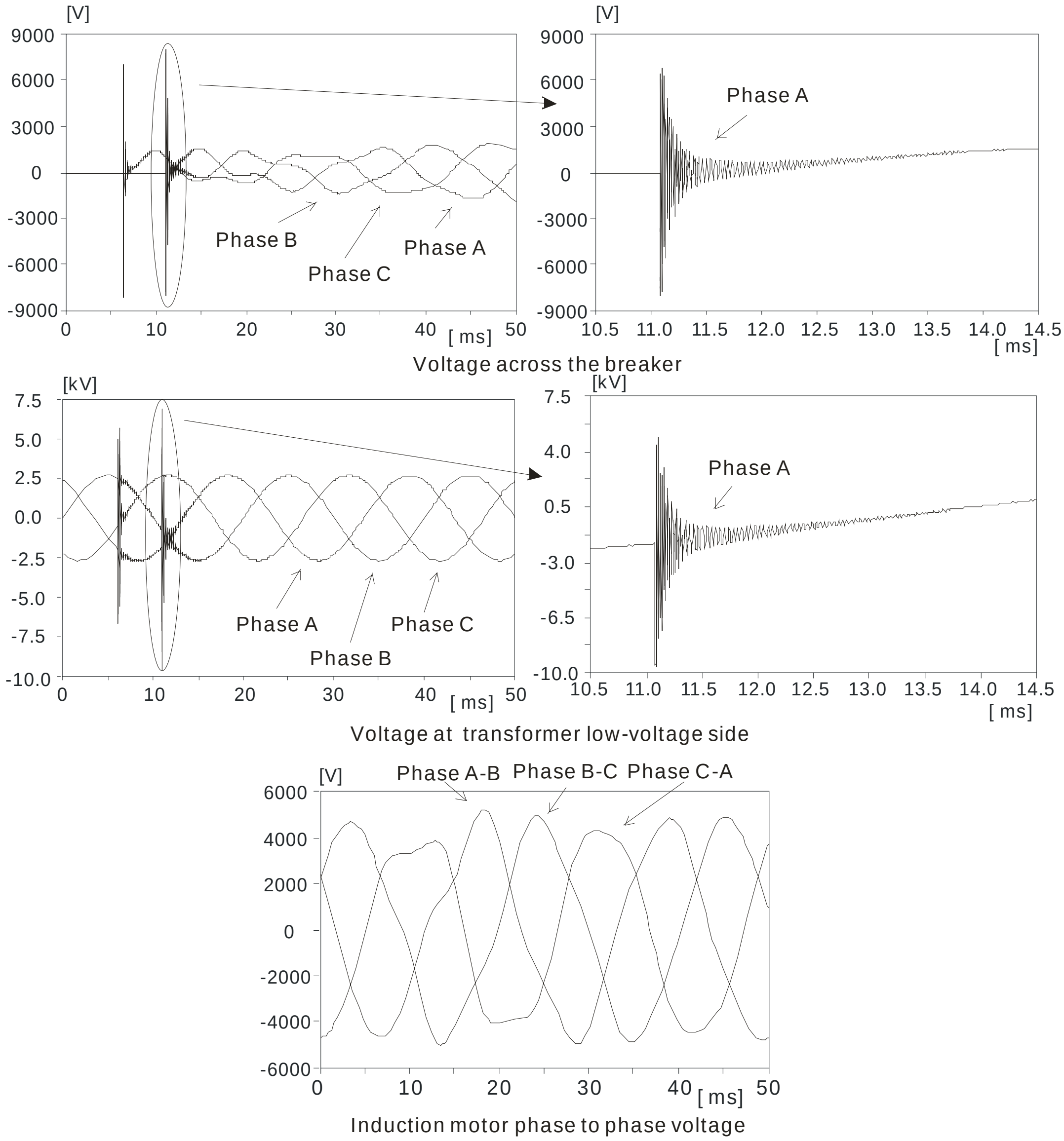

Figure 6-4 Transient voltage response at different locations without arrester connected

Had the arrester been installed correctly the overvoltages would have been reduced, as shown in Figure 6-5, where the overvoltage generated at the transformer low-voltage side is reduced to about 2.6 p.u.

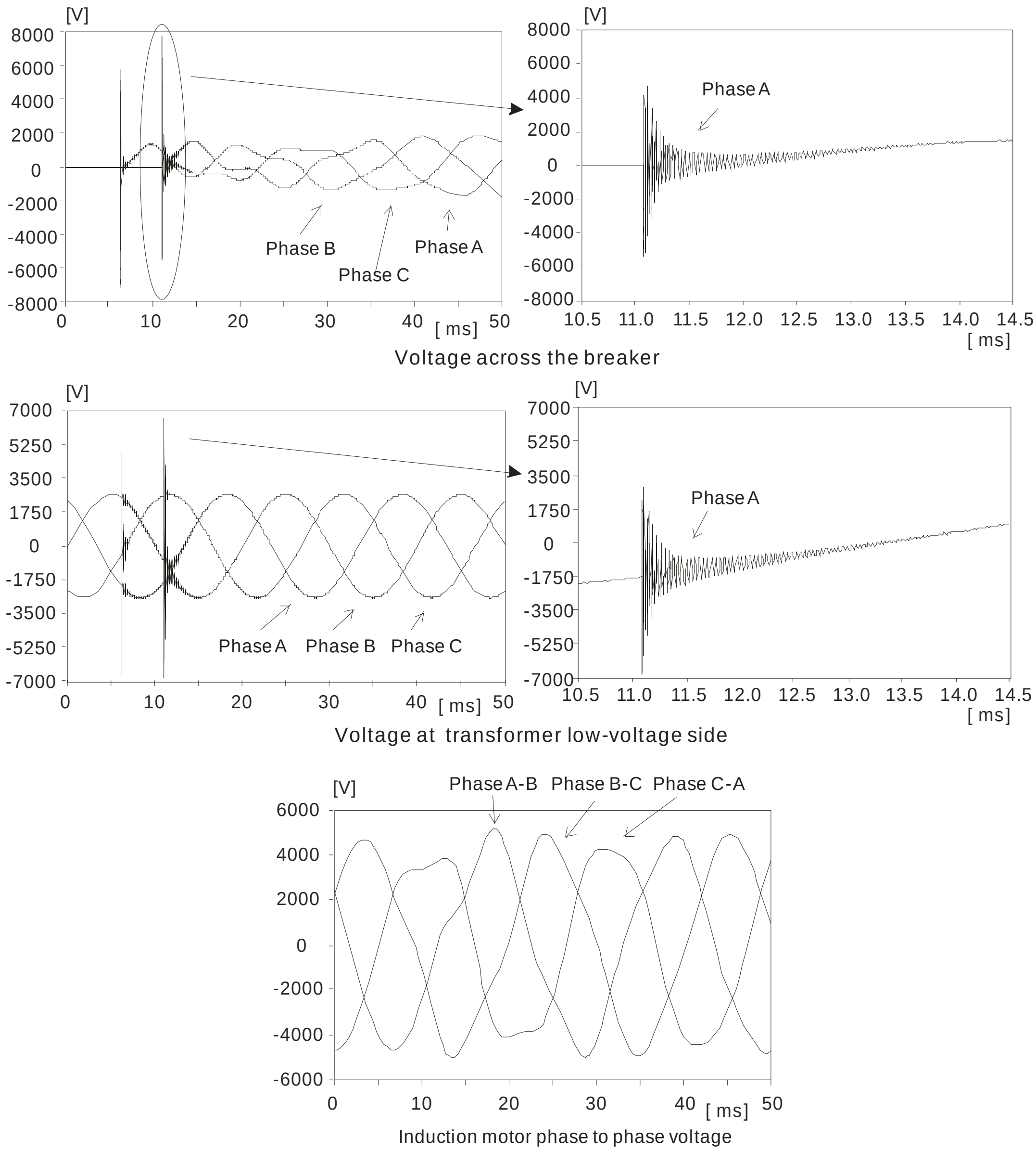

Figure 6-5 Transient voltage response at different locations with arrester connected

The simulation results show, as expected, that the chopping current level has a direct impact on the overvoltage produced on the transformer low voltage side. This is because the abrupt change of current results in energy exchange of the transformer winding leakage inductance and the stray capacitance to ground, leading to significant suppression peaks and high frequency oscillation.

6.1.3 Statistical overvoltages and risk-of-failure

Monte Carlo methods were used to determine the statistical overvoltages, and the results for various cases, with and without arresters are shown in Figures 6-6 to 6-11. Based on a sample of 100 switchings, the 2% overvoltage, V_2, was found to be some 5.9 p.u., or 15.9kV. As discussed, the transformer failed owing to a flashover of a gap between the high and low voltage leads. The 50% flashover voltage of the gap, assuming an inhomogeneous field is estimated to be some 20 kV. Assuming a standard deviation of 8%, the 90% flashover voltage, U_{90} is around 18kV. The statistical safety factor, defined as U_{90}/V_2 is thus 1.15, and this corresponds to a risk of failure of approximately 10^{-3} (IEC 1996), or one flashover of the gap in 1000 operations. The transformer was in service for some three years, and assuming at least one switching per day, the results of the study are consistent with the failure in the field.

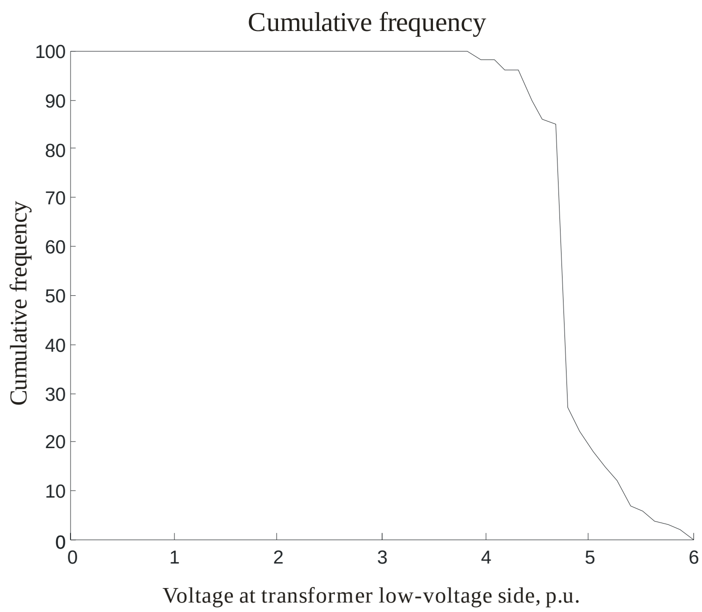

Figure 6-6 Cumulative frequency of voltage at transformer low-voltage side without arresters connected

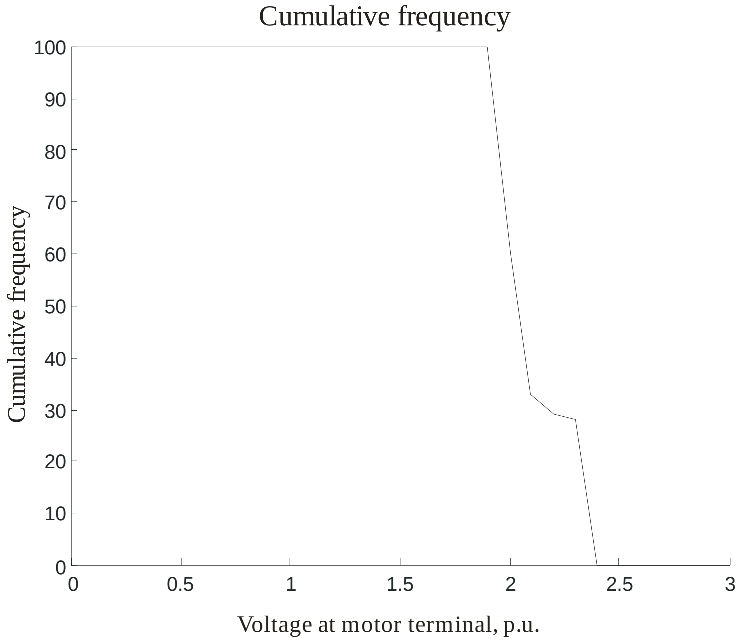

Figure 6-7 Cumulative frequency of voltage at motor terminal without arresters connected

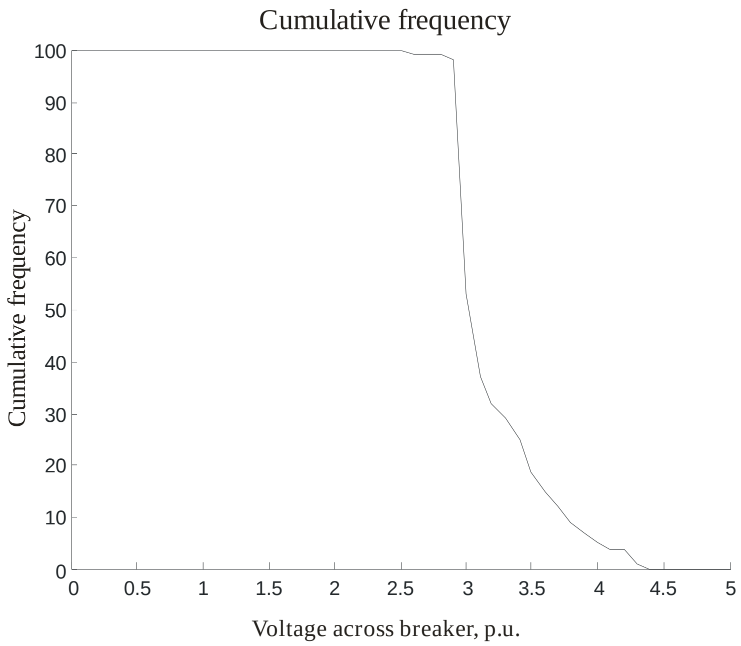

Figure 6-8 Cumulative frequency of voltage across breaker without arresters connected

Statistical overvoltages were also evaluated for the case with arresters connected properly (not the actual connection) and the results are shown in Figures 6-9, 6-10, and 6-11. For all locations, the overvoltages do not exceed 3 p.u., and it is unlikely that the transformer would have failed had the arresters been properly installed.

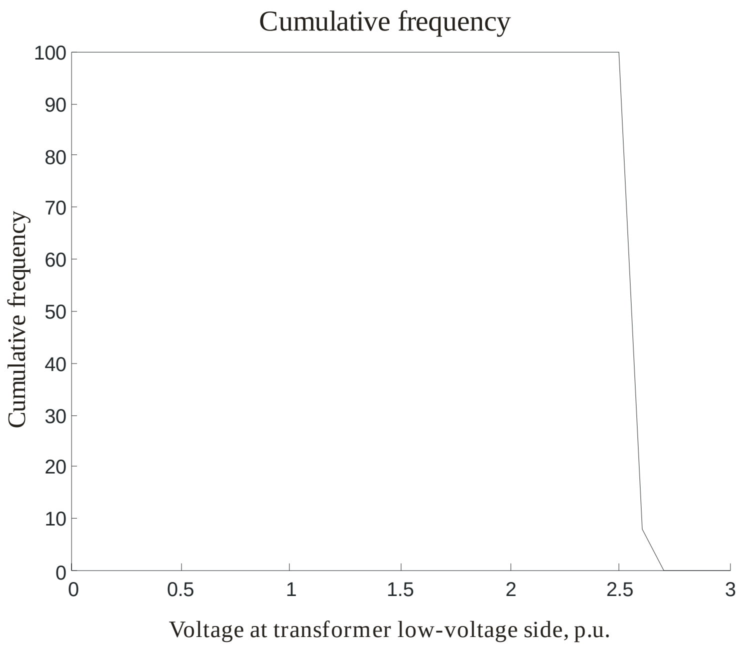

Figure 6-9 Cumulative frequency of voltage at transformer low-voltage side with arresters connected

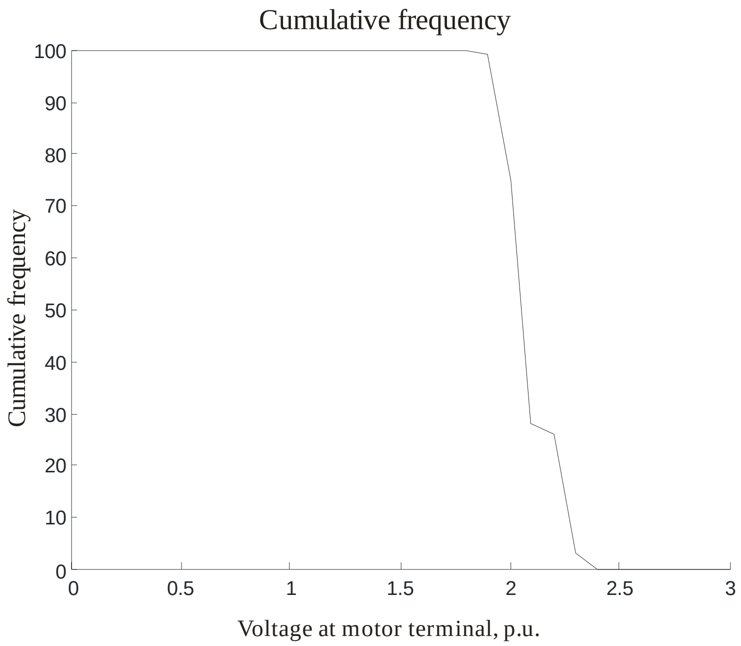

Figure 6-10 Cumulative frequency of voltage at motor terminal with arresters connected

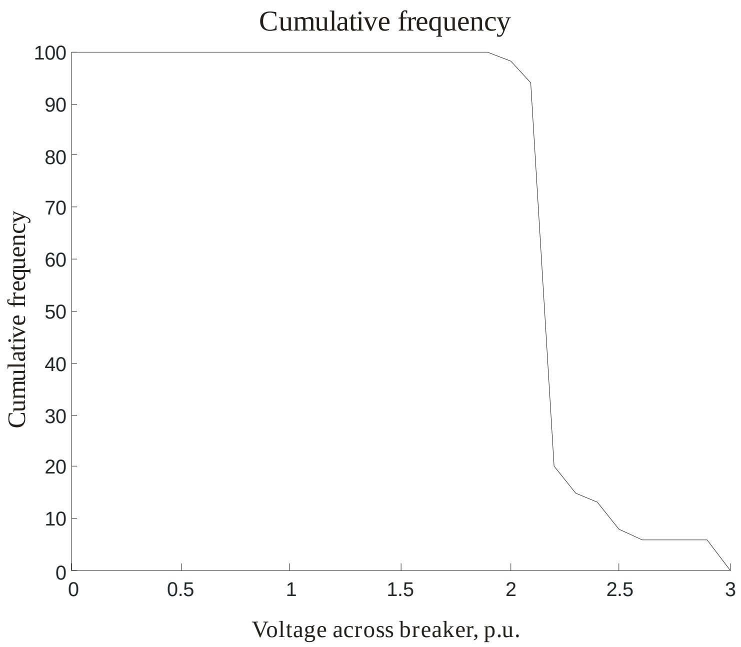

Figure 6-11 Cumulative frequency of voltage across breaker with arresters connected

6.2 INDUSTRIAL INSTALLATION IN HONG KONG –PUMP MOTORS

In this installation, the existing oil circuit breakers were to be replaced with VCBs and a study was commissioned to determine if onerous overvoltages would result from VCB switching operations, and the effectiveness of the surge protection devices proposed. The stochastic VCB model developed in this research was used in the study, as well as models of the cables, motors, transformers and surge arresters.

6.2.1 Simulation network and parameters

The general schematic diagram of the supply circuit is shown in Figure 6-12. There are totally 4 motors which can be run at the same time and only one induction motor is connected to the system in the simulation which demonstrates the overvoltage on the load side, for comparison with site measurements.

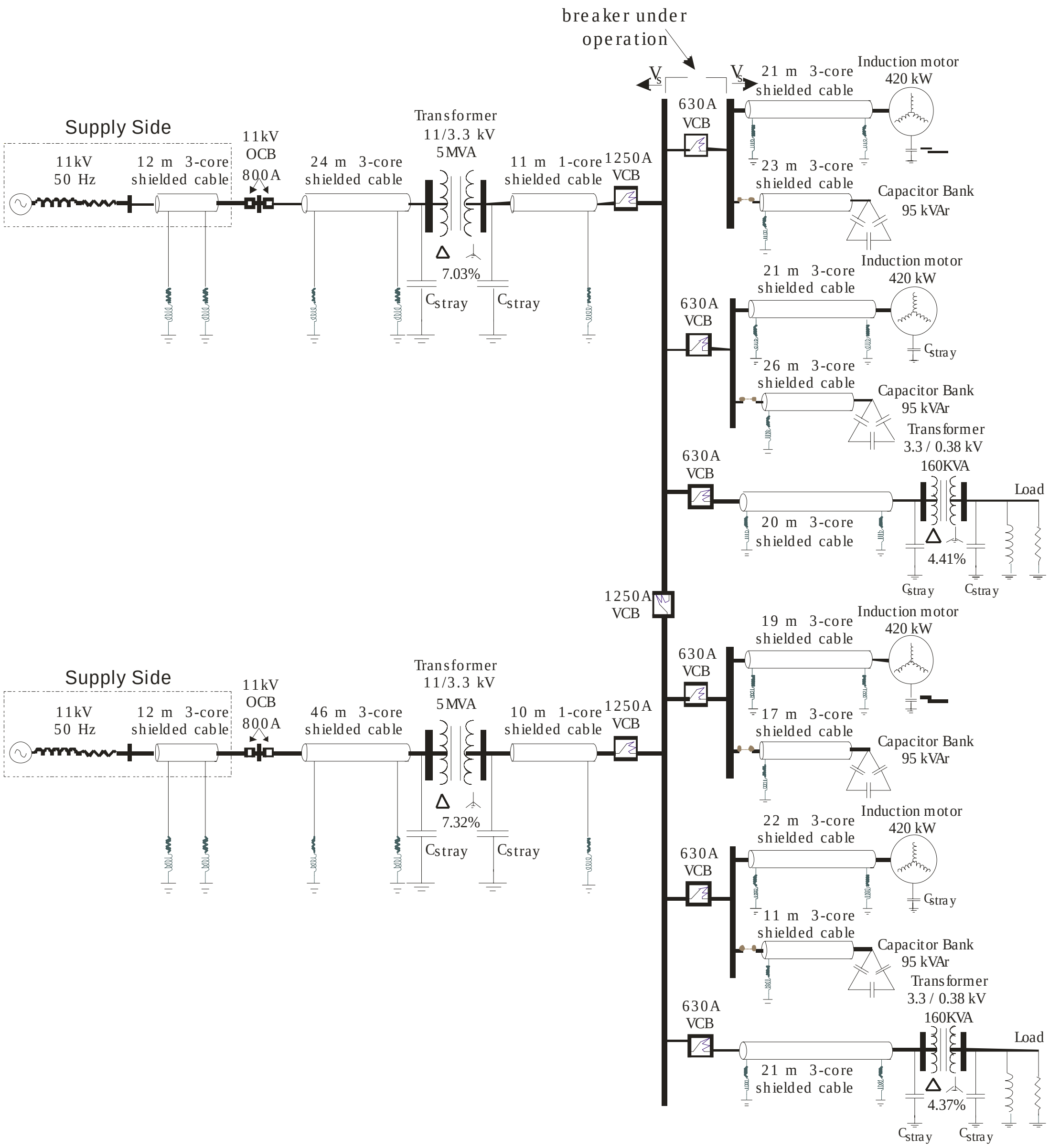

Figure 6-12 General schematic diagram of the pump motor installation

The fault level of the incoming supply points is given as 350MVA. The configuration and the length of cables used in the network are shown in Table 6-1.

Cable Circuit		No., core No., Size, Type of cables	Measured diameter of cables	Length of cables
From	To			
11kV incoming supply point	Station transformer 11 kV cable box termination	1 No. 3/C 400mm^2 PILC / SWA / PVC	75mm	36m
3.3 kV cable box termination of station transformer	Cable box termination of VCB incoming supply	6 Nos. 1/C 630mm^2 PILC / AWA / PVC	50mm	11m
Cable termination of VCB panel	Cable box termination of motor	1 No. 3/C 120mm^2 PVC / SWA / PVC	40mm	21m
Cable termination of VCB panel	Capacitor bank termination	1 No. 3/C 120mm^2 PVC / SWA / PVC	40mm	23m
Cable box termination of VCB station auxiliary transformer	Cable box terminal of station auxiliary transformer	1 No. 3/C 120mm^2 PVC / SWA / PVC	40mm	20m

Table 6-1 Configuration of cables

The incoming transformers in the simulation are 5MVA, delta/wye, 11kV/3.3kV with leakage impedance 7.03%. The auxiliary transformers in the simulation are 160kVA, delta/wye, 3.3kV/380V with leakage impedance 4.41%. The corresponding parameters are shown in Table 6-2 and Table 6-3 respectively based on the factory test report of the transformers given by the manufacturer.

Leakage impedance	7.03%
Resistance across magnetizing branch: Rmag (High frequency model)	50kΩ
Primary leakage resistance: R_p	0.2539Ω
Primary leakage inductance: L_p	8.0826mH
Secondary leakage resistance: R_s	$7.618 \times 10^{-3}\Omega$
Secondary leakage inductance: L_s	0.24248mH
First knee point: I / ϕ pair	1.072A / 49.52 Vs
Rated voltage at primary side	11kV
Rated voltage at secondary side	1.905kV

Table 6-2 Parameters of incoming transformer model

Leakage impedance	4.41%
Resistance across magnetizing branch: Rmag (High frequency model)	50kΩ
Primary leakage resistance: R_p	0.448Ω
Primary leakage inductance: L_p	16.26mH
Secondary leakage resistance: R_s	1.98 x 10-3Ω
Secondary leakage inductance: L_s	0.063mH
First knee point: I / ϕ pair	1.072A / 49.52 Vs
Rated voltage at primary side	3.3kV
Rated voltage at secondary side	220V

Table 6-3 Parameters of auxiliary transformer model

The relevant parameters for modelling the VCB were supplied by the manufacturer and are shown in Appendix F. These parameters include the nominal chopping current value, dielectric strength characteristic of the gap and the quenching capability of the high frequency current. The chopping current value is represented by a Gaussian distribution with 15% standard deviation from 8A which was provided by the manufacturer.

The dielectric strength curves supplied by the manufacturer do not suggest a linear relationship between arcing time (i.e. contact distance) and dielectric strength. Indeed, the withstand voltage reaches a maximum value after around 5mm of separation for the breaker with 630A rated current and some 10 mm of separation for breaker with 1250A rated current. The withstand curves are shown in Figures 6-13 and 6-14.

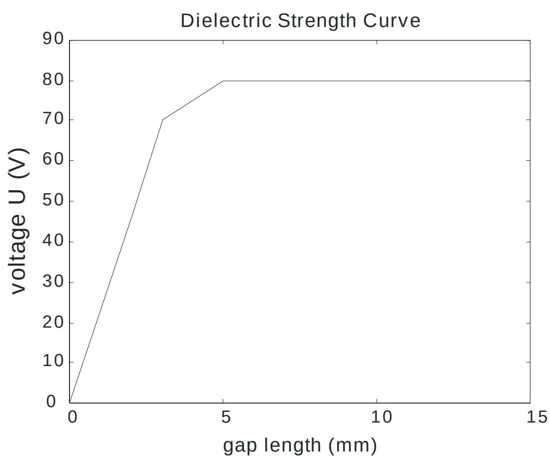

Figure 6-13 630 A rated current

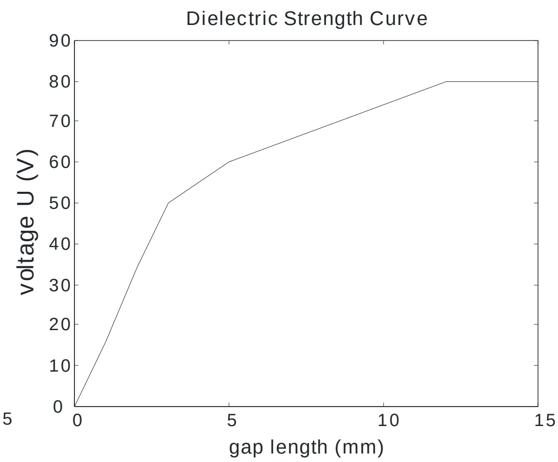

Figure 6-14 1250 A rated current

As shown in the figures the dielectric strength can be approximated by a linear relation in the first few microseconds. After that the curves reach a ‘saturation’ value.

This suggests that in this case there exists a chance the breaker can never be successfully opened after a certain duration.

From the information given by the manufacturer, the quenching capability of high frequency current at zero crossing of VCB is 400 A/μs and 100 A/μs for the breaker with 630A rated current and that with 1250 A rated current respectively.

The parameters of the high frequency model of the induction motor were calculated based on the method described in Chapter 3. The parameters of the d-q model were found based on the data sheet of the induction motor provided by the manufacturer. R_e, which represents the damping of the high frequency branch was 3kΩ, and C_g, which represents the winding-to-ground capacitance was 3.2nF.

A linear load of 80kVA with 0.8 power factor is assumed at the secondary side of the 160kVA station auxiliary transformers: it was assumed that during normal operation, the secondary side of the transformer should not be under full load or no load operation, consequently half load operation is assumed. The capacitor value for the capacitor bank is equivalent to 95kVAr and 210kVAr rating for low speed motor and high speed motor respectively. The characteristics of the arrester were obtained from the manufacturer's data sheets, and the V/I curve is shown in Appendix F.

6.2.2 Field measurements – period and set up

Field measurements were performed in August 2003 to September 2003 for the Low Speed (LS) operation of Motor #4, and on 10 March 2004 for the High Speed (HS) operation of Motor #4. Two measurements were taken for the high speed operation, while several were carried out for low speed operation.

A Hioki Recorder 8855 together with two high voltage (HV) probes was used for the measurements. The voltages probes were attached to the R-phase and Y-phase on load side of the associated VCB of Motor #4. Figure 6-15 shows the connections of the two high voltage probes onto the cable terminals at the back of the VCB. Both HV probes have a ratio of 1000:1 with a bandwidth of more than 1 MHz for 3.3 kV input. And the current probe has a ratio of 1V:100A. Figure 6-16 shows the overall arrangement of the setup.

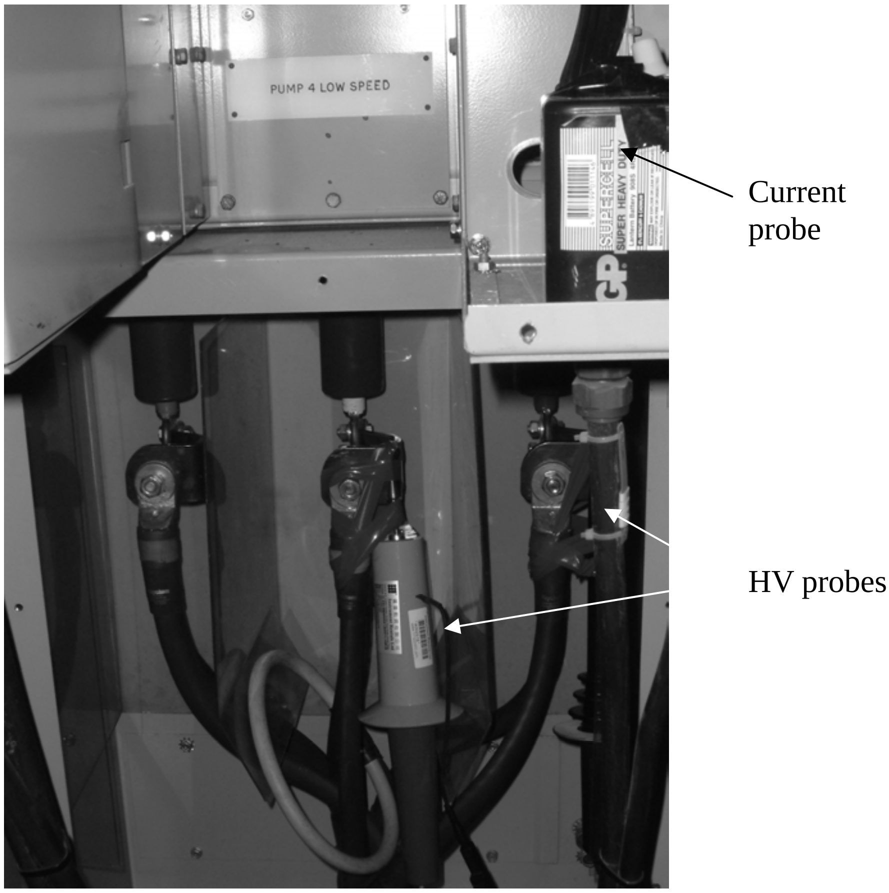

Figure 6-15 The connection of the two HV probes and the current probe onto the cable terminals at the back of the VCB

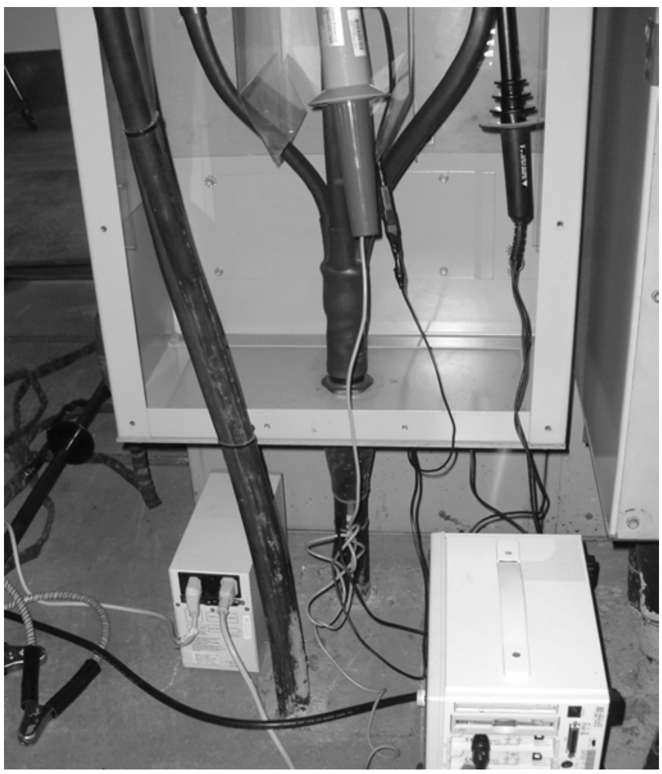

Figure 6-16 The overall arrangement of the setup

6.2.3 Simulation results

Typical waveform of TRV and motor voltage following opening of VCB

The overvoltages generated are stochastic, and one of the typical cases is shown in Figure 6-17. The TRV is small and as expected comprises different frequency components. The figure also shows the induction motor single phase voltage. The maximum magnitude is lower than 1.2 p.u.

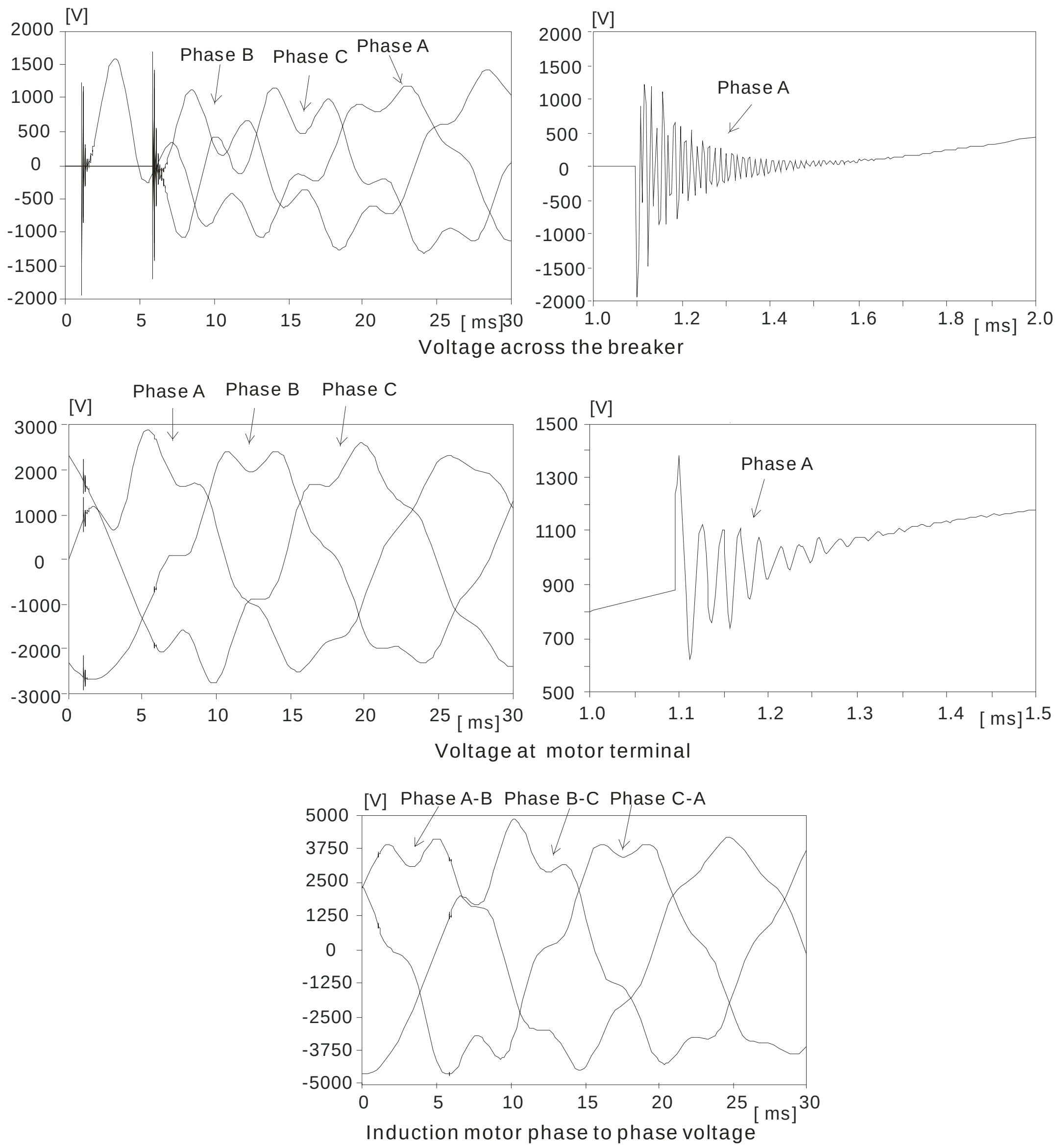

Figure 6-17 Transient voltage response at motor terminal and across the breaker with running motor

Disconnection of starting induction motor

The study has shown that the switching the VCB with starting motor generated onerous overvoltages. Typical voltage waveforms related to switching at motor starting are shown in Figure 6-18. The results show that the overvoltages resulting from current chopping following opening of the VCB can build up to 3 p.u..

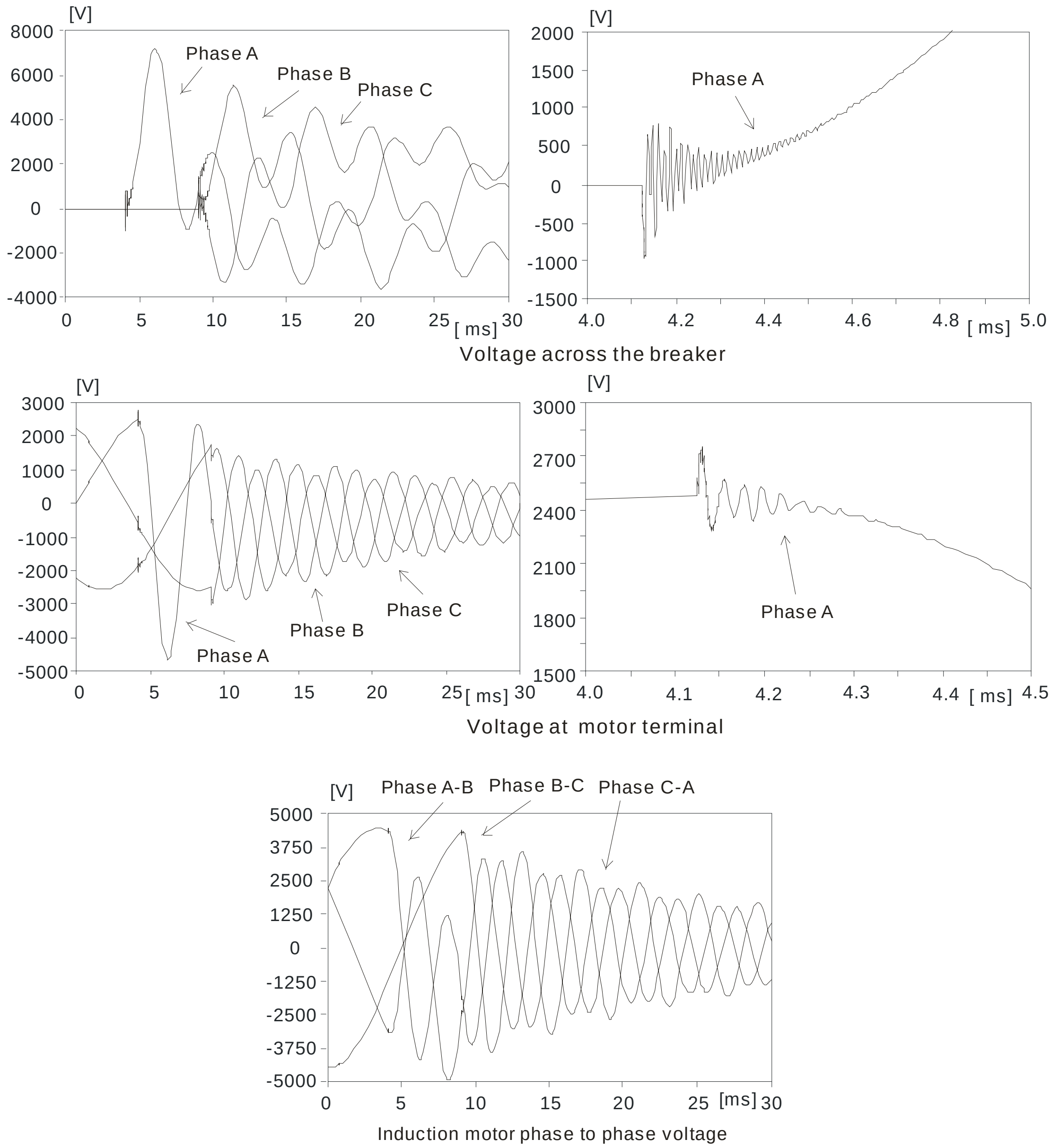

Figure 6-18 Transient voltage response at motor terminal and across the breaker with starting motor

Disconnection of power factor capacitors

The study has shown that with the power factor correction capacitors connected the VCBs will not generate onerous overvoltages. However if the capacitor bank is not connected high overvoltages are likely. Typical voltage waveforms from the study without the capacitor banks connected are shown in Figure 6-20. The results show that the overvoltages resulting from current chopping following opening of the VCB can build up to 5 p.u. However, when a 3 kV rated arrester is connected at the load side of the VCB (as shown as Figure 6-19), the overvoltages are limited to less than 2 p.u..

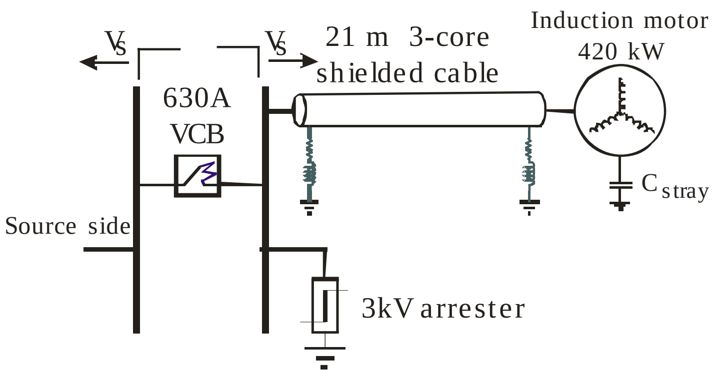

Figure 6-19 Single line diagram of the circuit without the capacitors

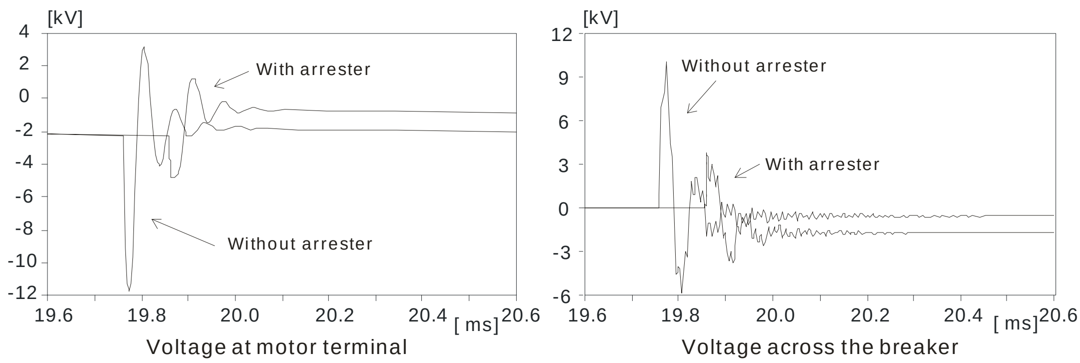

Figure 6-20 Transient voltage response at motor terminal and across the breaker without capacitors

6.2.4 Comparison of simulation results with field measurements

A typical result from field measurements is shown in Figure 6-21. This shows some high frequency ringing of very small magnitude at the point of switching OFF, and again some low frequency (several hundred Hz) voltage distortions around the switching OFF point. The waveform of simulation result is shown in Figures 6-22. For both cases, current chopping was shown to result in high frequency, low magnitude voltage ringing at the point of current chopping, followed by some low frequency (in the order of several hundreds of Hz) voltage distortion of moderate magnitude.

The simulation results for the switching of the induction motors compare well with the field measurements. For the low frequency voltage distortions, the waveforms produced by both simulation and field measurements are very close in both magnitude and frequency.

For the high frequency ringing, the simulation results give somewhat higher magnitudes, which, however, are not onerous and would not overstress the motor. The differences are to be expected, since simulation in a high bandwidth simulation the damping of the high frequency phenomena are usually understated. Furthermore, the measurement results are limited by the bandwidth of the measuring system, and the magnitudes of the high frequency ringing are also probably understated. Overall, however, the comparison of the field and simulation results is quite good.

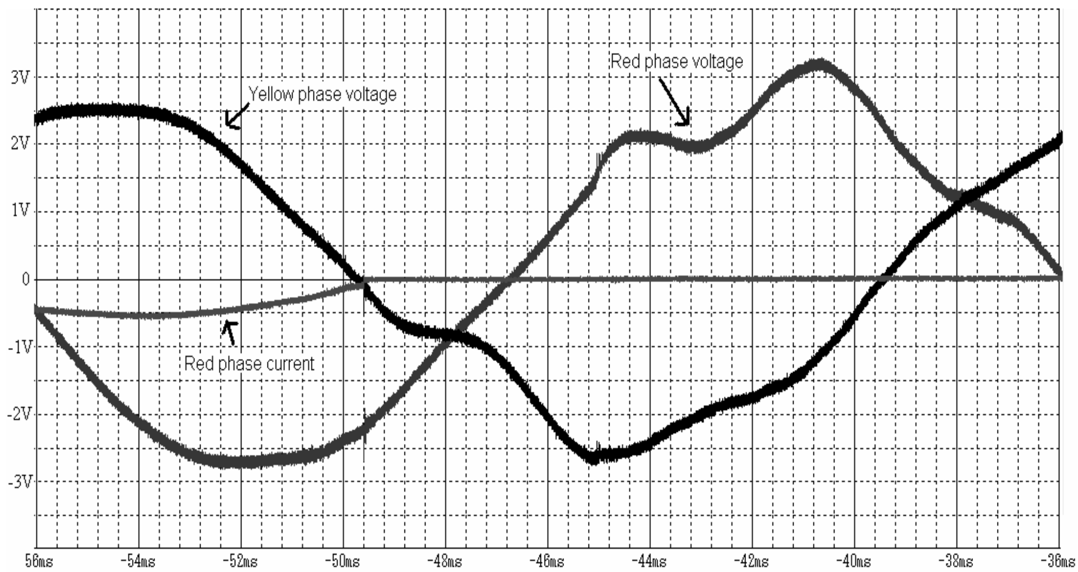

Figure 6-21 Field test results – voltage at load side of the breaker (Ratio of HV probe – 1000:1)

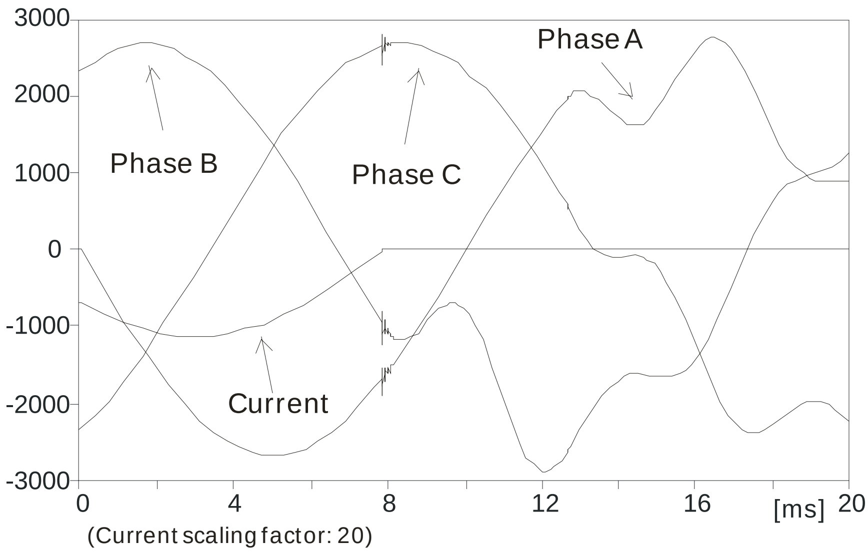

Figure 6-22 Simulation results – voltage at load side of the breaker

6.2.5 Statistical overvoltages

Monte Carlo methods were used to determine the statistical overvoltages. The distribution curves of statistical overvoltages at different locations for the case with the power factor correction capacitors are shown in Figures 6-23 and 6-24. The presence of the power factor correction capacitors limits the overvoltages. For both the TRV and the voltage at motor terminal, the overvoltages do not exceed 2 p.u..

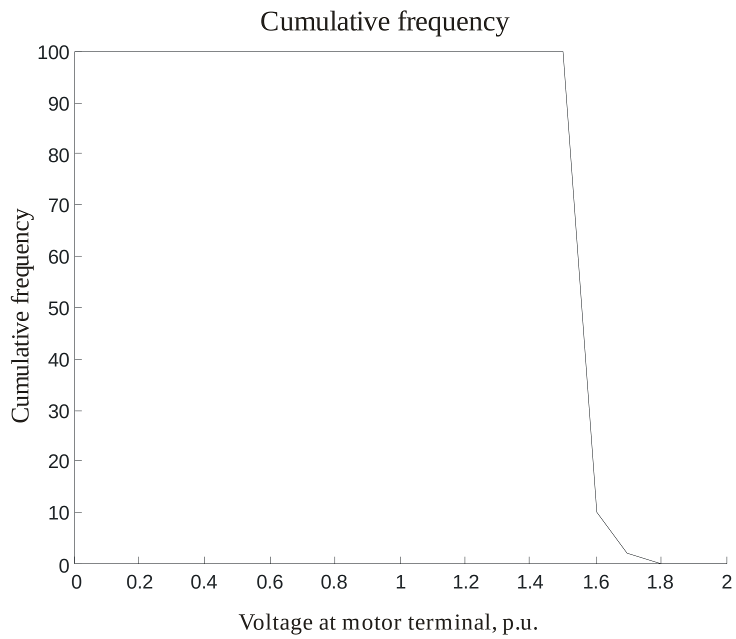

Figure 6-23 Cumulative frequency of voltage at motor terminal with the power factor correction capacitors

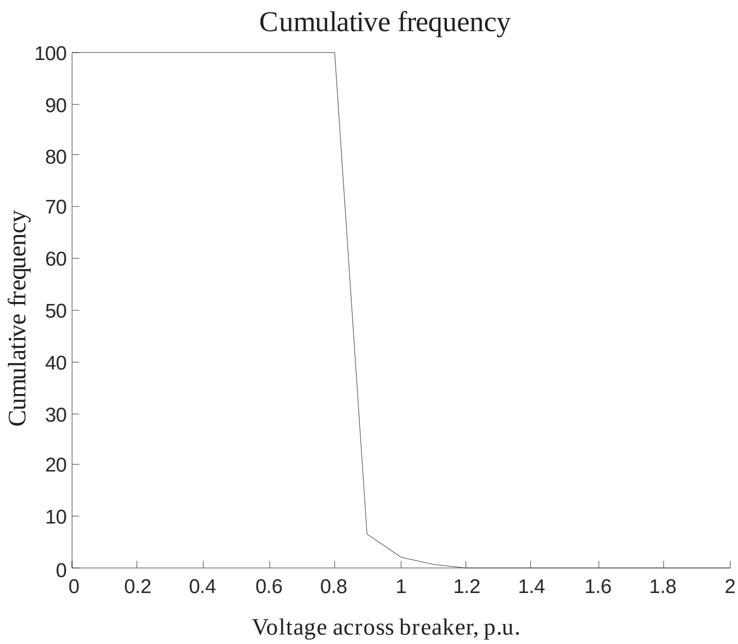

Figure 6-24 Cumulative frequency of voltage across breaker with the power factor correction capacitors

Statistical overvoltages were also determined for cases without power factor correction capacitors and the results are shown in Figures 6-25 and 6-26. As shown in Figure 6-25, the 50% overvoltages is around 4 p.u. at the motor terminal and results for the TRV are similar. Consequently, without the presence of the power factor correction capacitors severe overvoltages may occur.

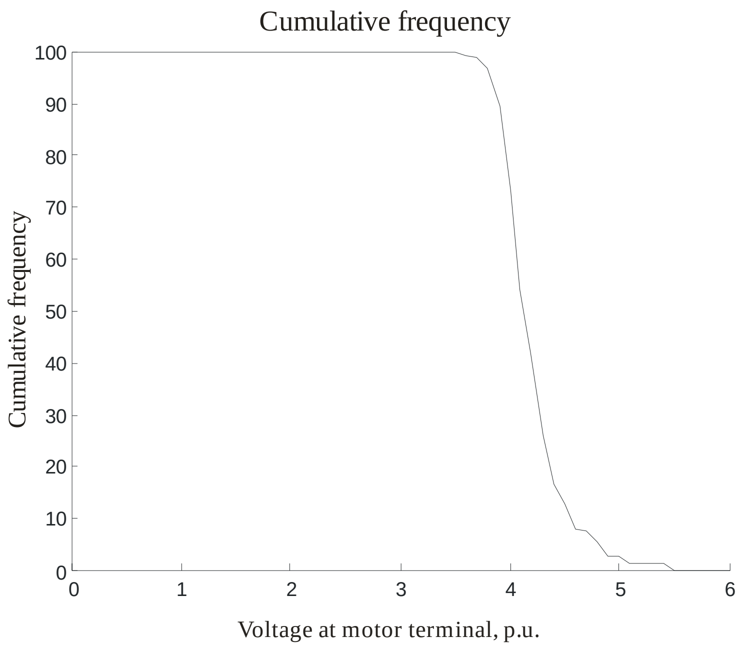

Figure 6-25 Cumulative frequency of voltage at motor terminal without power factor correction capacitors

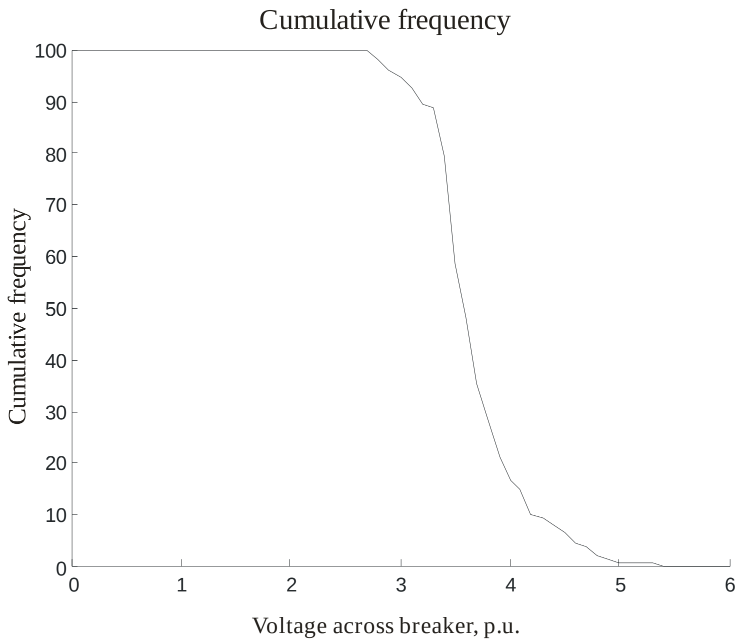

Figure 6-26 Cumulative frequency of voltage across breaker without power factor correction capacitors

Moreover, statistical overvoltages were determined for the case without the power factor correction capacitors but with arresters connected at the motor terminal. The results are shown in Figure 6-27 and 6-28. For all locations, the overvoltages generated do not exceed 3.5 p.u..

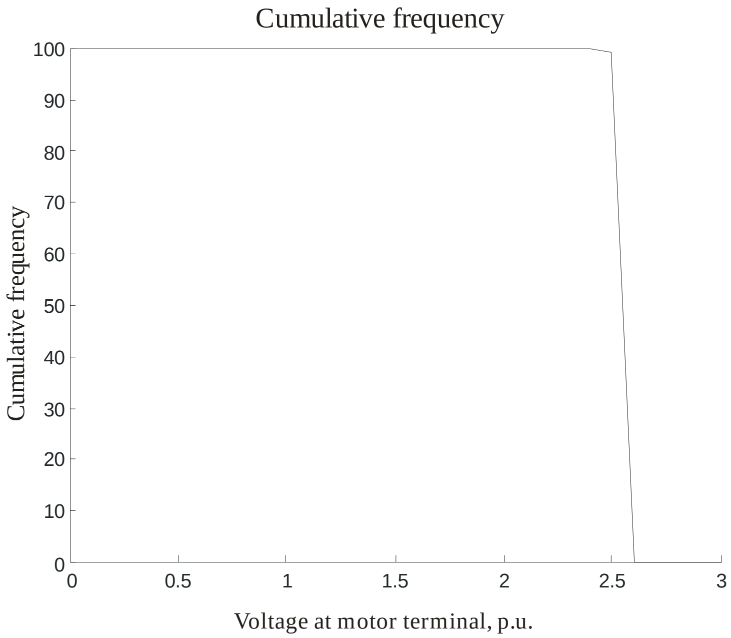

Figure 6-27 Cumulative frequency of voltage at motor terminal without the power factor correction capacitors but with arresters connected

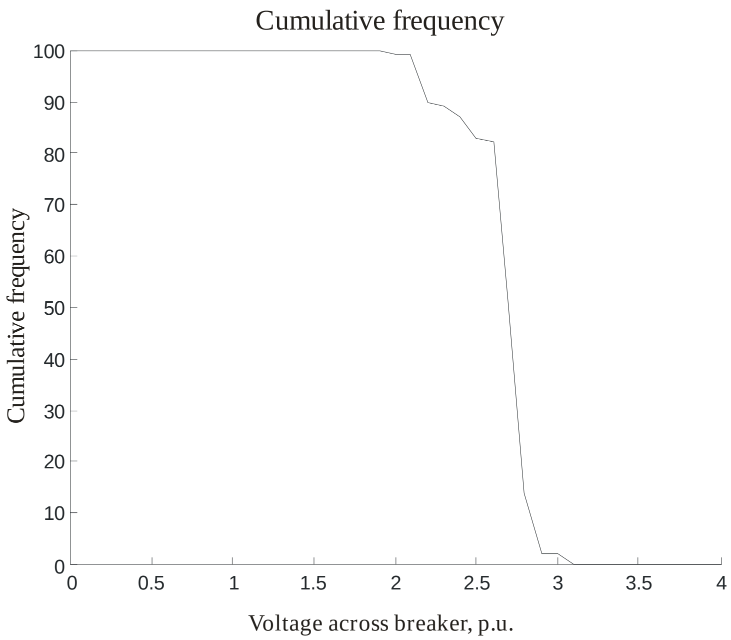

Figure 6-28 Cumulative frequency of voltage across breaker without the power factor correction capacitors but with arresters connected

Additionally, statistical overvoltages were determined for the case of motor starting. Figures 6-29 and 6-30 show the cumulative frequency curves of the voltage at motor terminal and the TRV with power factor correction capacitors. The overvoltages generated are more severe than the case with the running motor. The overvoltage at motor terminal is less than 3 p.u. and the TRV overvoltages does not exceed 4 p.u..

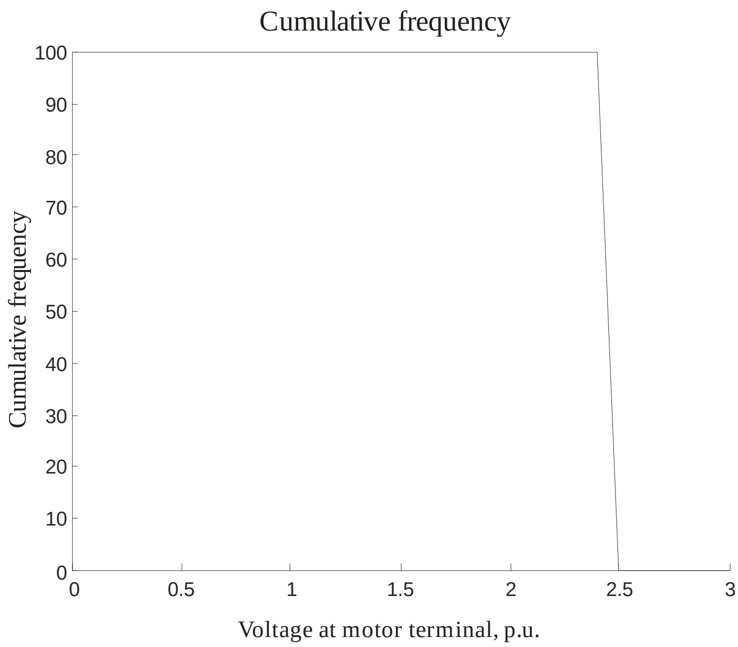

Figure 6-29 Cumulative frequency of voltage at motor terminal with power factor correction capacitors with starting motor

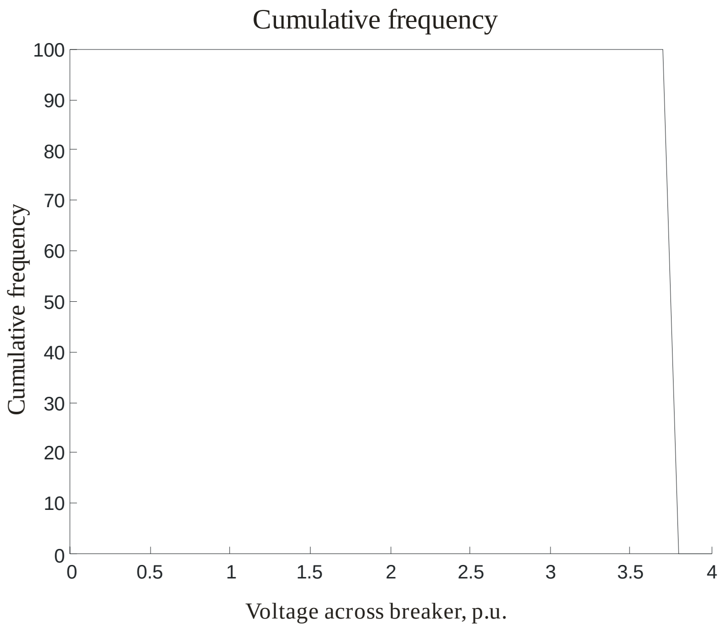

Figure 6-30 Cumulative frequency of voltage across breaker with power factor correction capacitors with starting motor

Figure 6-31 and 6-32 show the results of cases without power factor correction capacitors. As shown in Figure 6-31, the 50% overvoltages are around 4 p.u. at the motor terminal and results for the TRV are similar. The 2% overvoltage is more than 12 p.u. in both locations. When compared to the same case with the running motor, more severe overvoltages occur.

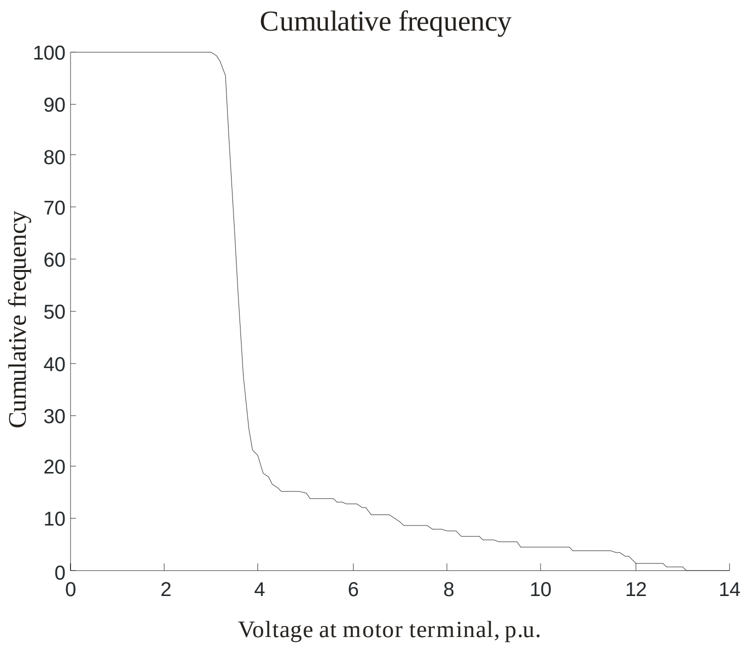

Figure 6-31 Cumulative frequency of voltage at motor terminal without power factor correction capacitors with starting motor

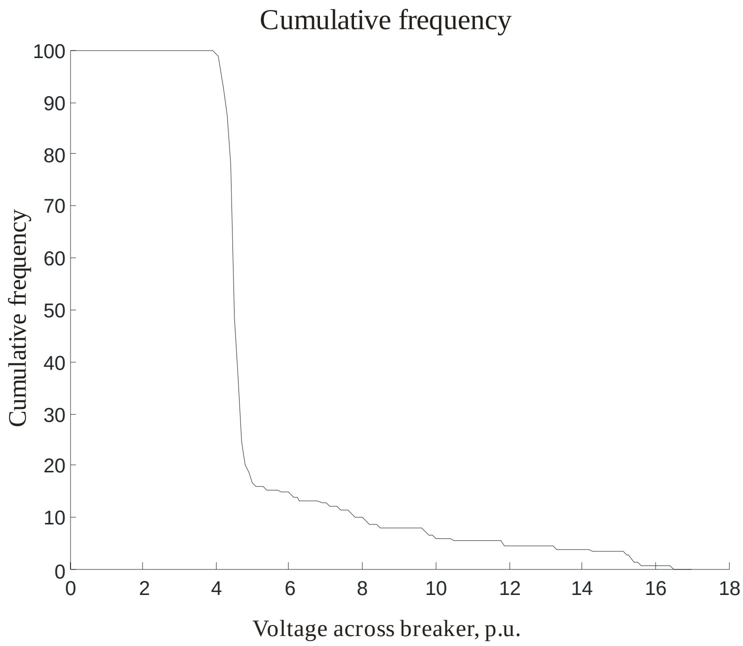

Figure 6-32 Cumulative frequency of voltage across breaker without power factor correction capacitors with starting motor

Finally, statistical overvoltages were studied for the case without the power factor correction capacitors but with arresters connected at the motor terminal. The results are shown in Figure 6-33 and 6-34. The overvoltage at motor terminal is limited to less than 4 p.u. and the TRV overvoltage does not exceed 9 p.u..

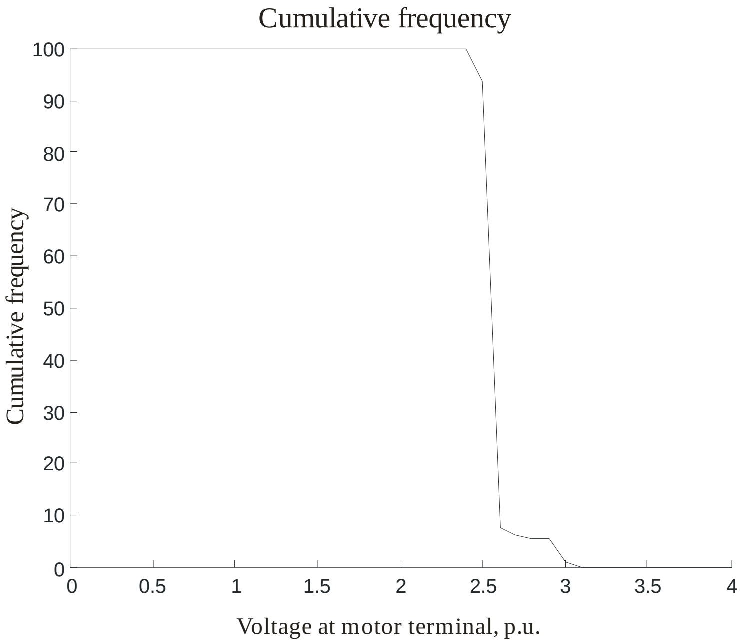

Figure 6-33 Cumulative frequency of voltage at motor terminal without power factor correction capacitors but with arresters connected with starting motor

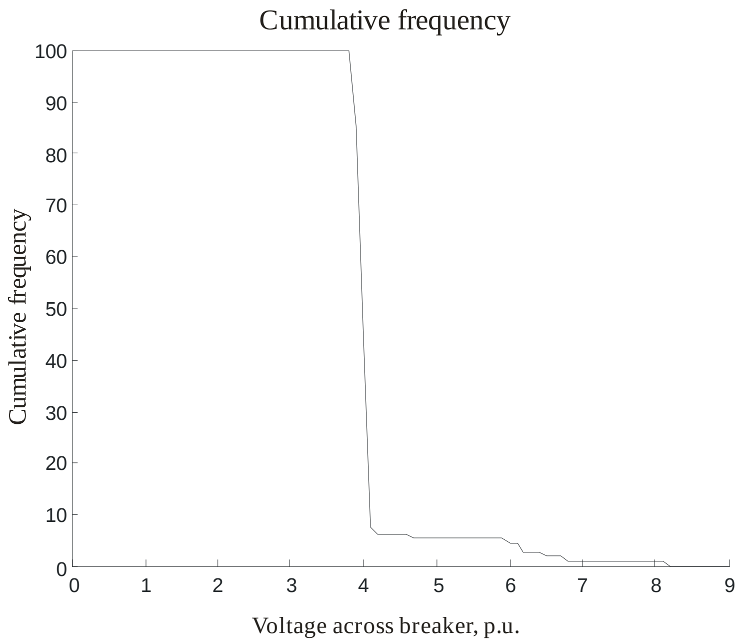

Figure 6-34 Cumulative frequency of voltage across breaker without power factor correction capacitors but with arresters connected with starting motor

CHAPTER 7 CONCLUSIONS

In this research, a stochastic model of vacuum circuit breakers was developed and used in EMTP to study system overvoltages resulting from virtual current chopping. The statistical properties of the arcing time, chopping current, dielectric strength, and quenching capability were taken into account.

Other circuit element models, induction motors, transformers and cables, which are required to represent the correct propagation media and termination impedances for incoming surges were also developed. They were incorporated for the studies of switching overvoltages and these models reflect the required termination impedance at both operating frequency and high frequencies.

Forty-eight breaker models were applied to study the TRV generated under different switching conditions with an evaluation circuit. Monte Carlo methods were used, with 100 shots for each of the cases. Some combinations of the breaker characteristics lead to reignition/voltage escalation problems. For example, high escalation voltages were found to be more likely to occur when the arcing time was short, or the rate of change of the dielectric strength was in the middle range, or the termination mode was mode A (successfully interrupt at the end of the high frequency reignition sequence), or if the quenching capability decreased with time.

The results of the statistical TRV calculation show that the rate-of-change of the dielectric strength and the arcing time of the breaker are the most important factors for the estimation of the TRV, while the influence of the quenching capability on the escalation voltage is less pronounced. It was suggested to consider the middle range of the rate-of-change of the dielectric strength to look for the worst case in order to provide the most appropriate protection scheme when estimating the overvoltages resulting from the operation of vacuum circuit breakers.

Parametric sensitivity studies were performed in order to determine parameters and combinations of parameters most likely to lead to onerous overvoltages. The results presented have shown that the most significant factor governing the severity of overvoltages generated is the operating mode of the motor at the time of switching.

When switching off a starting induction motor, onerous overvoltages can occur. Also, the shorter the cable connecting to the motor to the breaker, the more severe the overvoltages generated. On the other hand, the presence of the power factor correction capacitors precludes the production of serious overvoltages.

The effects of the short circuit ratio, transformer connection, grounding practices of the cable sheath, length of the cable connecting the motor to the power factor correction capacitors and the rating of the power factor correction capacitors on the overvoltages severity were found to have less impact.

The performances of different protection measures were evaluated. It was found that the most effective way of reducing overvoltages is through the connection of an arrester across the breaker. The results also demonstrate the importance of the location and installation method of the protective devices. Even with short lead lengths, the fast-front overvoltages generated by the breaker can result in a protective level higher than the clamping voltage of the arrester at the terminals of the equipment.

Two case studies were carried out based on typical industrial installations in Hong Kong. The statistical overvoltages generated at the low-voltage side of a transformer which failed after the opening operation of a VCB in a paper mill were found to be significantly high. An evaluation of the risk-of-failure, based on an approximation of the breakdown voltage of the gap where the flashover occurred resulted in an estimate of one failure per 1000 operations. The transformer was in service for some three years, and assuming at least one switching per day, the results of the study are consistent with the failure in the field.

Another study dealing with VCB switching of pump motors indicated that statistical phase-to-ground overvoltages were as high as 6 p.u. when the power factor capacitor were not connected and overvoltage protection is required. While capacitors are usually found near large induction motors, smaller motors and transformers may need overvoltage protection. In general, it is prudent to install surge arresters to protect against unforeseen events. Field measurements of the switching overvoltages were made in this study and the measured waveforms compared well with the corresponding waveforms obtained from the simulation results, and this serves to verify the model. The simulation gave somewhat more pessimistic results, however even the pessimistic results indicate that the vacuum circuit breakers do not produce onerous overvoltages in this installation, largely because of the presence of the power factor correction capacitors.

In summary, the main contributions in this thesis are (i) the development of improved stochastic models of vacuum circuit breakers, (ii) the development of hybrid models of induction motors and transformers valid over a wide bandwidth, (iii) parametric sensitivity studies, including effects of cable and motor grounding, power factor correction, cable lengths, etc, (iv) stochastic studies aimed at determining representative overvoltages in industrial power delivery networks, and (v) evaluation of the effectiveness of overvoltage protection measures. Future work should be aimed at obtaining more field results, which would help with further refinement of the models.

REFERENCE

[1] Avila-Rosales, J. and Alvarado, F. L., "Nonlinear frequency dependent transformer model for Electromagnetic Transient studies in power systems," IEEE Transactions on Power Apparatus and Systems, Vol. PAS-101, No.11, November 1982, pp.281-288

[2] Benn, L. C., Buton, B. and Harley, R. G.., "Online converter fed induction motor impulse response identification and parameter extraction using pseudorandom modified PWM," Diagnostics for Electric Machines, Power Electronics and Drives 2003, Atlanta, 24-26 Aug. 2003, pp.70 - 75

[3] Boglietti, A. and Carpaneto, E., "Induction motor high frequency model," Industry Applications Conference, 1999. Thirty-Fourth IAS Annual Meeting Conference Record of the 1999 IEEE, Volume: 3, 3-7 Oct. 1999, pp.1551 -1558

[4] CIGRE W. G. 33.02, Internal Overvoltages, "Guidelines for representation of network elements when calculating transients," 1994

[5] Chaly, A. M. and Chalaya, A. T., "The influence of a vacuum circuit breaker and circuit parameters on switching overvoltages generated during interruption of starting motors," IEEE 17th International Symposium on Discharges and Electrical Insulation in Vacuum, Berkeley, 1996, pp. 244 - 248

[6] Chimklai, S. and Marti, J. R., "Simplified three phase transformer model for electro magnetic transients study," IEEE Transaction on Power Delivery, Vol. 10, No. 3, July, 1995, pp.1316 – 1325

[7] Colombo, E., Costa, G. and Piccarreta, L., "Results of an investigation on the overvoltages due to a vacuum circuit breaker when switching an H.V. motor," IEEE Transaction on Power Delivery, Vol 3, No.1 , January 1988, pp.205-213

[8] deLeon, F. and Semlyen, A., "Reduced order model for transformer transients," IEEE Transaction on Power Delivery, Vol. 7, No.1, January 1992, pp.361-369

[9] Dick, E. P., Gupta, B. K., Pillai, P., Narang, A. and Sharma, D. K., "Equivalent circuits for simulating switching surges at motor terminals," IEEE Transactions on Energy Conversion, Vol. 3, No. 3, September 1988, pp.696-704

[10] Dommel, H. W., "EMTP theory book volume 1," Bonneville Power Administration, August 1986

[11] Eichenberg, J. P., Hennenfent, H. and Lilijestrand, L., "Multiple restrikes phenomenon when using vacuum circuit breakers to start refiner motors," Pulp and Paper Industry Technical Conference, Maine, June 1998, pp.266-273

[12] Glinkowski, M. T., Gutierrez, M. R. and Braun, D., "Voltage escalation and reignition behavior of vacuum generator circuit breakers during load shedding" IEEE Transactions on Power Delivery, Vol. 12, No. 1, January 1997, pp.219-226

[13] Grandi, G., Casadei, D. and Massarini, A., "High frequency lumped parameter model for AC motor windings," Proc. EPE'97, Vol.2, Trondheim, Norway, 1997, pp.578 – 583

[14] Greenwood, A. and Glinkowski, M., "Voltage escalation in vacuum switching operations," IEEE Transactions on Power Delivery, Vol. 3, No. 4, October 1988, pp. 1698-1706

[15] Greenwood, A. and Glinkowski, M., "Some interruption criteria for short high-frequency vacuum arcs," IEEE Transactions on Plasma Science, Vol. 17, No. 5, October 1989, pp.741-743

[16] Greenwood, A., "Vacuum switchgear," IEE Power Series 18, 1994

[17] Helmer, J. and Lindmayer, M., "Mathematical modelling of the high frequency behaviour of vacuum interrupters and comparison with measured transients in power systems," IEEE 17th International Symposium on Discharges and Electrical Insulation in Vacuum, Berkeley, 1996, pp.323-331

[18] IEC standard 60664-1, "Insulation coordination for equipment within low voltage systems," April 2000

[19] IEC standard 71-2, "Insulation Co-ordination – Part 2: Application guide", August 1996

[20] IEEE Working Group 15.08.09, "Power system overvoltages: Analysis, modelling and case studies (video) 1999," IEEE Power Engineering Society Summer Meeting

[21] Keradec, J. P., “Equivalent circuit for coupled multi-layers transformer,” Journal of Physic. France 4, April 1994, pp.751 – 773

[22] Kosmac, J. and Zunko, P., “A statistical vacuum circuit breaker model for simulation of transient overvoltages” IEEE Transactions on Power Delivery, Vol. 10, No. 1, January 1995, pp.294-300

[23] Krause P. C. K. and Carlsen, K., “Analysis and hybrid computer simulation of multi-conductor transmissions systems,” IEEE Transactions on Apparatus and Systems, Vol. PAS-91, Mar / Apr 1972, pp. 465-447

[24] Lindmayer, M. and Czarnecki, L., “Measurement and statistical simulation of virtual current chopping in vacuum switches,” 11th International symposium on discharges and electrical insulation in Vacuum, Berlin, 1984, pp.253-260

[25] Martzloff, F. D. and Hahn, G. J., “Low Cost Surge Counter,” Declassified GE TIS Report 64GL166, 1970

[26] Meyer, W. S. and Liu, T. H., “Alternative Transients Program (ATP) Rule Book,” Canadian / American EMTP User Group

[27] Miri, A. M., “Different methods for modelling the transient behaviour of 3-phase high voltage power transformers and deviations in the results,” Proceedings of IPST’97, June 22 – 26, Seattle, pp. 111-116

[28] Morched, A., Marti, L. and Ottevangers, J., “A high frequency transformer model for the EMTP,” IEEE Transaction on Power Delivery, Vol. 8, No.3, July 1993, pp.1615-1626

[29] Moreira, A. F., Lipo, T. A., Venkataramanan, G.. and Bernet, S., “Modelling and evaluation of dv/dt filters for AC drives with high switching speed,” Proceedings of 9th European Conference Power Electronics and Applications (EPE’01), Graz, Austria, Aug, 27-29, 2001, CD Rom

[30] Moreira, A. F., Lipo, T. A., Venkataramanan, G.. and Bernet, S., “High-frequency modelling for cable and induction motor overvoltage studies in long cable drives,” Industry Applications, IEEE Transactions on , Volume: 38 Issue: 5 , Sept.-Oct. 2002, pp.1297 -1306

[31] Phaniraj, S. and Phadke, A. G.., "Modeling of circuit breakers in the Electromagnetic Transients Program," IEEE Transactions on Power Systems, Vol. 3, No. 2, May 1988, pp.799-805

[32] Reckleff, J. G., Nelson, J. K., Musil, R. J. and Wenger, S., "Characterization of fast rise-time transients when energizing large 13.2kV motors," IEEE Transactions on Power Delivery, Vol. 3, No. 2, April 1988, pp.627-636

[33] Skibinski, G., Kerkman, R., Leggate, D., Pankau, J. and Schlegel, D., "Reflected wave modelling techniques for PWM AC motor drives," Proceeding of IEEE APEC'98, Vol. 2, Anaheim, CA, Feb, 15-19, 1998, pp.1021-1029

[34] Smeets, R. P. P., "The origin of current chopping in vacuum arcs" IEEE Transactions on Plasma Science, Vol. 17, No. 2, April 1989, pp.303-310

[35] Smeets, R. P. P., Kaneko, E. and Ohshima, I., "Experimental characterization of arc instabilities and their effect on current chopping in low-surge vacuum interrupters," IEEE Transactions on Plasma Science, Vol. 20, No. 4, August 1992, pp.439-446

[36] Smeets, R. P. P., Funahashi, T., Kaneko, E. and Ohshima, I., "Types of reignition following high-frequency current zero in vacuum interrupters with two types of contact material," IEEE Transactions on Plasma Science, Vol. 21, No. 5, October 1993, pp.478-483

[37] Snider, L. A., "Analysis of a Transformer Failure", Investigative Report November 1997.

[38] Soysal, O. O., "A method for wide frequency range modelling of power transformers and rotating machines," IEEE Transcations On Power Delivery, Vol. 8, No.4, October 1993, pp. 1802 – 1810

[39] St-Jane, G.. and Wang, R. F., "Equivalence between direct and synthetic interruption tests on high voltage circuit breakers," IEEE Transactions on Power Apparatus and Systems, July / August 1983, pp. 2216 – 2223

[40] Thomas, D. W. P., Pereira, E. T., Christopoulos C. and Howe, A. F., "The Simulation of Circuit Breaker Switching Using a Composite Cassie-Modified

Mayr Model," IEEE Transactions on Power Delivery, Vol. 10, No. 4 , October 1995, pp.1829-1835

[41] Thuries, E., Doan, P. V., Dayet J. and Joyeux-Bouillon, B., "Synthetic testing method for generator circuit breakers," IEEE Transactions on Power Delivery, January 1986, pp. 179 – 184

[42] Ueda T. et al, "A frequency-dependent model transformer for transfer voltage study," Proceedings of IPST'97, June 22 – 26, Seattle, pp. 105-110

[43] Ueno, N., Toya, H., Murai, Y. and Okada, M., "Monte-Carlo simulation of overvoltage generation in the inductive current interruption by vacuum interrupters," IEEE Transactions on Power Apparatus and Systems, Vol. PAS-103, No. 3, March 1984, pp.236-241

[44] Vaessen, P. T. M., "Transformer model for high frequencies," IEEE Transactions on Power Delivery, Vol. 3, No. 4, October 1988, pp.1761-1768

[45] von Jouanne, A. V., Rendusara, D. and Enjeti, P. N., "Filtering techniques to minimize the effect of long motor leads on PWM inverter-fed AC motor drive systems," IEEE Transaction on Industry Applications, Vol. 32, July – Aug 1996, pp. 919-926

[46] Wilcox, D. J., "Theory of transformer modelling using modal analysis," IEE Proceedings - Generation, Transmission and Distribution, IEE Proceedings C , Volume: 138 , Issue: 2 , March 1991, pp.121-128

[47] Wilcox, D. J. et al., "Application of modified modal theory in the modelling of practical transformers," Proc. IEE, Vol. 139, No.6, November 1992, pp. 513-520

[48] Wilcox, D. J., and Mchale, T. P., "Modified theory of modal analysis for the modelling of multi-winding transformers," Proceedings of IEE, Vol. 139, No.6, November 1992, pp. 505-511

[49] Wills, J. R., Brock, G.. J. and Edmonds, J. S., "Derivation of induction motor models from standstill frequency response tests," IEEE Transactions on Energy Conversion, Vol. 4, No. 4, December 1989, pp. 608 – 615

APPENDIX A: CIRCUIT BREAKER STATISTICAL STUDY CASE

Case No.	Tcon (µs from current zero)	U (V)		*di/dt* (A / µs)	
		A	B	C	D
1	200 - 300	50	0	0	100
2	100 - 200	50	0	0	100
3	0 - 100	50	0	0	100
4	200 - 300	30	1000	0	100
5	100 - 200	30	1000	0	100
6	0 - 100	30	1000	0	100
7	200 - 300	20	0	0	100
8	100 - 200	20	0	0	100
9	0 - 100	20	0	0	100
10	200 - 300	2	0	0	100
11	100 - 200	2	0	0	100
12	0 - 100	2	0	0	100
13	200 - 300	50	0	0	600
14	100 - 200	50	0	0	600
15	0 - 100	50	0	0	600
16	200 - 300	30	1000	0	600
17	100 - 200	30	1000	0	600
18	0 - 100	30	1000	0	600
19	200 - 300	20	0	0	600
20	100 - 200	20	0	0	600
21	0 - 100	20	0	0	600
22	200 - 300	2	0	0	600
23	100 - 200	2	0	0	600
24	0 - 100	2	0	0	600

Case No.	Tcon (μs from current zero)	U (V)		*di/dt* (A / μs)	
		A	B	C	D
25	200 - 300	50	0	-0.034	255
26	100 - 200	50	0	-0.034	255
27	0 - 100	50	0	-0.034	255
28	200 - 300	30	1000	-0.034	255
29	100 - 200	30	1000	-0.034	255
30	0 - 100	30	1000	-0.034	255
31	200 - 300	20	0	-0.034	255
32	100 - 200	20	0	-0.034	255
33	0 - 100	20	0	-0.034	255
34	200 - 300	2	0	-0.034	255
35	100 - 200	2	0	-0.034	255
36	0 - 100	2	0	-0.034	255
37	200 - 300	50	0	0.31	155
38	100 - 200	50	0	0.31	155
39	0 - 100	50	0	0.31	155
40	200 - 300	30	1000	0.31	155
41	100 - 200	30	1000	0.31	155
42	0 - 100	30	1000	0.31	155
43	200 - 300	20	0	0.31	155
44	100 - 200	20	0	0.31	155
45	0 - 100	20	0	0.31	155
46	200 - 300	2	0	0.31	155
47	100 - 200	2	0	0.31	155
48	0 - 100	2	0	0.31	155

APPENDIX B: CIRCUIT BREAKER STATISTICAL RESULTS

Case No.	Mean Reignition Voltage [p.u.]	Mean No. of reignitions	Max. No. of Reignitions
1	1.441	0.525	1
2	7.172	14.653	34
3	15.780	38.792	52
4	10.971	41.594	65
5	10.142	47.703	67
6	9.001	55.446	67
7	5.754	57.030	67
8	5.864	68.218	82
9	5.123	89.079	107
10	1.273	89.653	107
11	1.273	56.446	74
12	1.273	9.386	37
13	1.478	2.099	4
14	2.234	25.347	72
15	7.156	110.703	131
16	9.238	179.970	202
17	11.782	211.764	222
18	12.817	244.347	264
19	12.508	373.267	390
20	12.637	400.119	421
21	12.738	439.109	454
22	1.273	89.653	107
23	1.273	56.446	74
24	1.273	9.386	37

Case No.	Mean Reignition Voltage [p.u.]	Mean No. of reignitions	Max. No. of Reignitions
25	1.478	2.099	4
26	4.462	17.535	41
27	12.669	60.406	78
28	15.768	84.386	99
29	16.318	107.802	116
30	16.743	127.624	142
31	8.697	141.97	154
32	8.551	158.149	174
33	8.131	188.644	208
34	0.174	89.653	107
35	0.180	56.446	74
36	0.102	9.386	37
37	1.475	2.099	4
38	3.422	16.396	36
39	8.426	58.802	78
40	9.586	127.842	149
41	10.676	159.436	170
42	11.357	188.604	205
43	11.838	568.416	586
44	11.913	597.109	627
45	12.143	644.178	662
46	1.273	89.653	107
47	1.273	56.446	74
48	1.273	9.386	37

APPENDIX C: CIRCUIT BREAKER STATISTICAL RESULTS

Mean Reignition Voltage

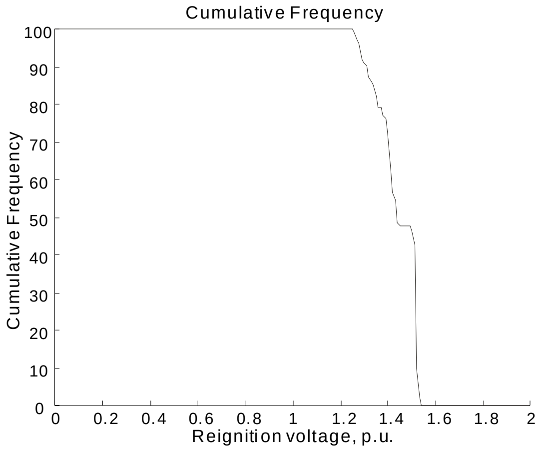

Case 1

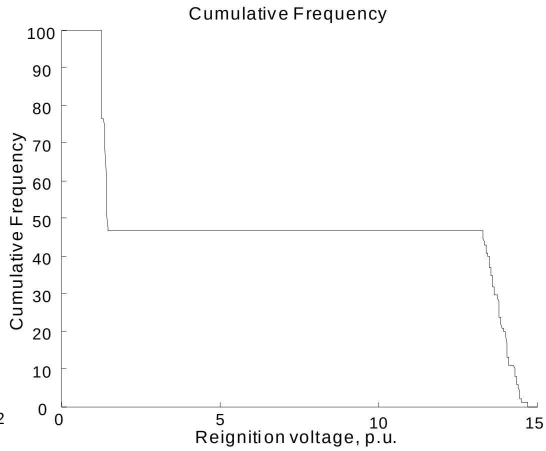

Case 2

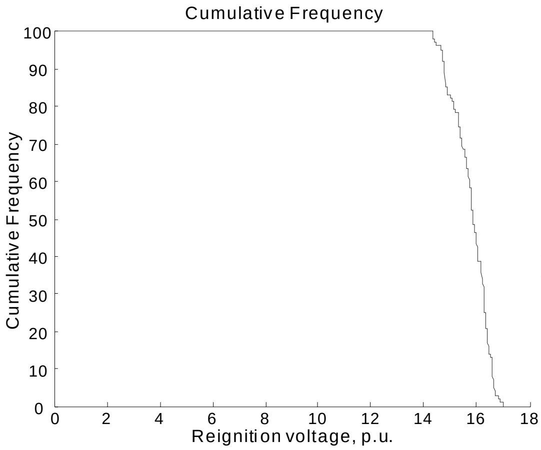

Case 3

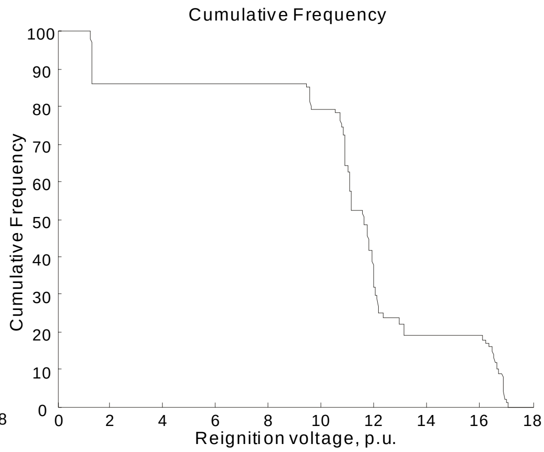

Case 4

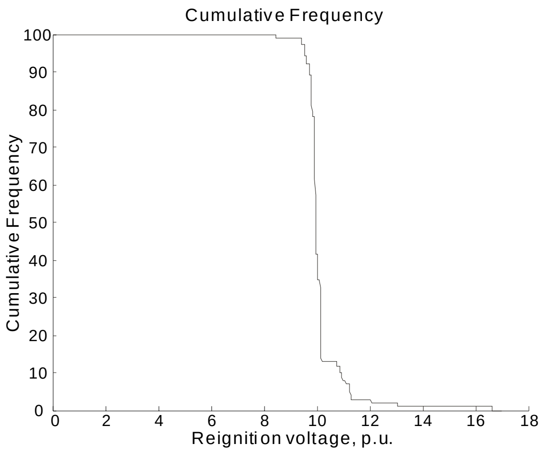

Case 5

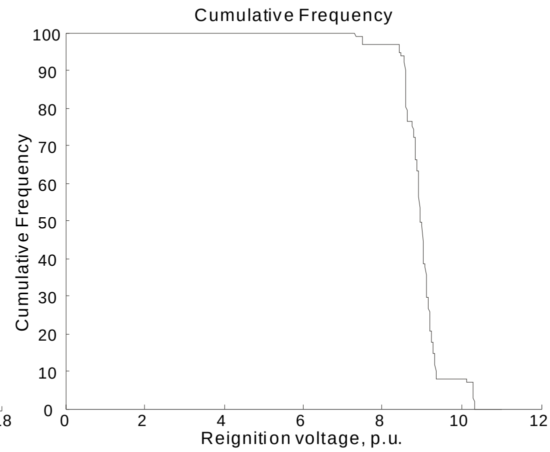

Case 6

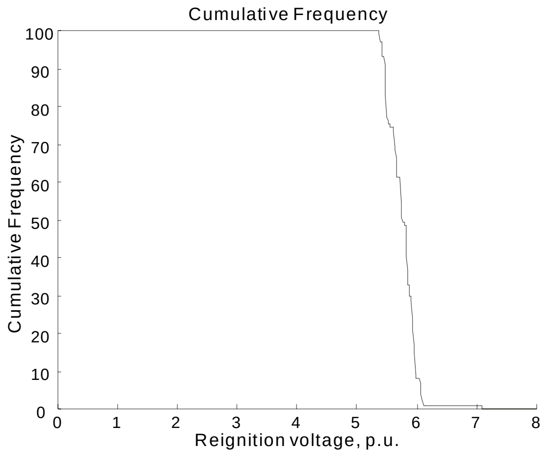

Case 7

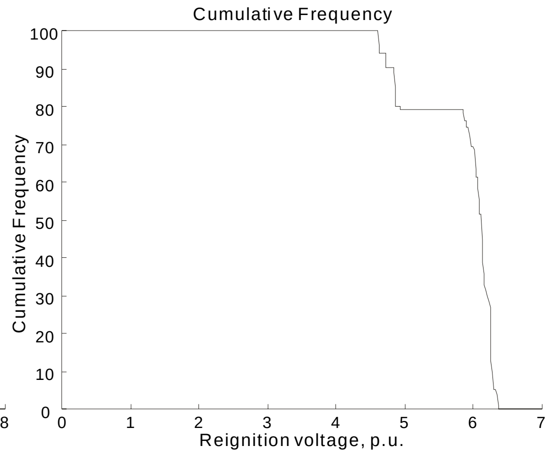

Case 8

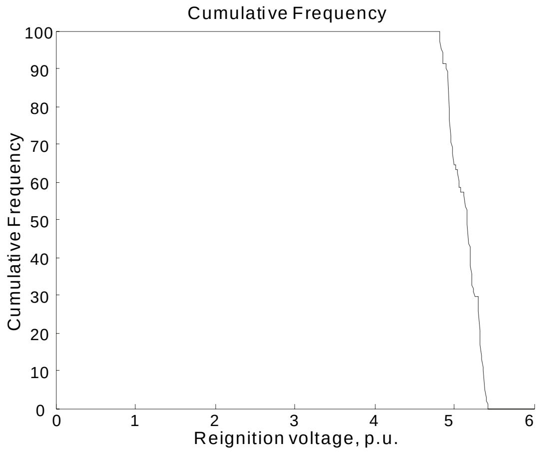

Case 9

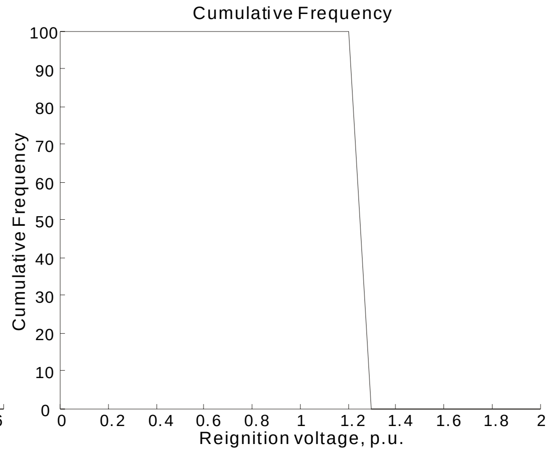

Case 10

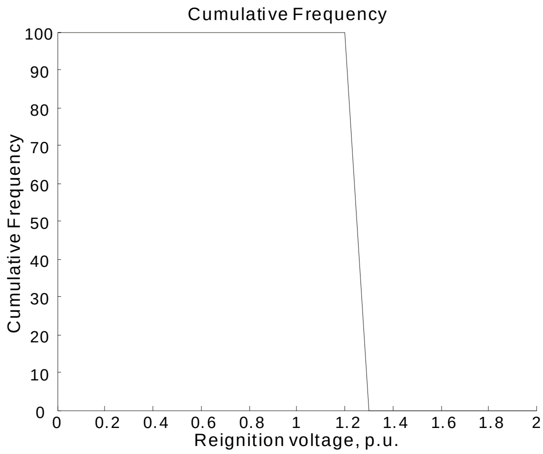

Case 11

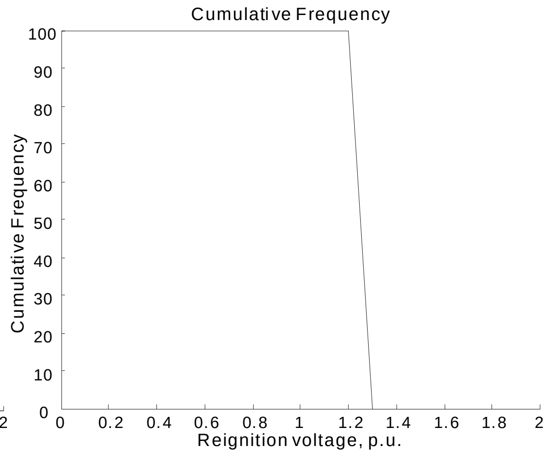

Case 12

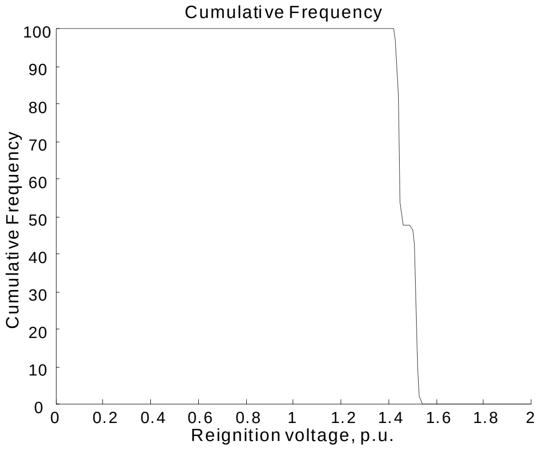

Case 13

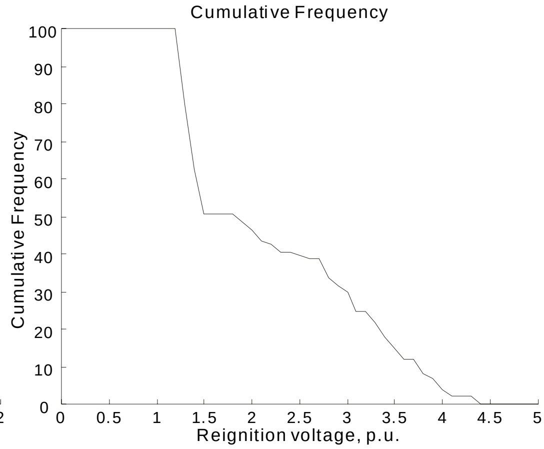

Case 14

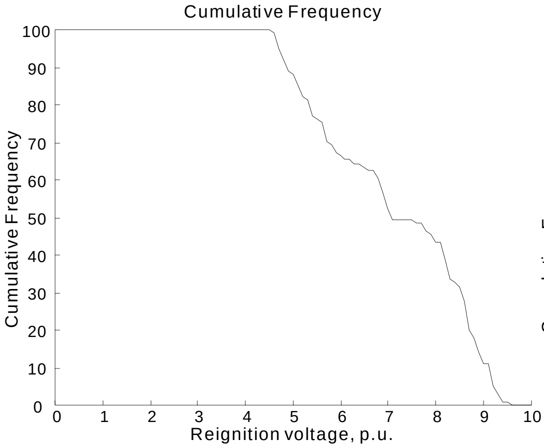

Case 15

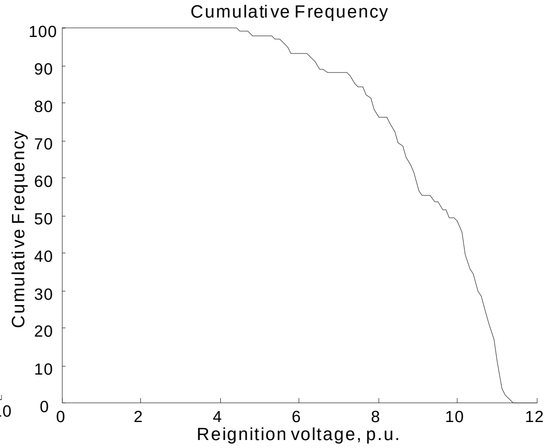

Case 16

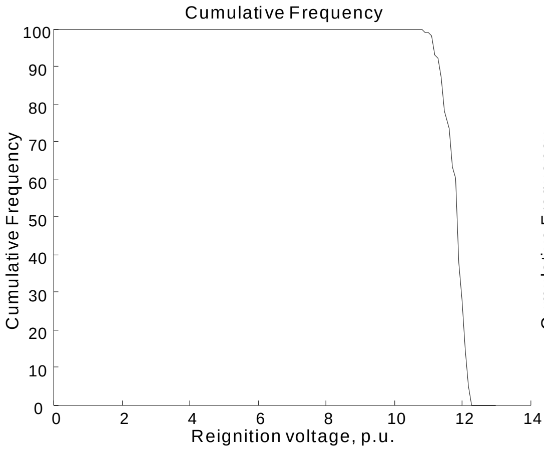

Case 17

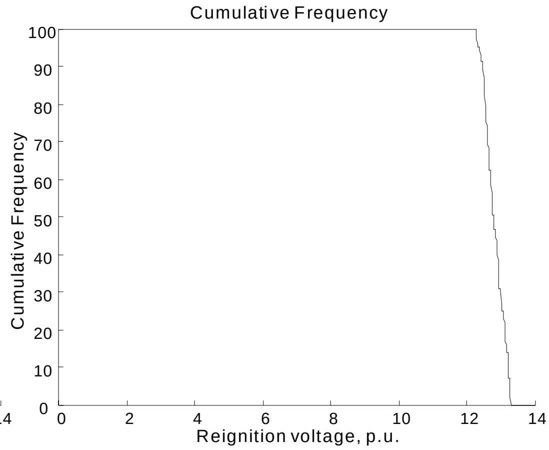

Case 18

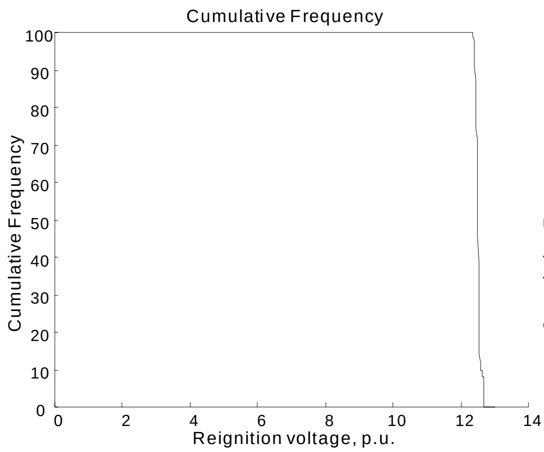

Case 19

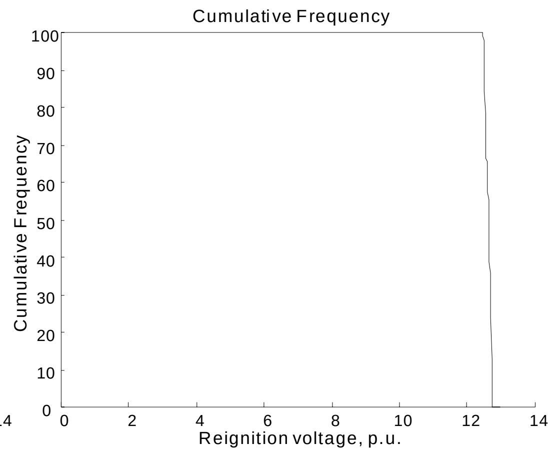

Case 20

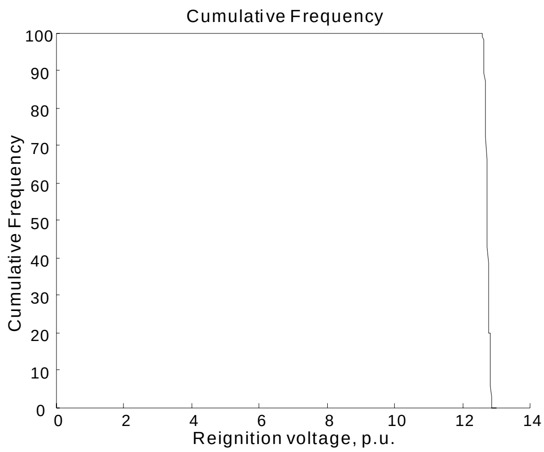

Case 21

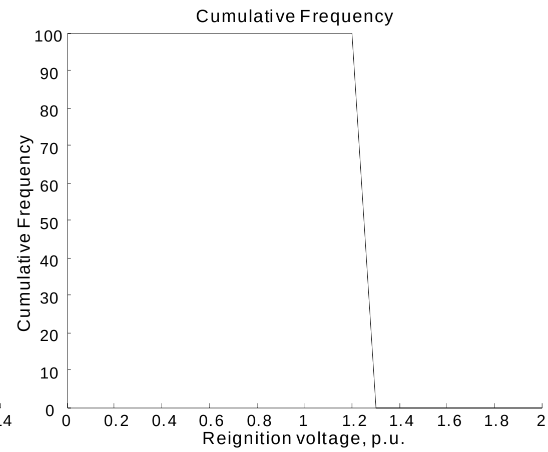

Case 22

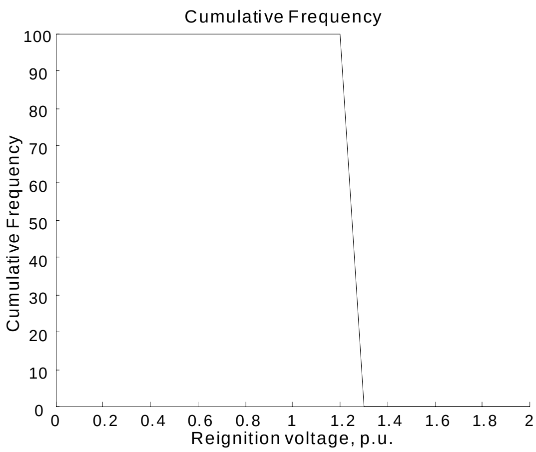

Case 23

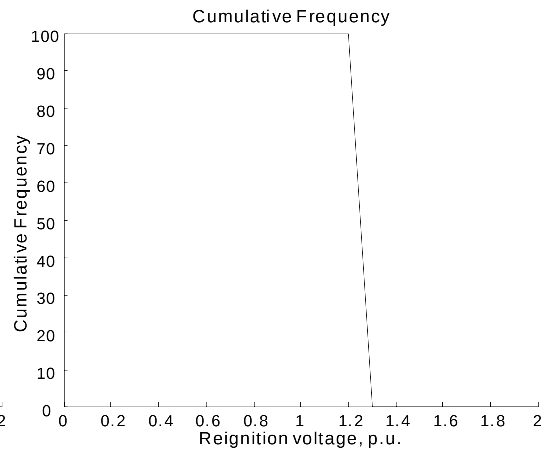

Case 24

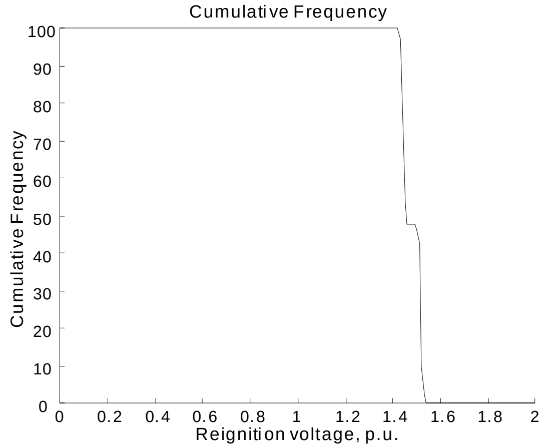

Case 25

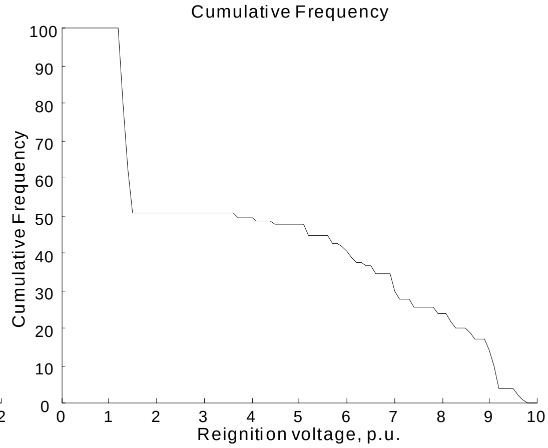

Case 26

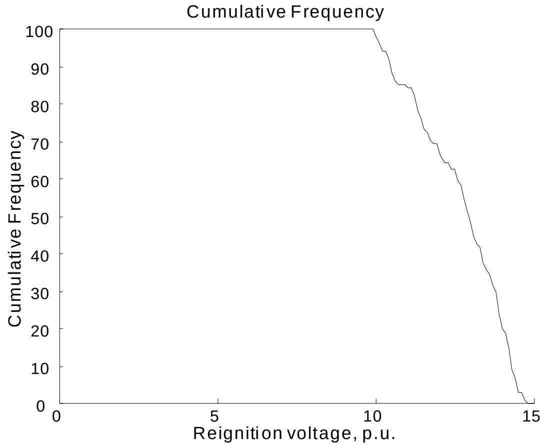

Case 27

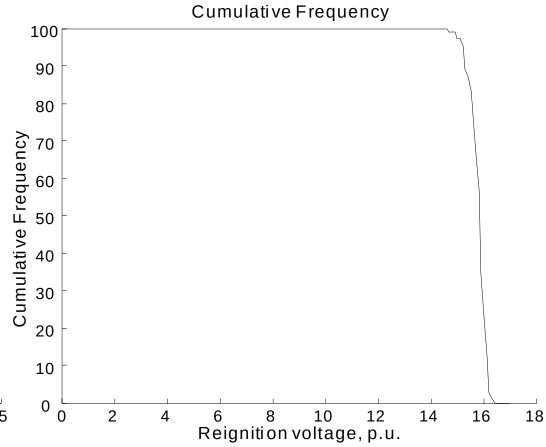

Case 28

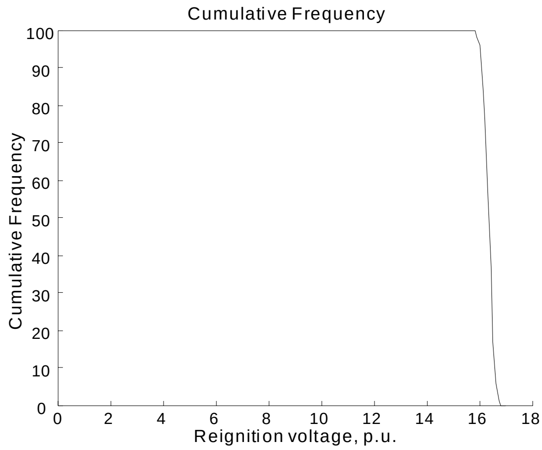

Case 29

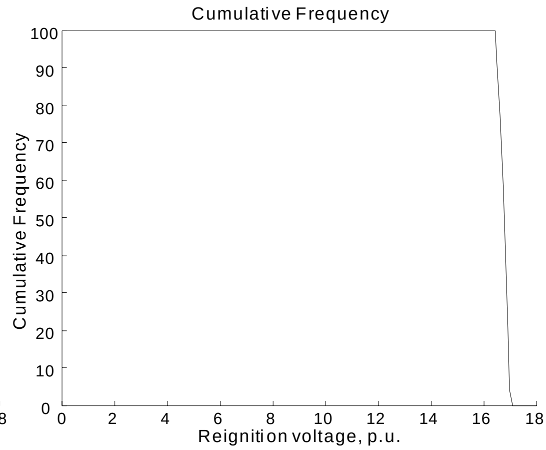

Case 30

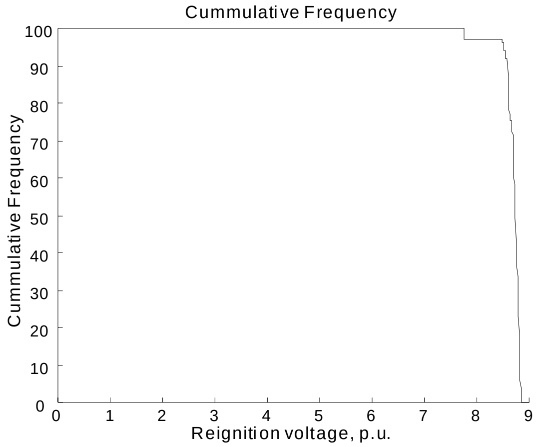

Case 31

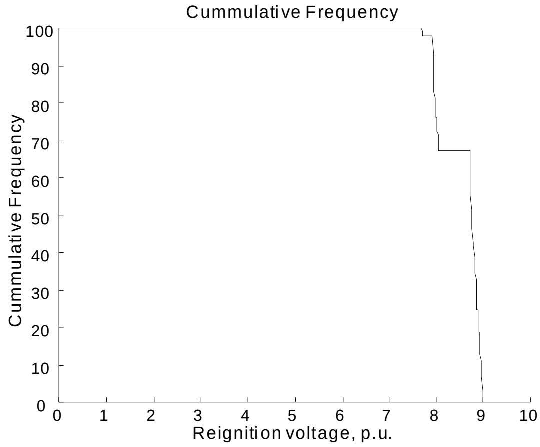

Case 32

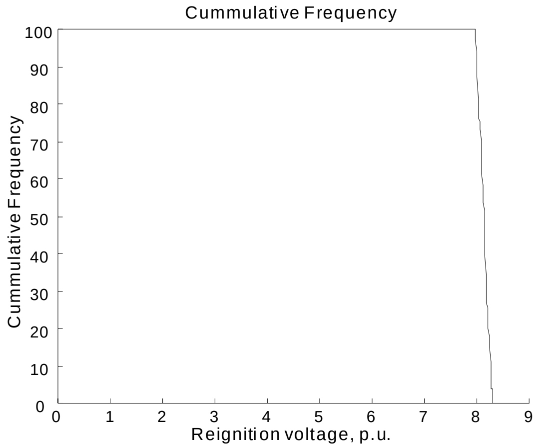

Case 33

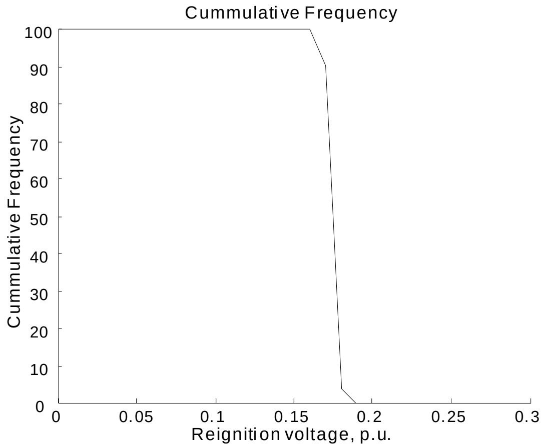

Case 34

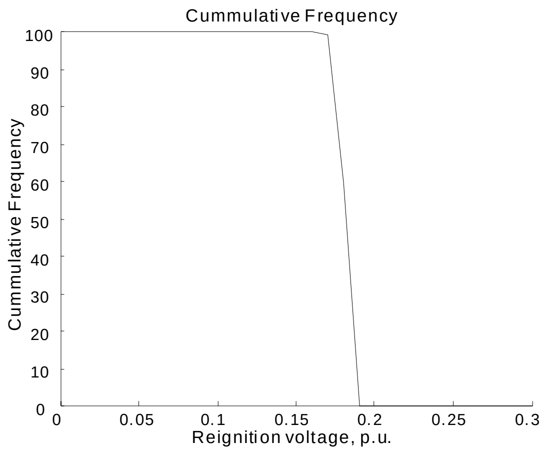

Case 35

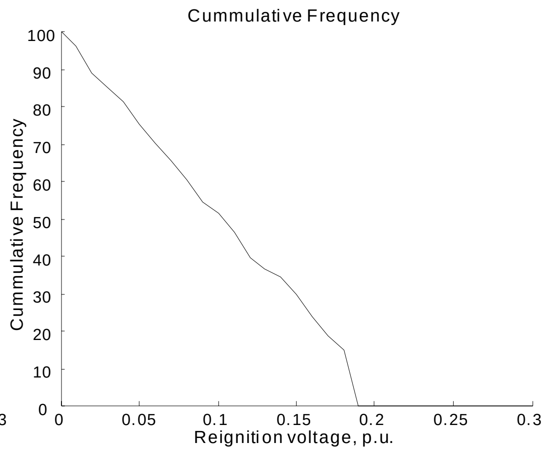

Case 36

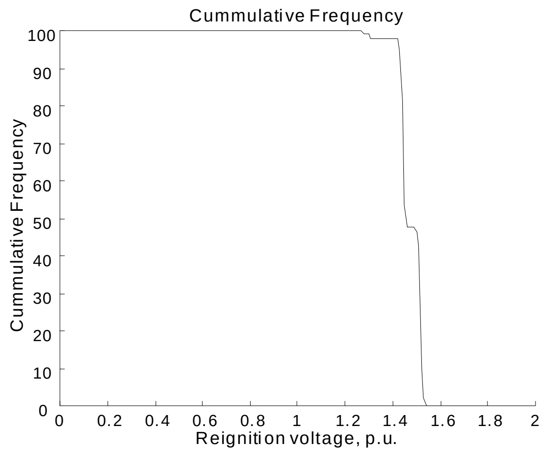

Case 37

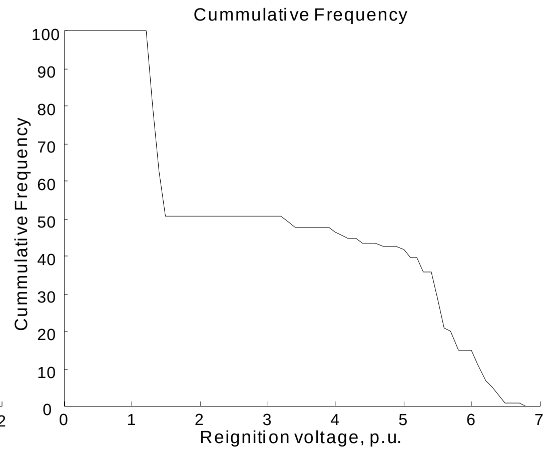

Case 38

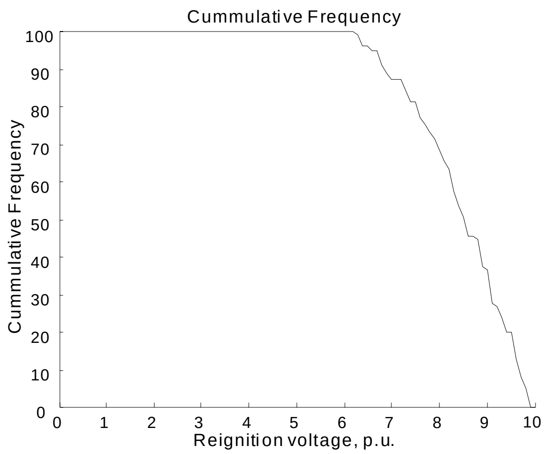

Case 39

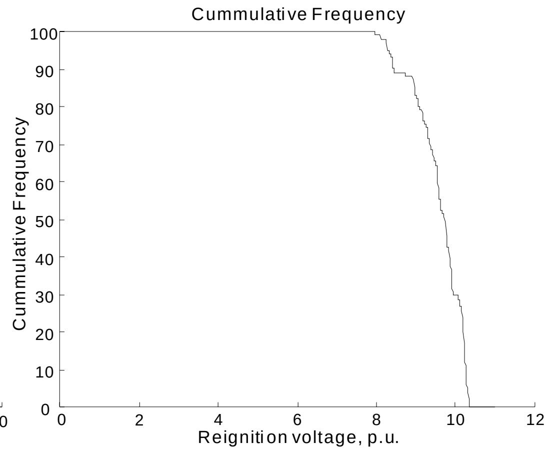

Case 40

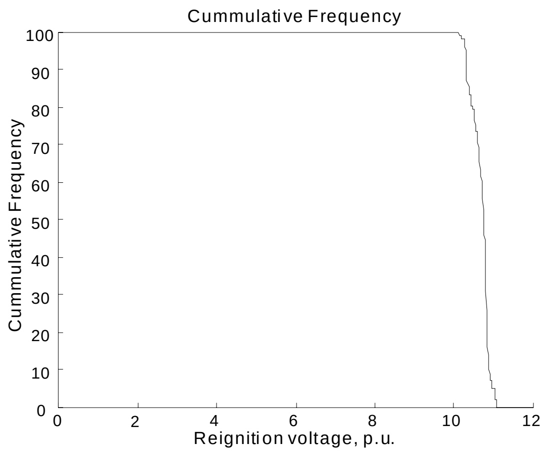

Case 41

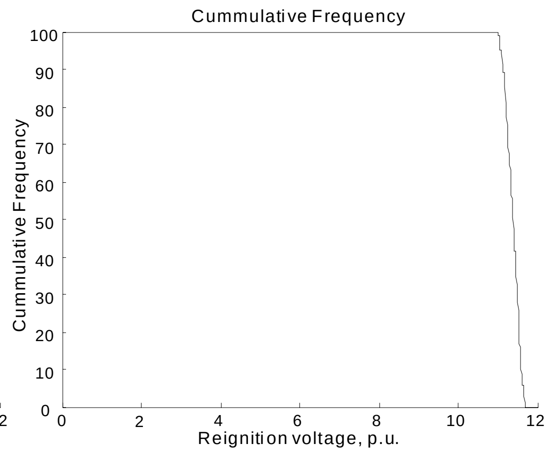

Case 42

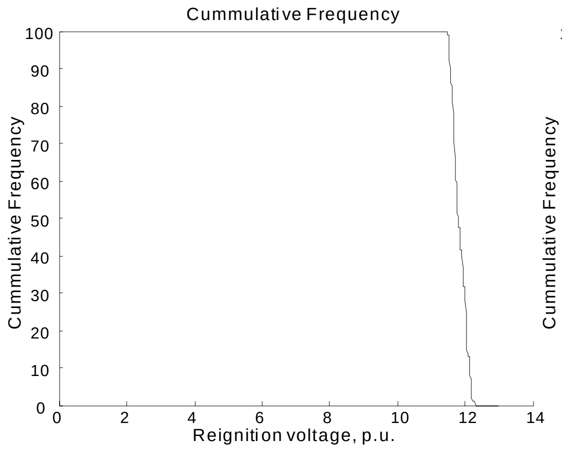

Case 43

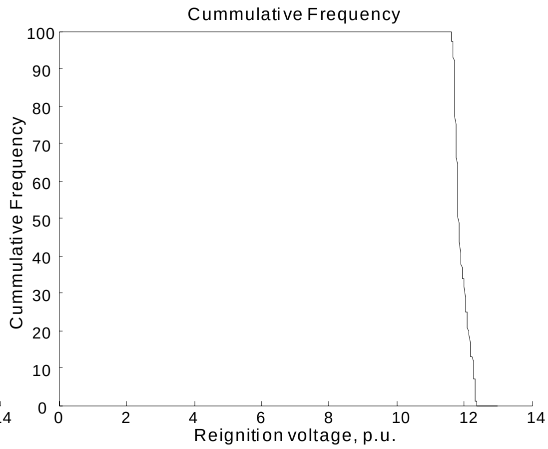

Case 44

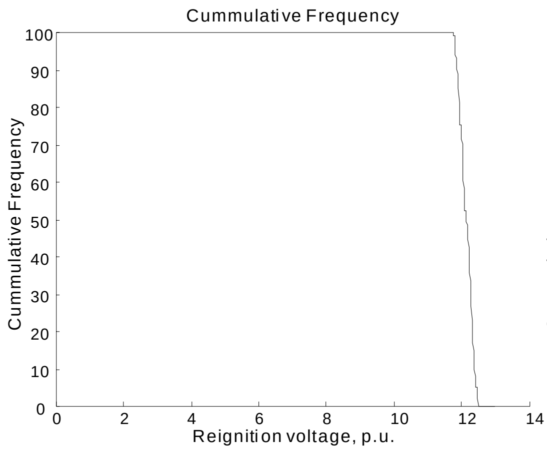

Case 45

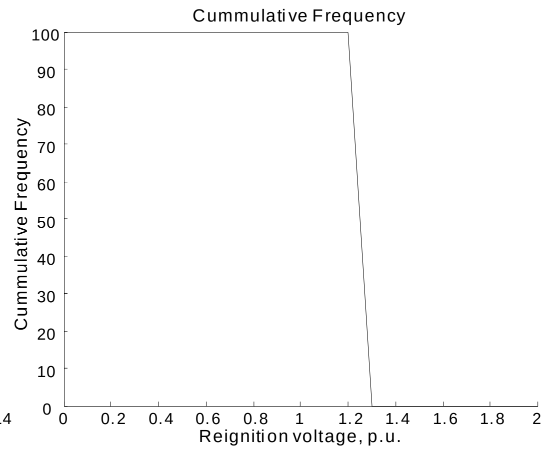

Case 46

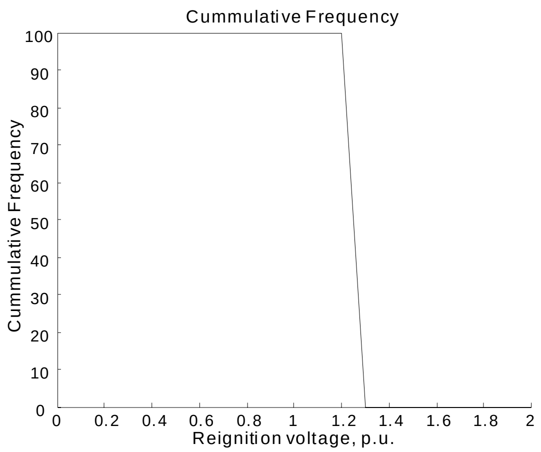

Case 47

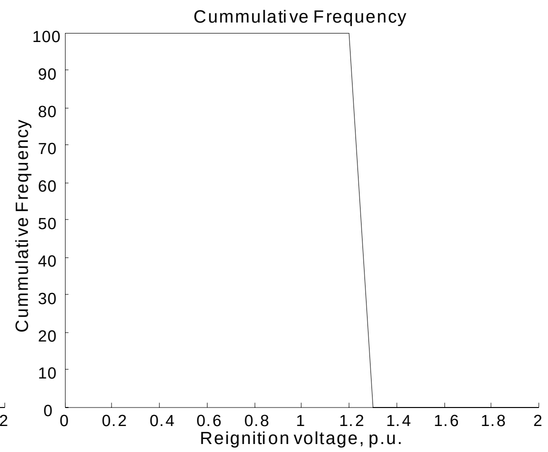

Case 48

Mean Frequency of Reignitions

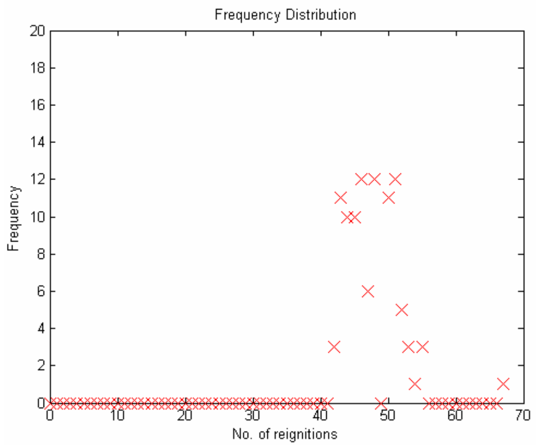

Case 1

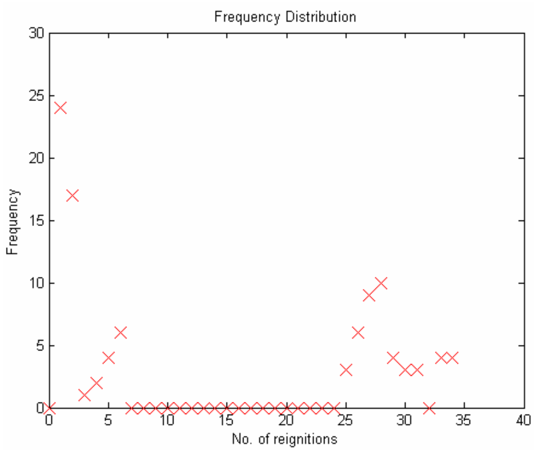

Case 2

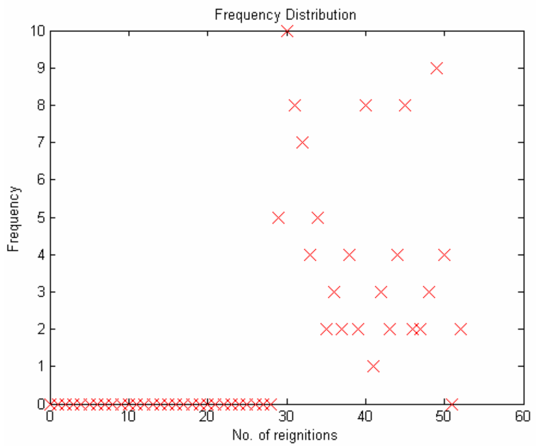

Case 3

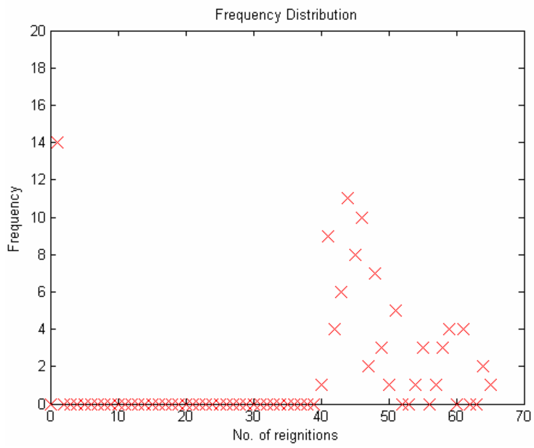

Case 4

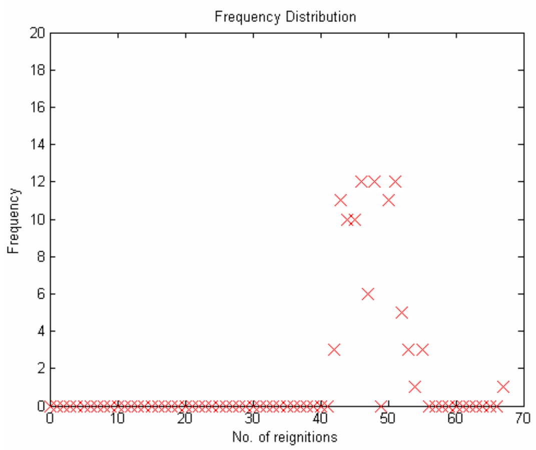

Case 5

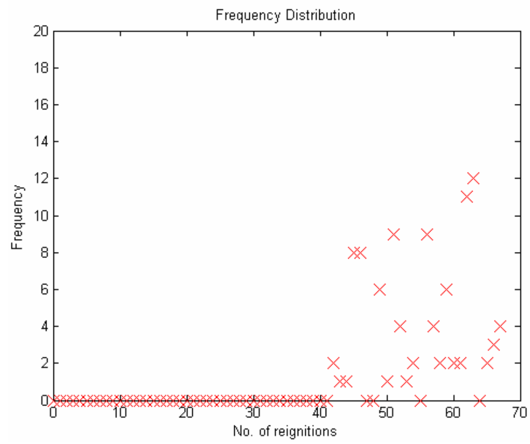

Case 6

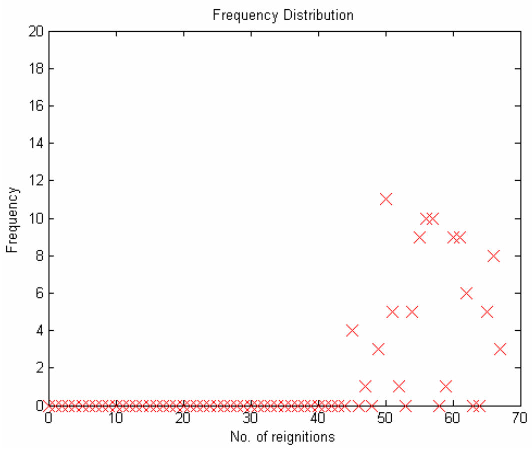

Case 7

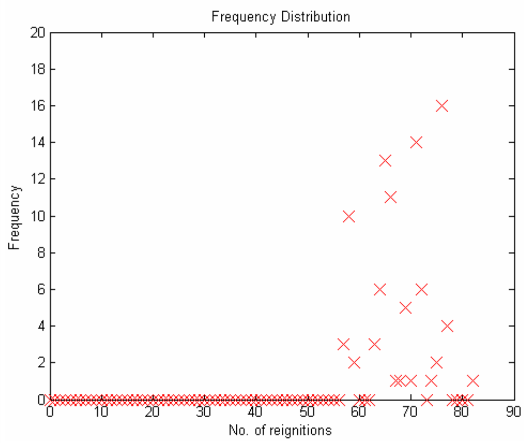

Case 8

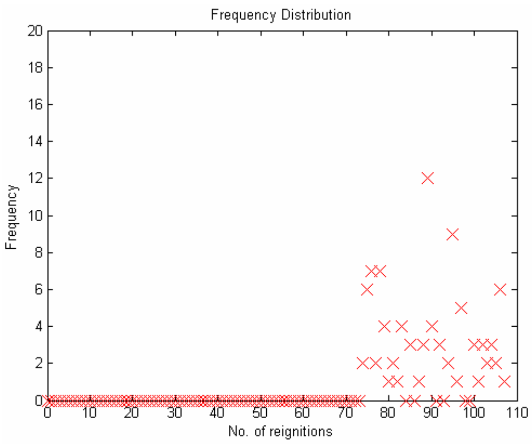

Case 9

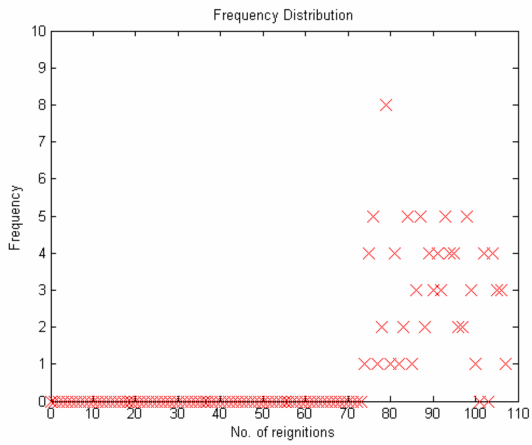

Case 10

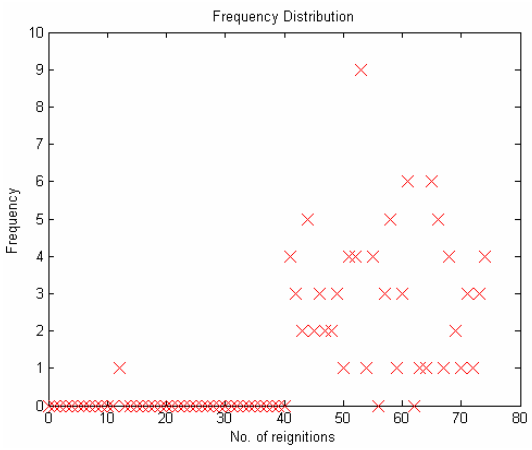

Case 11

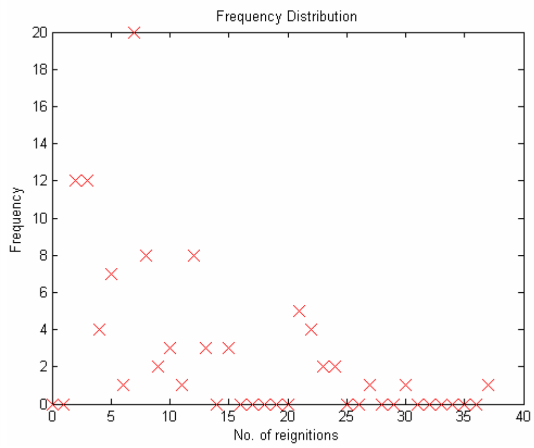

Case 12

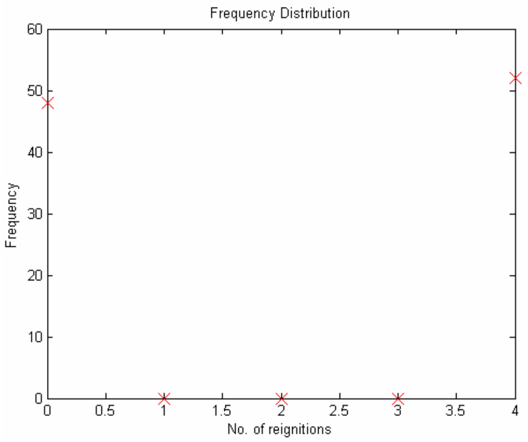

Case 13

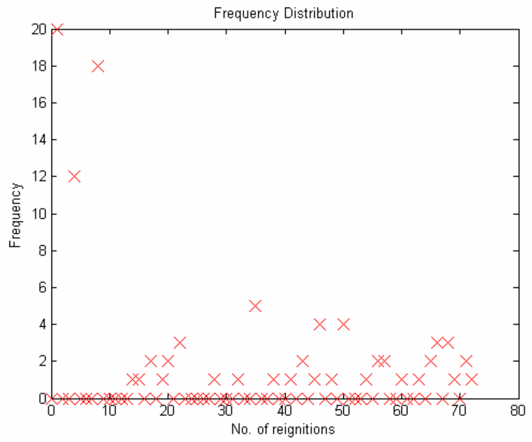

Case 14

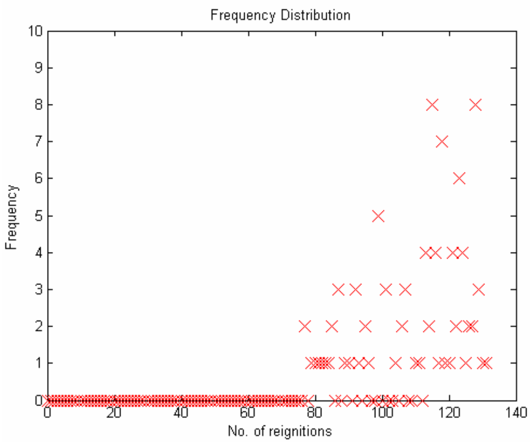

Case 15

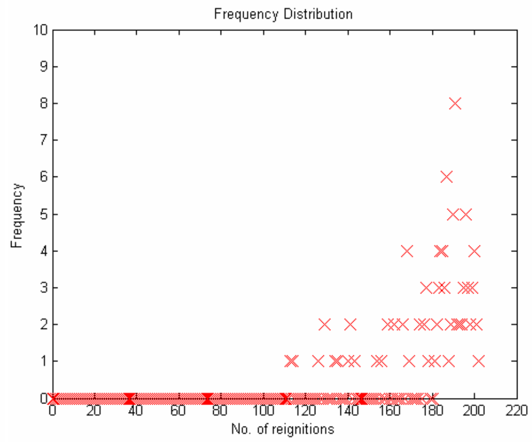

Case 16

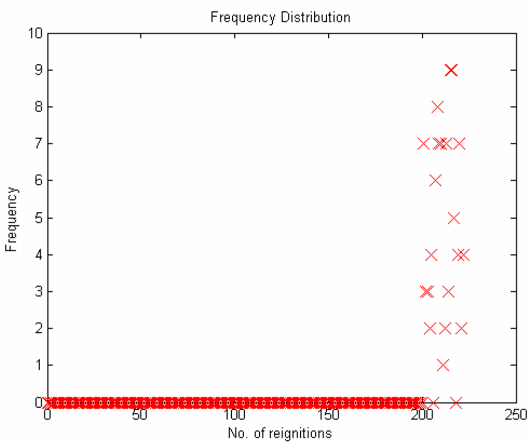

Case 17

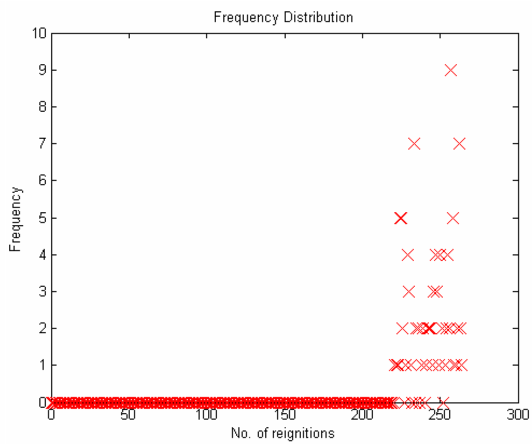

Case 18

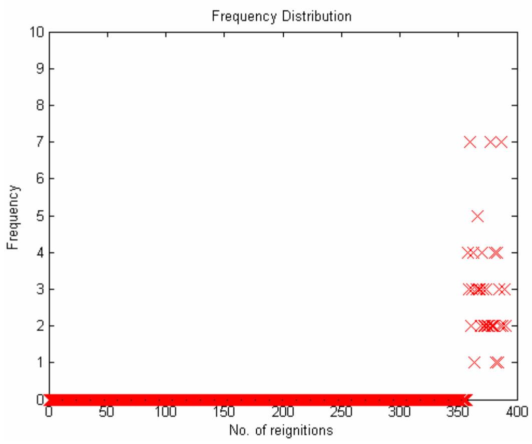

Case 19

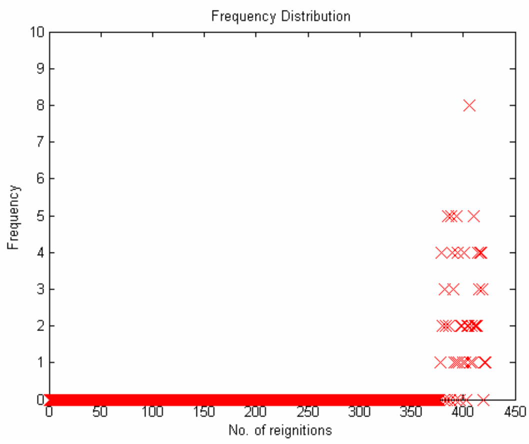

Case 20

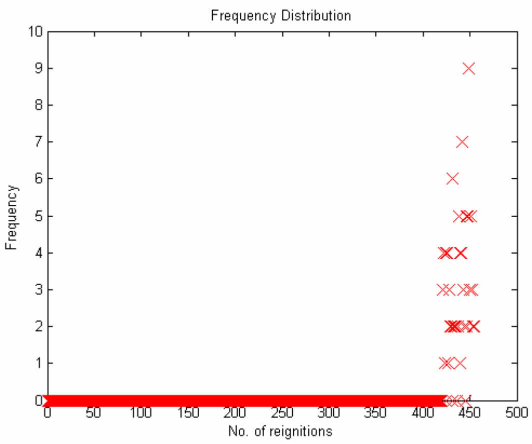

Case 21

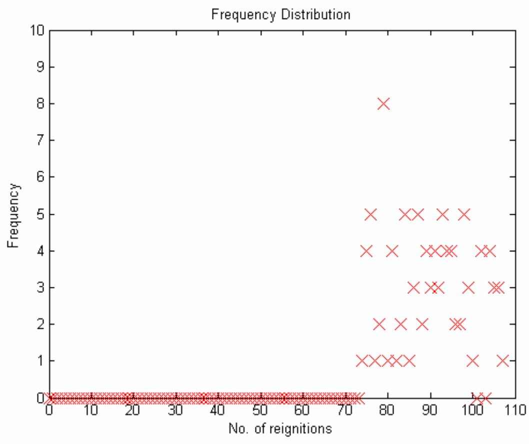

Case 22

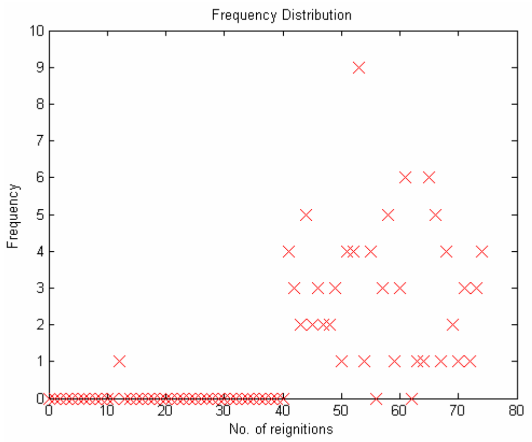

Case 23

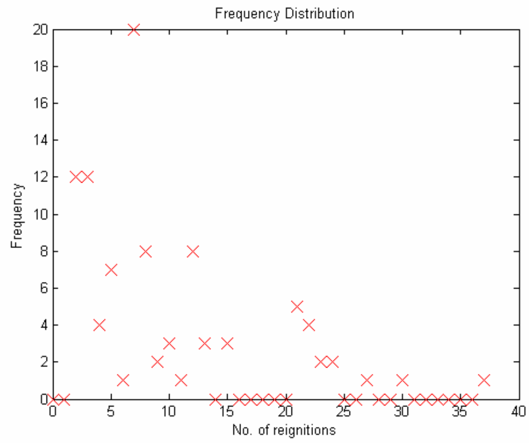

Case 24

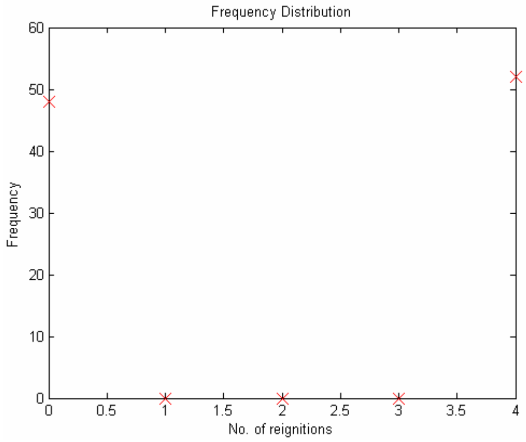

Case 25

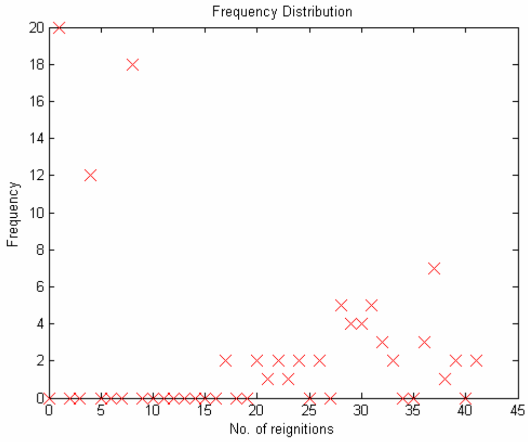

Case 26

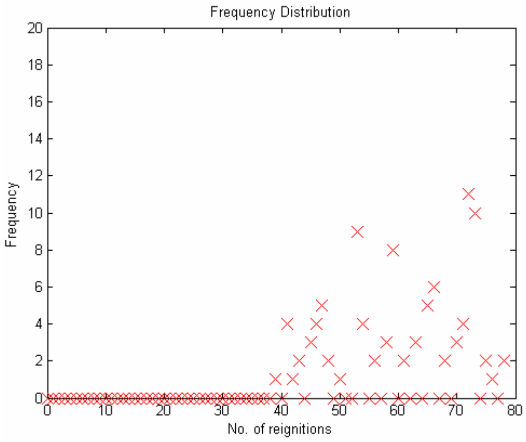

Case 27

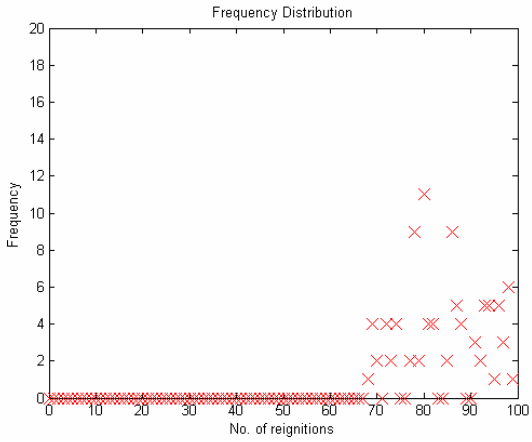

Case 28

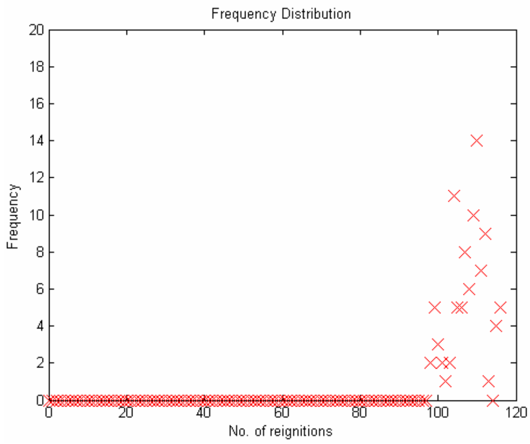

Case 29

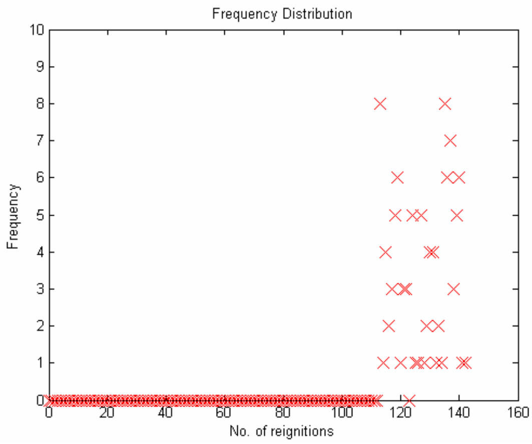

Case 30

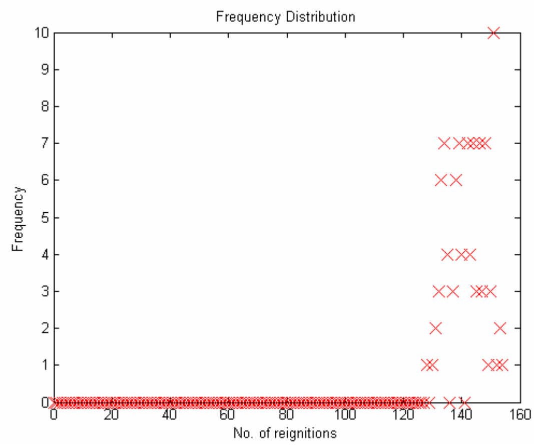

Case 31

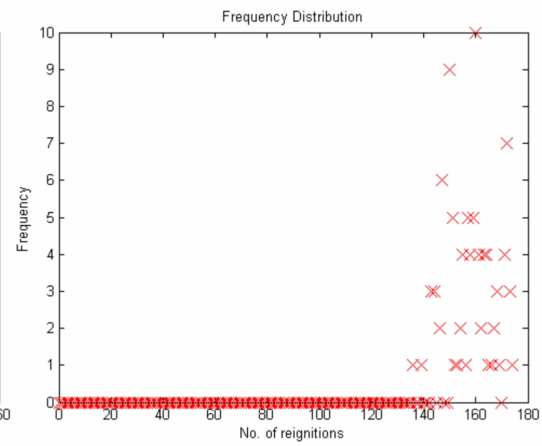

Case 32

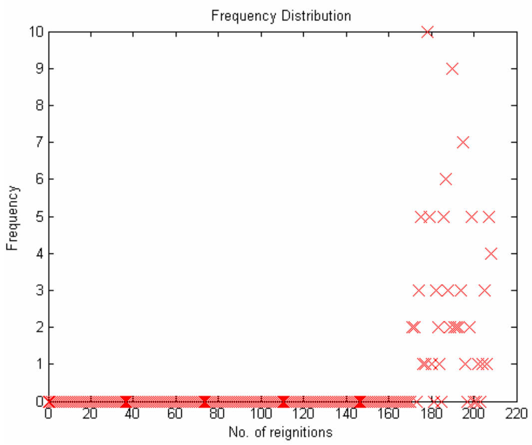

Case 33

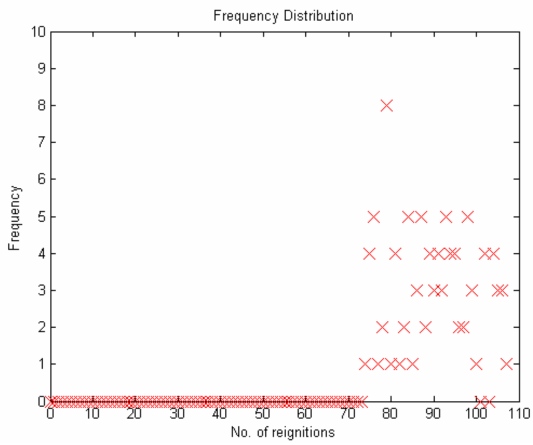

Case 34

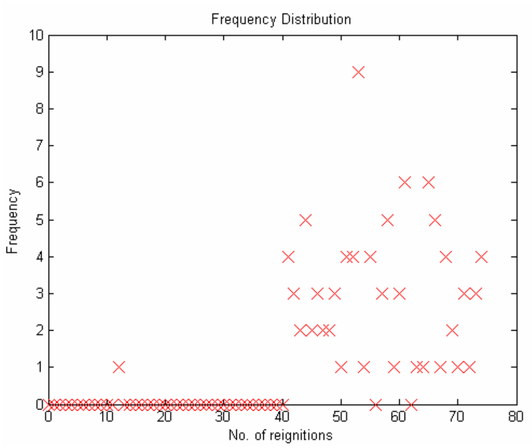

Case 35

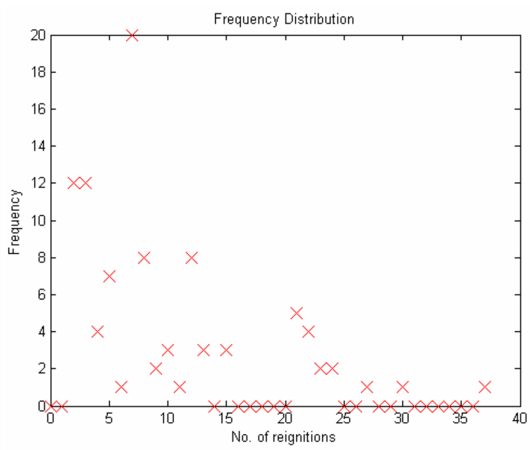

Case 36

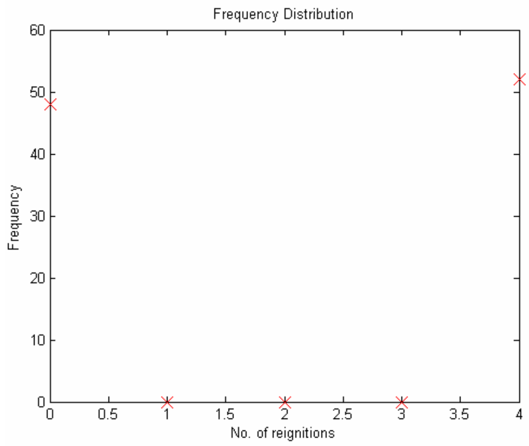

Case 37

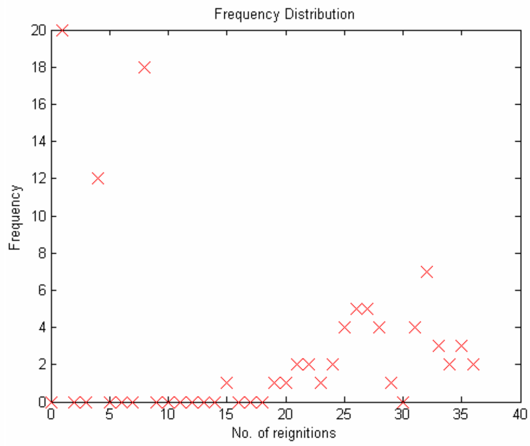

Case 38

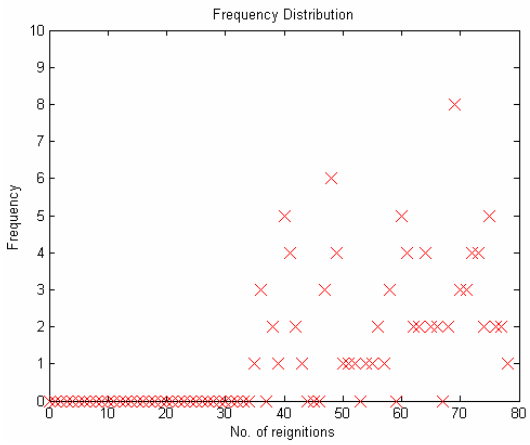

Case 39

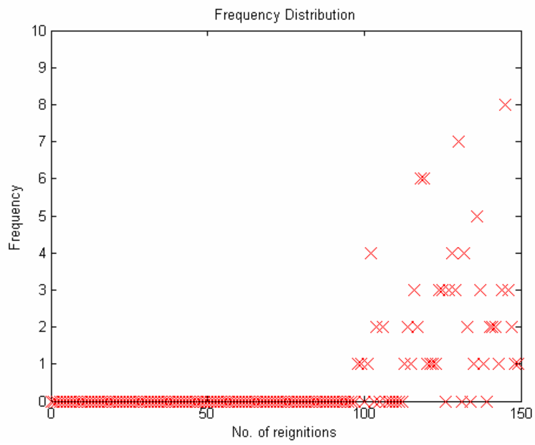

Case 40

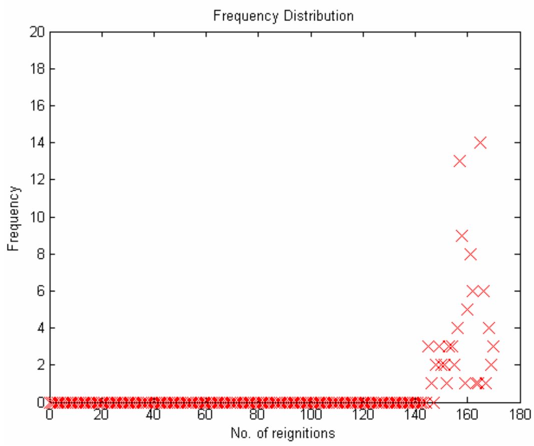

Case 41

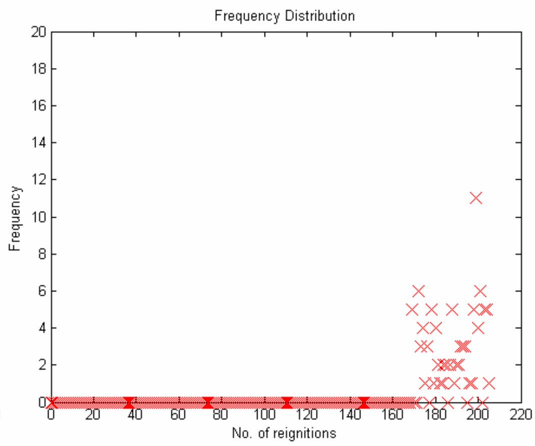

Case 42

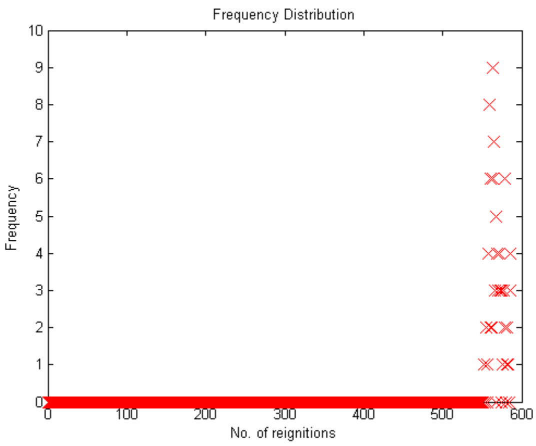

Case 43

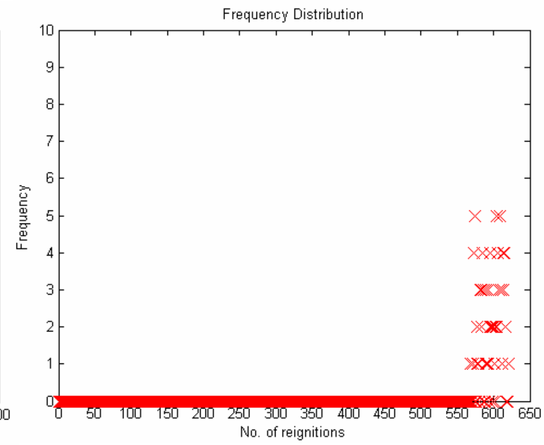

Case 44

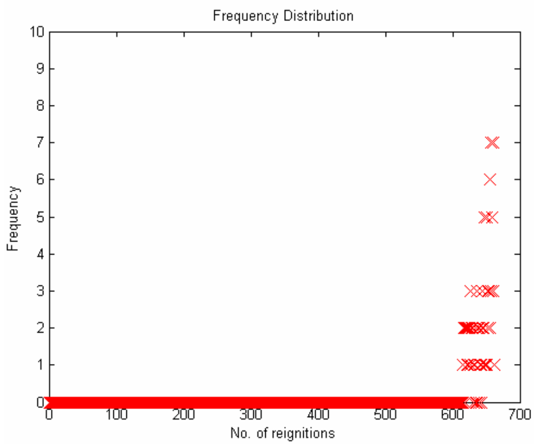

Case 45

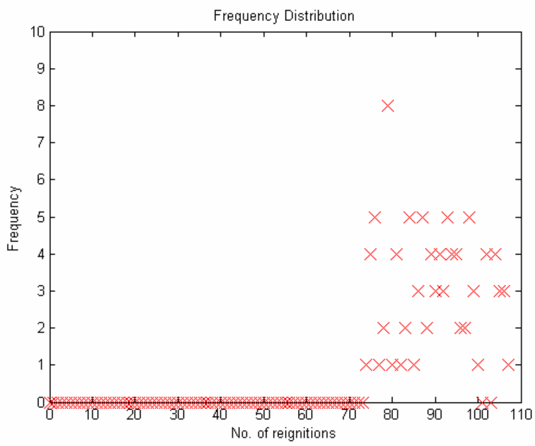

Case 46

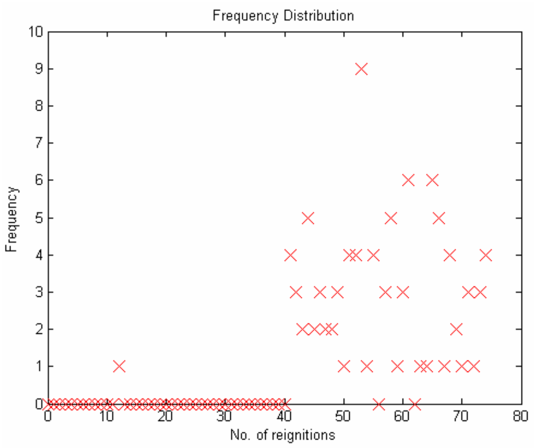

Case 47

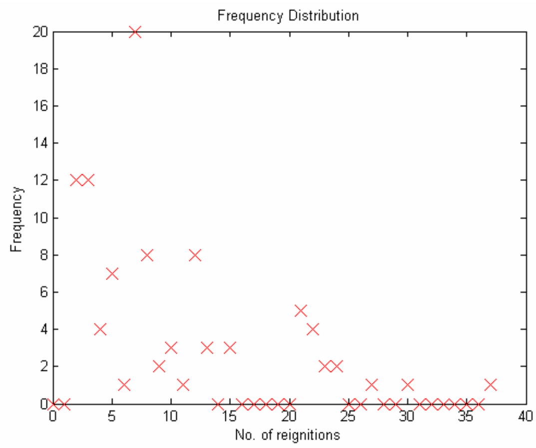

Case 48

APPENDIX D: OTHER CIRCUIT PARAMETER STATISTICAL RESULTS

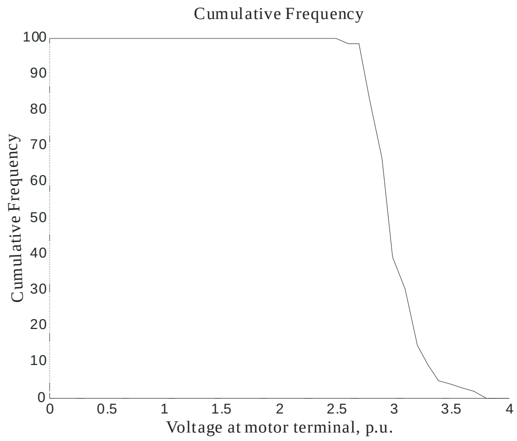

Case 1

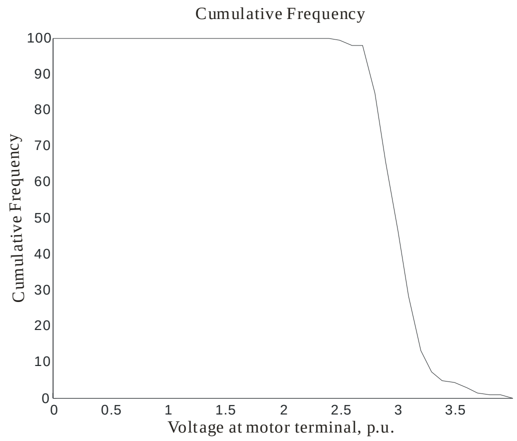

Case 2

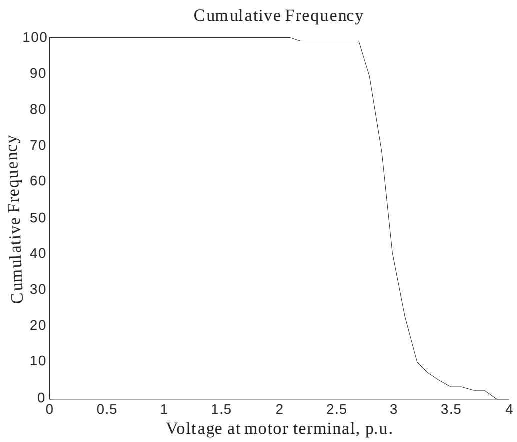

Case 3

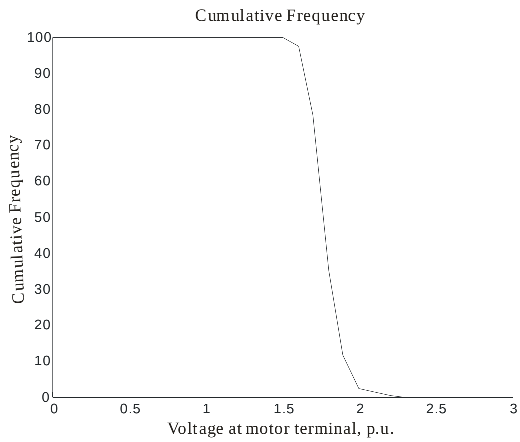

Case 4

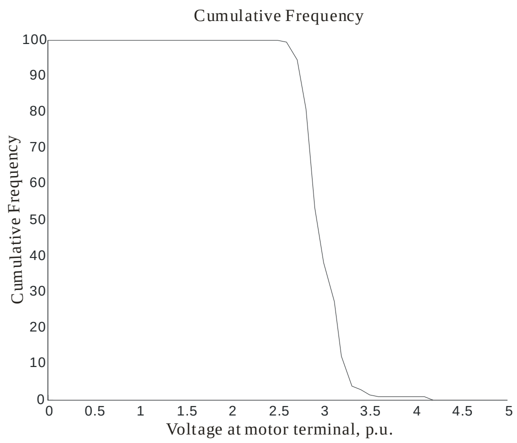

Case 5

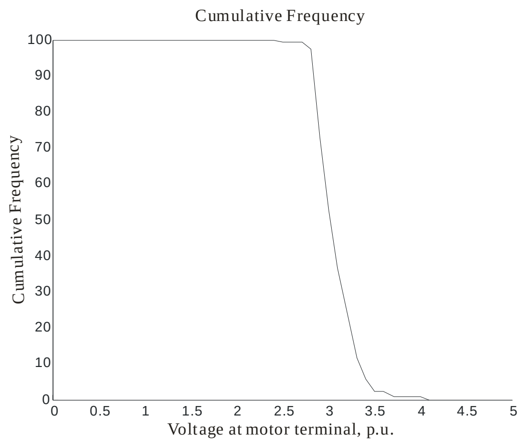

Case 6

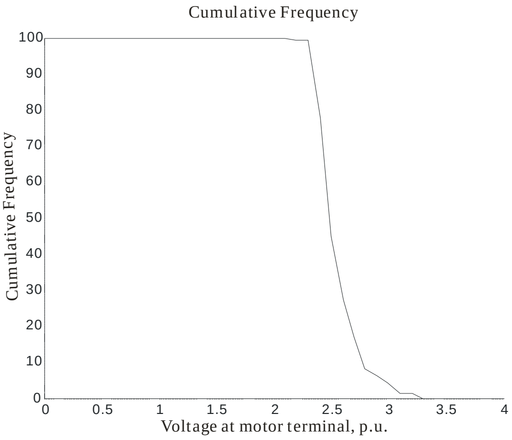

Case 7

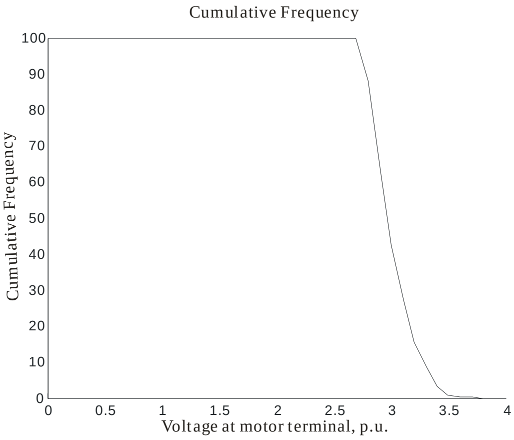

Case 8

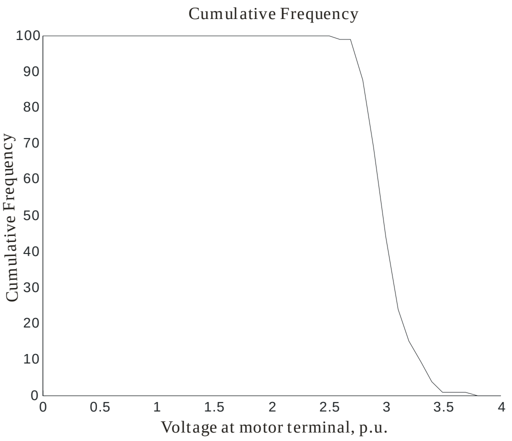

Case 9

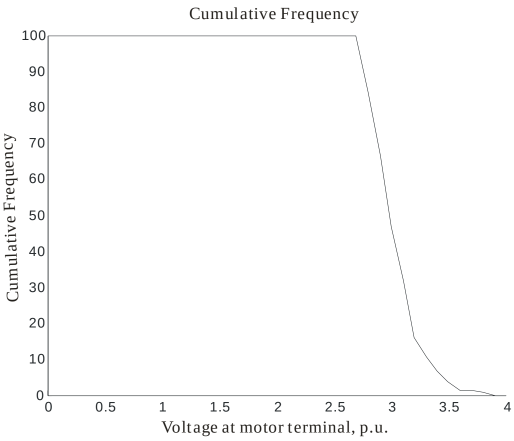

Case 10

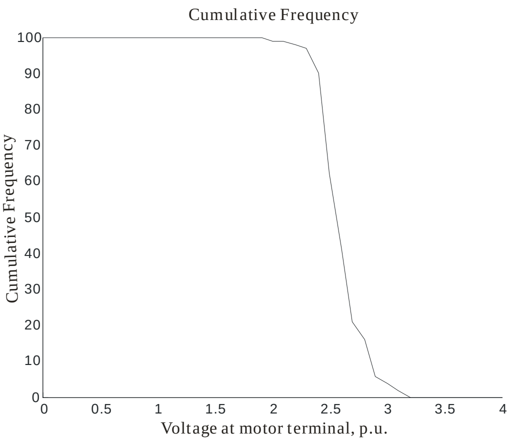

Case 11

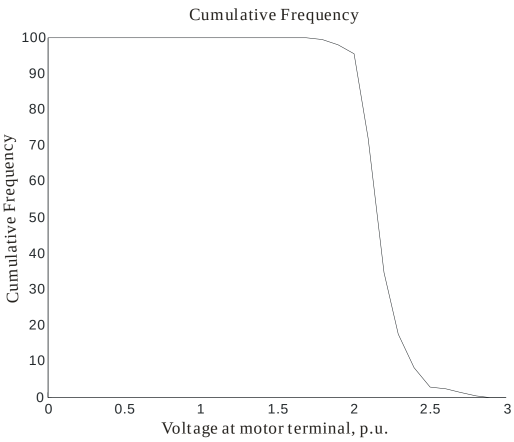

Case 12

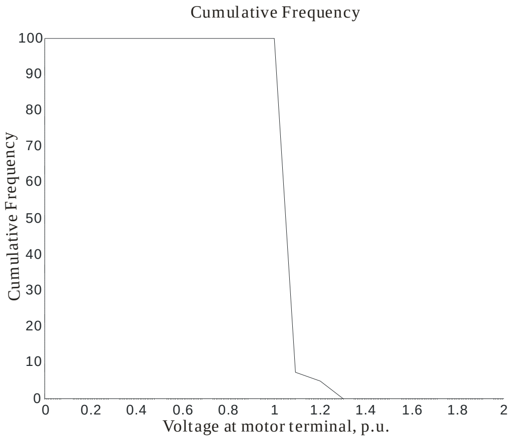

Case 13

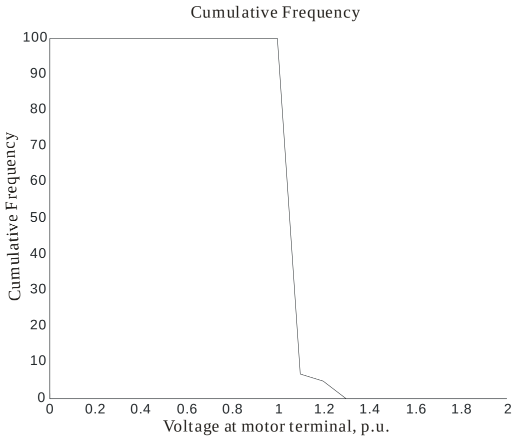

Case 14

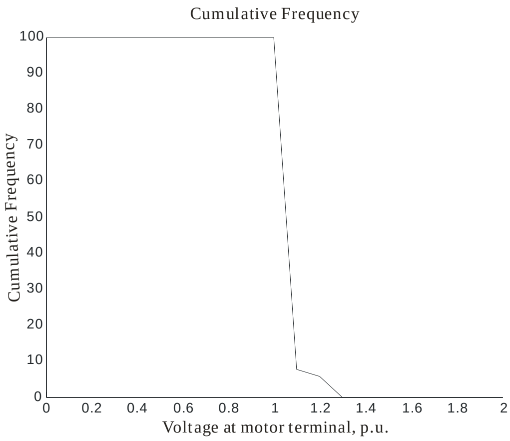

Case 15

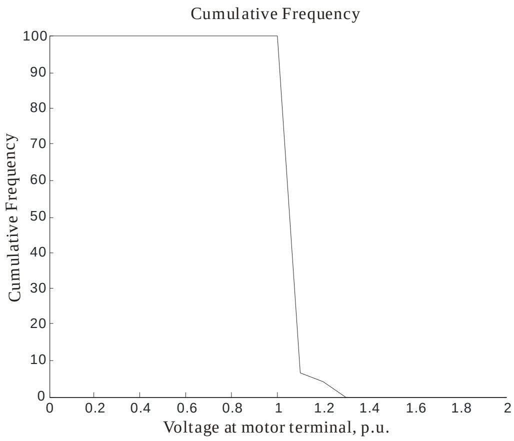

Case 16

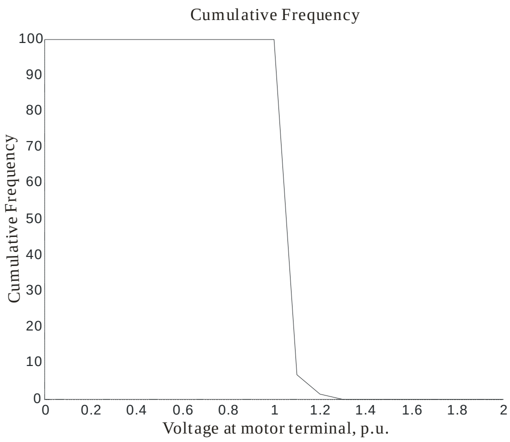

Case 17

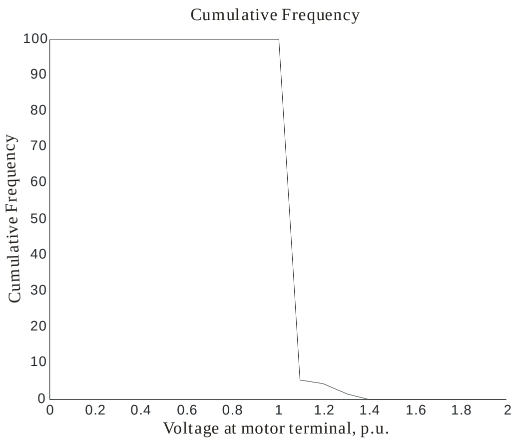

Case 18

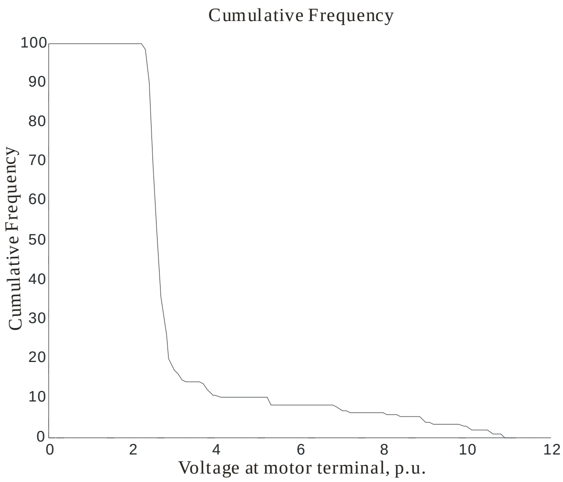
Cumulative Frequency
Cumulative Frequency
100
90
80
70
60
50
40
30
20
10
0
0
2
4
6
8
10
12
Voltage at motor terminal, p.u.

Case 19

APPENDIX E: PROTECTIVE MEASURES STATISTICAL RESULTS

Voltage at motor terminal

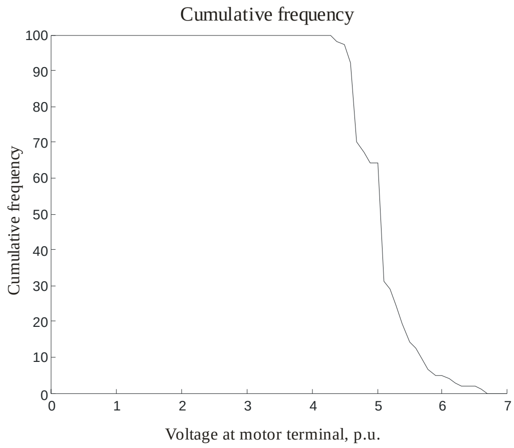

Case 1

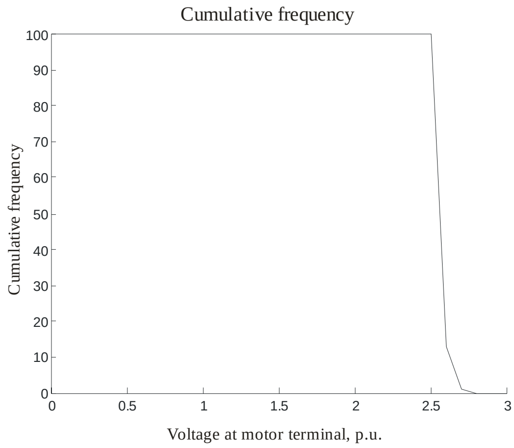

Case 2

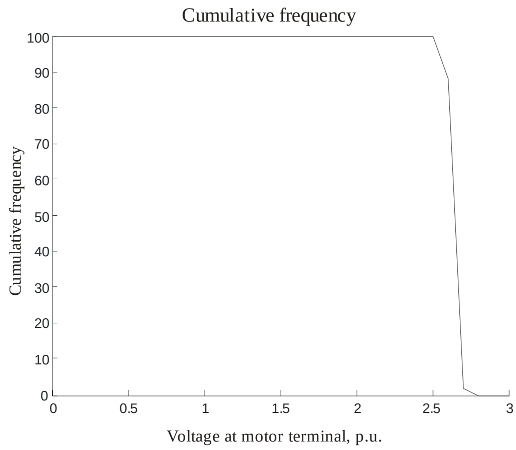

Case 3

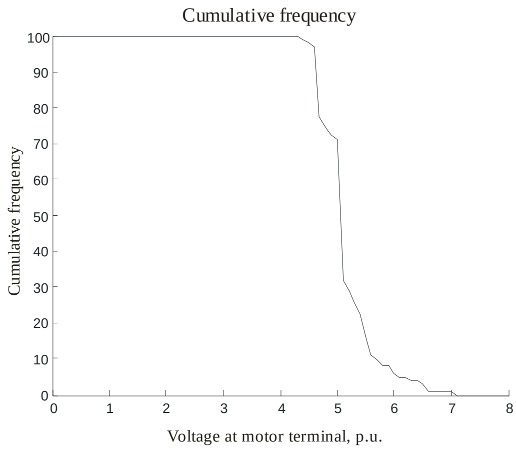

Case 4

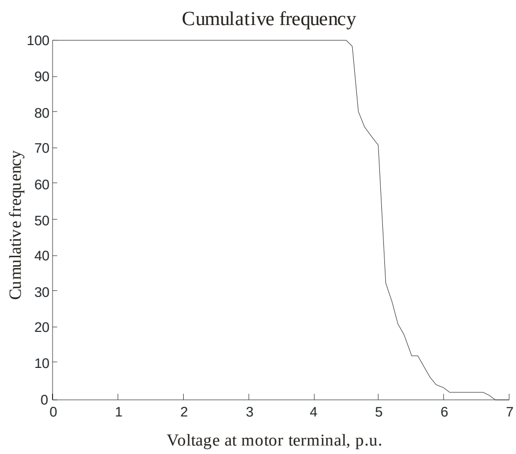

Case 5

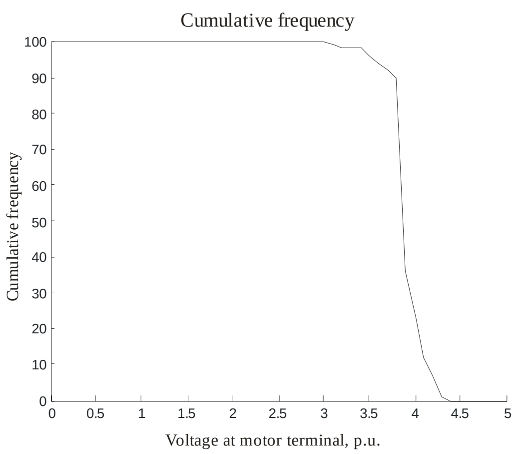

Case 6

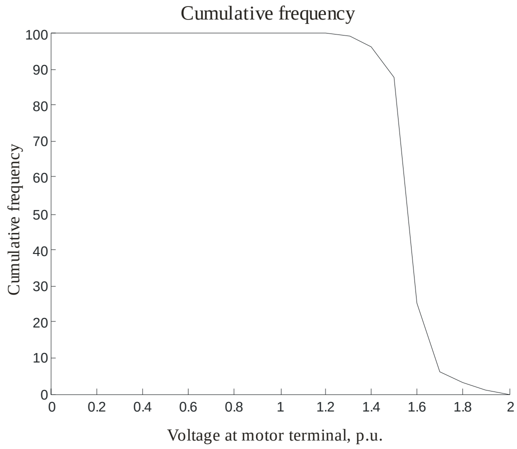
Cumulative frequency
Cumulative frequency
100
90
80
70
60
50
40
30
20
10
0
0
0.2
0.4
0.6
0.8
1
1.2
1.4
1.6
1.8
2
Voltage at motor terminal, p.u.

Case 7

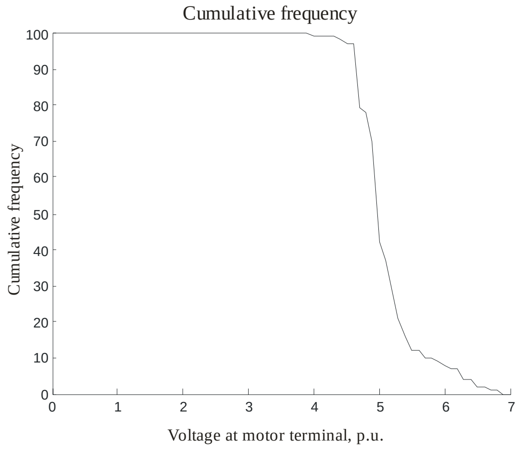
Cumulative frequency
Cumulative frequency
100
90
80
70
60
50
40
30
20
10
0
0
1
2
3
4
5
6
7
Voltage at motor terminal, p.u.

Case 8

Voltage across breaker

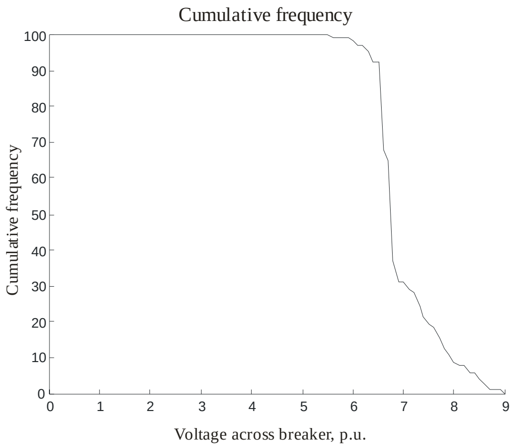

Case 1

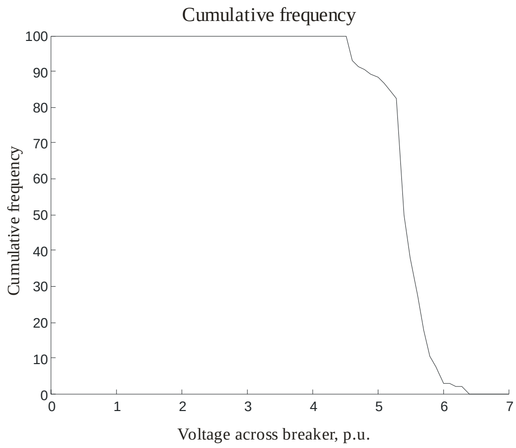

Case 2

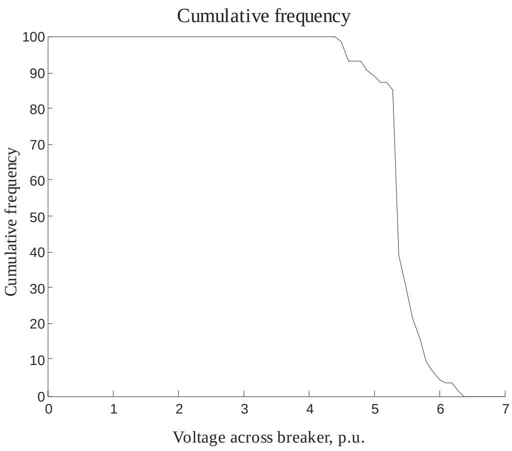

Case 3

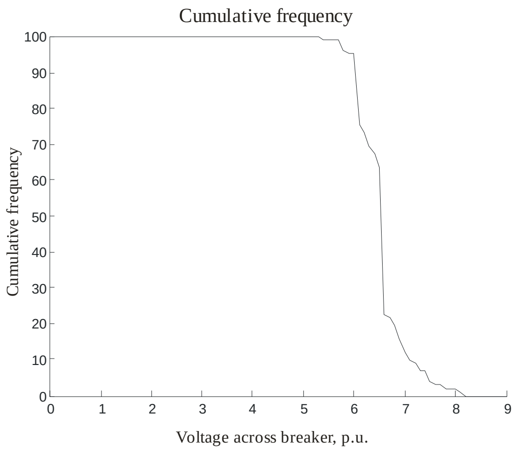

Case 4

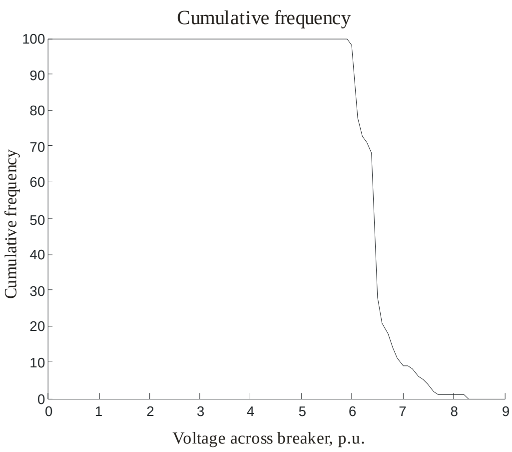

Case 5

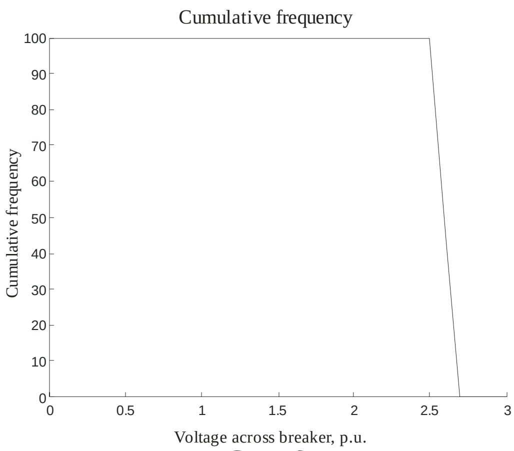

Case 6

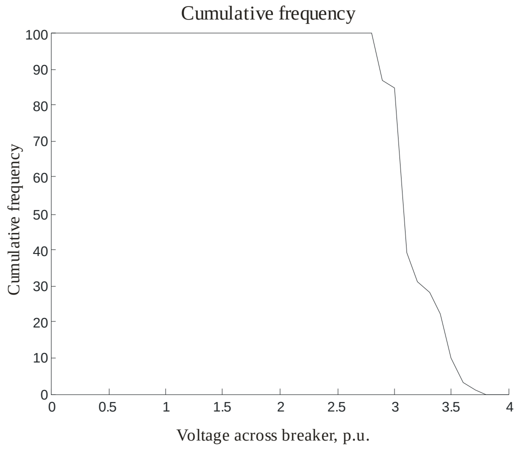
Cumulative frequency
Cumulative frequency
Voltage across breaker, p.u.
0
0.5
1
1.5
2
2.5
3
3.5
4
0
10
20
30
40
50
60
70
80
90
100

Case 7

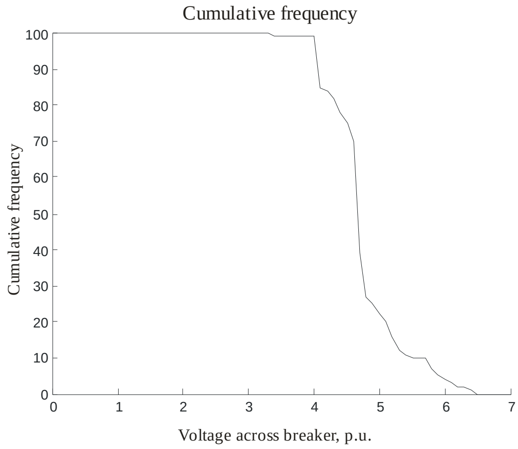
Cumulative frequency
Cumulative frequency
Voltage across breaker, p.u.
0
1
2
3
4
5
6
7
0
10
20
30
40
50
60
70
80
90
100

Case 8

Voltage at transformer low voltage side

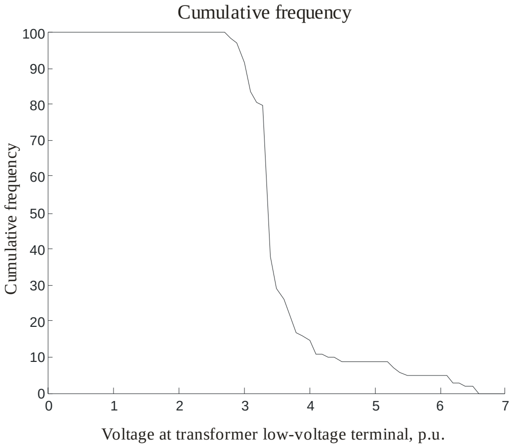

Case 1

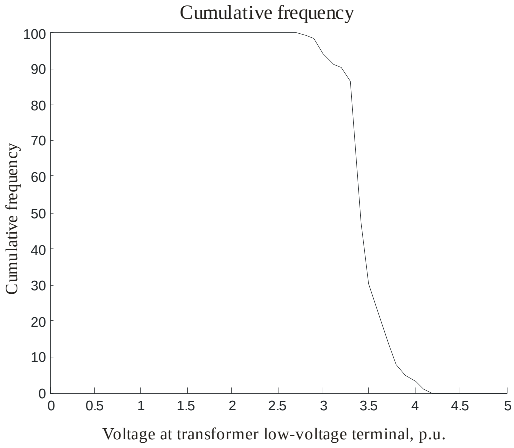

Case 2

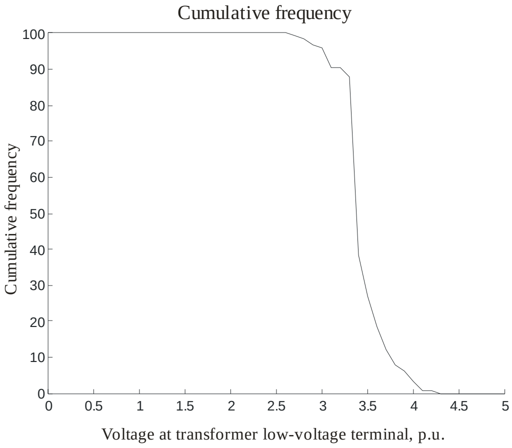

Case 3

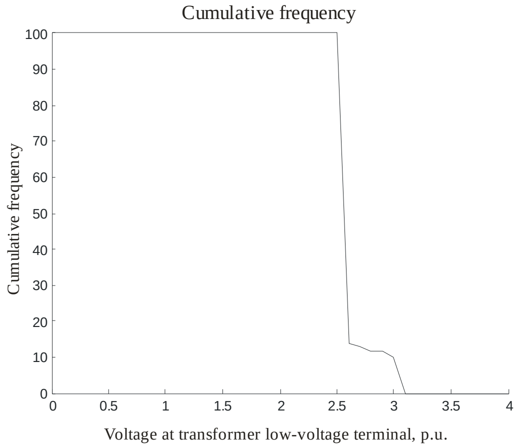

Case 4

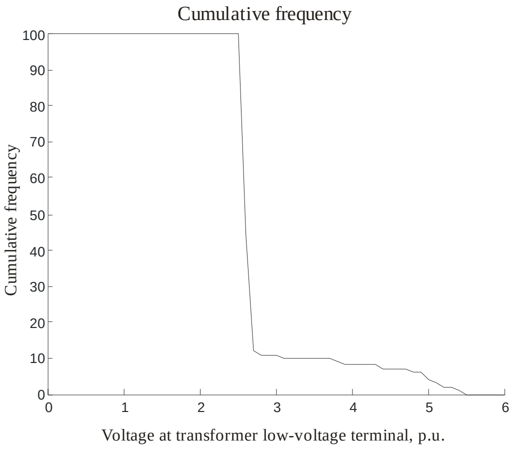

Case 5

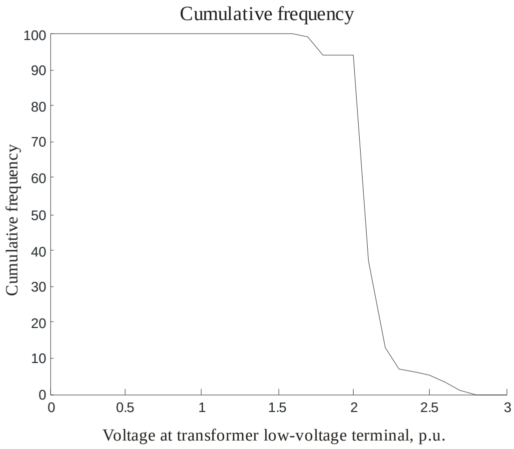

Case 6

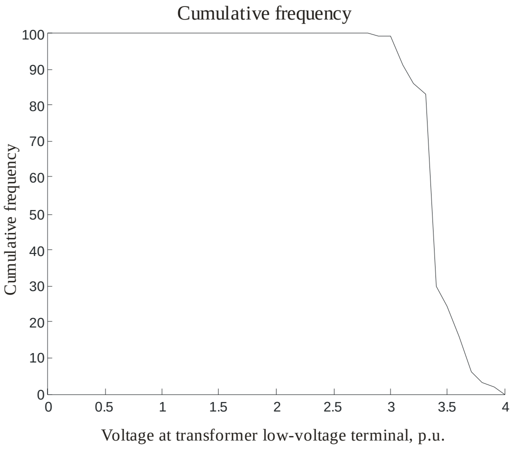
Cumulative frequency
Cumulative frequency
Voltage at transformer low-voltage terminal, p.u.
Case 7

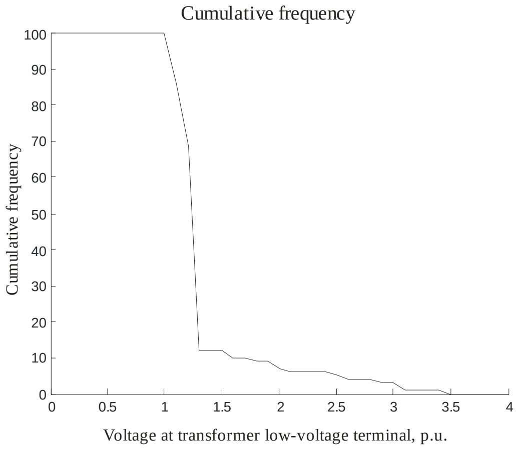
Cumulative frequency
Cumulative frequency
Voltage at transformer low-voltage terminal, p.u.
Case 8

APPENDIX F: Parameters from manufacturer

Characteristics of the VCB

1. ***Characteristics of surge arrestor.***
   (Please find the attached sheets)

2. ***Dielectric Strength of gap (withstand voltage curve) of VCB***

Gap Length (mm)	***Impulse (kV peak)***	
	DP-11	***DP-16***
1	16	23
2	34	46
3	50	70
5	60	80
12	80	80

3. ***Quenching capability of High frequency current at zero crossing of VCB.***

Possible to Interrupting dI/dt at current zero (A/micro-sec)	
DP-11	100
DP-16	400

4. ***Value of Chopping current.***

   The copping current of the VCB's will be as per WSD specification apart from the 1250A units which will have a chopping current value of 8A.

Characteristics of the arrester

Technical Characteristics

Characteristic	Unit	Value
Arrester type reference	-	HSRA3
Rated Voltage	kV rms	3
Continuous operating voltage	kV rms	2.4
Temporary overvoltage capability for 1 second	kV rms	3.6
Maximum residual voltages with 8/20µsec current wave (lightning surge):		
- 5kA	kV crest	7.9
- 10kA	kV crest	8.7
- 20kA	kV crest	9.6
Maximum residual voltages with: 30/60µsec current wave (switching surge):		
- 0.125kA	kV crest	6.0
- 0.5kA	kV crest	6.5
Steep current residual voltage at 10kA	kV crest	9.2
Nominal current rating	kA crest	10
Line discharge class	-	2
Overall height	mm	228
Nett weight	kg	1.8
Total creepage distance	mm	600

Characteristics of the arrester